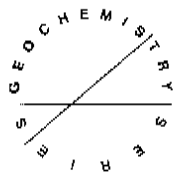

Using Geochemical Data:
Evaluation, Presentation, Interpretation

Hugh R. Rollinson

Longman Scientific & Technical

Copublished in the United States with
John Wiley & Sons, Inc., New York

Longman Scientific & Technical
Longman Group UK Limited
Longman House, Burnt Mill, Harlow
Essex CM20 2JE, England
and Associated Companies throughout the world.

Copublished in the United States with
John Wiley & Sons, Inc., 695 Third Avenue, New York, NY 10158

First published 1993

British Library Cataloguing-in-Publication Data
A catalogue record for this book is available from the British Library

ISBN 0 582 06701 4

Library of Congress Cataloging-in-Publication Data
A catalogue record for this book is available from the Library of Congress

ISBN 0 470 221542 (USA only)

Set by 8RR in 10/12 pt Ehrhardt.
Produced by Longman Singapore Publishers (Pte) Ltd.
Printed in Singapore

which they plot the fields of Archaean greenstone belt shales and Phanerozoic shales. Bjorlykke (1974) plotted the $(Al_2O_3+K_2O)/(MgO+Na_2O)$ content of shales and used it as an indicator of volcanic-arc provenance.

3.2.5 Discussion

For volcanic igneous rocks there is a variety of chemical classification schemes which work and which are simple to use, the best of which is the TAS diagram. Plutonic rocks are more problematic. An adequate classification scheme exists for granitic rocks in the O'Connor diagram but there is no simple and widely accepted classification for all plutonic rocks. Probably, the most comprehensive is the R1–R2 diagram of De la Roche *et al.* (1980) although this diagram is difficult both to understand and to apply.

3.3 Variation diagrams

A table of geochemical data from a particular igneous province, metamorphic terrain or sedimentary succession may at first sight show an almost incomprehensible variation in the concentration of individual elements. Given that the samples are likely to be geologically related, a major task for the geochemist is to devise a way in which the variation between individual rocks may be simplified and condensed so that relationships between the individual rocks may be identified. The device which is most commonly used and has proved invaluable in the examination of geochemical data is the variation diagram. This is a bivariate graph or scattergram on which two selected variables are plotted. Diagrams of this type were popularized as long ago as 1909 by Alfred Harker in his *Natural history of igneous rocks*, and one particular type of variation diagram, in which SiO_2 is plotted along the x-axis, has become known as the 'Harker diagram'.

An illustration of the usefulness of variation diagrams can be seen from a comparison of the data in Table 3.3 and the variation diagrams plotted for the same data (Figure 3.14). It is clear that the variation diagrams have condensed and rationalized a large volume of numerical information and show qualitatively that there is an excellent correlation (either positive or negative) between each of the major elements displayed and SiO_2. Traditionally this strong geochemical coherence between the major elements has been used to suggest that there is an underlying process which will explain the relationships between the major elements.

3.3.1 Recognizing geochemical processes on a major element variation diagram

Most trends on variation diagrams are the result of mixing. In igneous rocks the mixing may be that of two magmas, the addition and/or subtraction of solid phases during contamination or fractional crystallization, or mixing due to the addition of

Table 3.3 Chemical analyses of rocks from Kilauea Iki lava lake, Hawaii*

	1	2	3	4	5	6	7	8	9	10	11	12	13	14	15	16	17
SiO_2	48.29	48.83	45.61	45.50	49.27	46.53	48.12	47.93	46.96	49.16	48.41	47.90	48.45	48.98	48.74	49.61	49.20
TiO_2	2.33	2.47	1.70	1.54	3.30	1.99	2.34	2.32	2.01	2.73	2.47	2.24	2.35	2.48	2.44	3.03	2.50
Al_2O_3	11.48	12.38	8.33	8.17	12.10	9.49	11.43	11.18	9.90	12.54	11.80	11.17	11.64	12.05	11.60	12.91	12.32
Fe_2O_3	1.59	2.15	2.12	1.60	1.77	2.16	2.26	2.46	2.13	1.83	2.81	2.41	1.04	1.39	1.38	1.60	1.26
FeO	10.03	9.41	10.02	10.44	9.89	9.79	9.46	9.36	9.72	10.02	8.91	9.36	10.37	10.17	10.18	9.68	10.13
MnO	0.18	0.17	0.17	0.17	0.17	0.18	0.18	0.18	0.18	0.18	0.18	0.18	0.18	0.18	0.18	0.17	0.18
MgO	13.58	11.08	23.06	23.87	10.46	19.28	13.65	14.33	18.31	10.05	12.52	14.64	13.23	11.18	12.35	8.84	10.51
CaO	9.85	10.64	6.98	6.79	9.65	8.18	9.87	9.64	8.58	10.55	10.18	9.58	10.13	10.83	10.45	10.96	11.05
Na_2O	1.90	2.02	1.33	1.28	2.25	1.54	1.89	1.86	1.58	2.09	1.93	1.82	1.89	1.73	1.67	2.24	2.02
K_2O	0.44	0.47	0.32	0.31	0.65	0.38	0.46	0.45	0.37	0.56	0.48	0.41	0.45	0.80	0.79	0.55	0.48
P_2O_5	0.23	0.24	0.16	0.15	0.30	0.18	0.22	0.21	0.19	0.26	0.23	0.21	0.23	0.24	0.23	0.27	0.23
H_2O^+	0.05	0.00	0.00	0.00	0.00	0.08	0.03	0.01	0.00	0.06	0.08	0.00	0.09	0.02	0.04	0.02	0.04
H_2O^-	0.05	0.03	0.04	0.04	0.03	0.04	0.05	0.04	0.00	0.02	0.02	0.02	0.00	0.00	0.01	0.01	0.02
CO_2	0.01	0.00	0.00	0.00	0.00	0.11	0.04	0.02	0.00	0.00	0.00	0.01	0.00	0.01	0.01	0.01	0.01
Total	100.01	99.89	99.84	99.86	99.84	99.93	100.00	99.99	99.93	100.05	100.02	99.95	100.05	100.06	100.07	99.90	99.95

* From Richter and Moore (1966), courtesy of the US Geological Survey.

melt increments during partial melting. In sedimentary rocks trends on a variation diagram will also result from mixing, but in this case the mixing of chemically distinct components which contribute to the composition of the sediment. In metamorphic rocks, trends on a variation diagram will usually reflect the processes in the igneous or sedimentary precursor, masked to some degree by specific metamorphic processes such as metasomatism. In some instances, however, deformation may 'smear' together more than one rock type, giving rise to a mixing line of metamorphic origin.

Below we consider some of the more important mixing processes.

Fractional crystallization

Fractional crystallization is a major process in the evolution of many igneous rocks, and is frequently the cause of trends seen on variation diagrams for igneous rocks. The fractionating mineral assemblage is normally indicated by the phenocrysts present. A test of crystal fractionation may be made by accurately determining the composition of the phenocrysts using the electron microprobe and then plotting the compositions on the same graph as the rock analyses. If trends on a variation diagram are controlled by phenocryst compositions then it may be possible to infer that the rock chemistry is controlled by crystal fractionation. It should be noted, however, that fractional crystallization may also take place at depth and in this case the fractionating phases may not be represented in the phenocryst assemblage.

The importance of fractional crystallization was expounded at length by Bowen (1928) in his book *The evolution of the igneous rocks*; he argued that geochemical trends for volcanic rocks represent a 'liquid line of descent'. This is the path taken by residual liquids as they evolve through the differential withdrawal of minerals from the magma. The ideas of Bowen now need to be qualified in the light of modern findings in the following ways: (1) trends identical to those produced by crystal fractionation can also be produced by partial melting; (2) only phenocryst-poor or aphyric volcanic rocks will give a true indication of the liquid path; (3) rarely does a suite of volcanic rocks showing a progressive chemical change erupt as a time sequence. Thus even a highly correlated trend for phenocryst-free volcanic

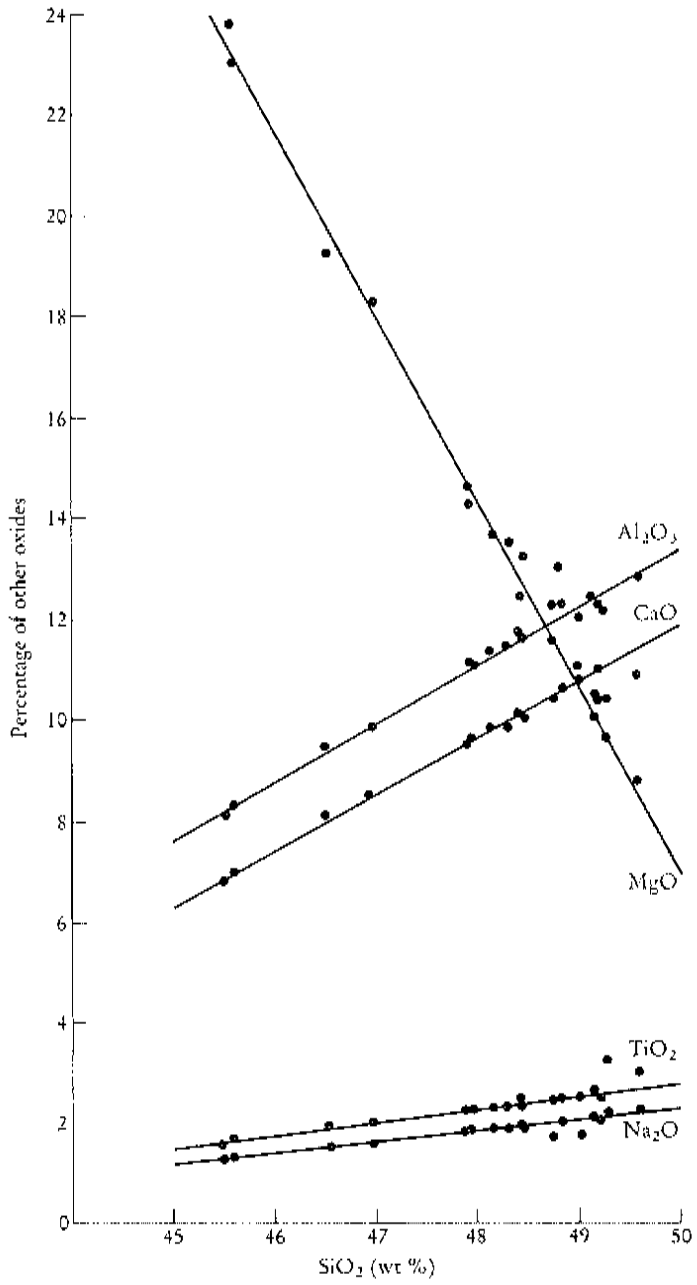

Figure 3.14 Bivariate plots of the oxides Al_2O_3, CaO, MgO, TiO_2, Na_2O vs SiO_2 in basaltic lavas from Kilauea Iki lava lake from the 1959–1960 eruption of Kilauea volcano, Hawaii (from Richter and Moore, 1966). The data are given in Table 3.3.

rocks on a variation diagram for a single volcano is unlikely to represent a liquid line of descent. Rather it is an approximation to a liquid line of descent of a bundle of similar, overlapping, subparallel lines of descent. Such lavas are not related to a

single parental magma but rather to a series of similar and related magmas (Cox *et al.*, 1979).

Assimilation and fractional crystallization

If phenocryst compositions cannot explain trends in a rock series and a fractional crystallization model does not appear to work, it is instructive to consider the possibility of simultaneous assimilation of the country rock and fractional crystallization. This process, often abreviated to AFC, was first proposed by Bowen (1928), who argued that the latent heat of crystallization during fractional crystallization can provide sufficient thermal energy to consume the wall-rock. Anderson and Cullers (1987) argued for an AFC model to explain the major element chemistry of a Proterozoic tonalite–trondhjemite suite hosted by Archean gneisses. The suite showed marked chemical variability but trends on Harker diagrams were not compatible with any simple fractionation scheme based upon the chemistry of minerals present, or once present, in the original melt. Their calculations showed, however, that if in addition to crystal fractionation the melt was contaminated with a small amount (*ca* 7 %) of the enclosing Archean gneiss, the observed trends were duplicated.

O'Hara (1980) has argued that contamination can result in the 'decoupling' of the major and trace element or isotope chemistry and is not always demonstrable from the major element data. For example, contamination of a basalt precipitating olivine, clinopyroxene and plagioclase will result in increased precipitation of fractionating minerals but may cause only a minor change in composition of the liquid as measured, for example, in its silica content. Trace element levels and isotope ratios, however, will be changed and provide a better means of recognizing assimilation.

Partial melting

Progressive fractional melting will show a trend on a variation diagram which is controlled by the chemistry of the solid phases being added to the melt. However, this can be very difficult to distinguish from a fractional crystallization trend on a major element variation diagram, for both processes represent crystal–liquid equilibria involving almost identical liquids and identical crystals. One situation in which progressive partial melting and fractional crystallization may be differentiated is if the two processes take place under different physical conditions. For example, if partial melting takes place at great depth in the mantle and fractional crystallization is a crustal phenomenon, then some of the phases involved in partial melting will be different from those involved in fractional crystallization.

Mixing lines in sedimentary rocks

Trends on variation diagrams for sedimentary rocks may result from the mixing of the different ingredients which constitute the sediment. There are a number of examples of this effect in the literature. Bhatia (1983), in a study of turbidite sandstones from eastern Australia, shows Harker diagrams in which there is a change in mineralogical maturity, i.e. an increase in quartz coupled with a decrease in the proportions of lithic fragments and feldspar (Figure 3.15). Argast and Donnelly (1987) show how strongly correlated trends may result from two-component (quartz–illite, quartz/feldspar–illite) mixing and curvilinear or scattered trends result from three-component mixing (quartz–illite–calcite).

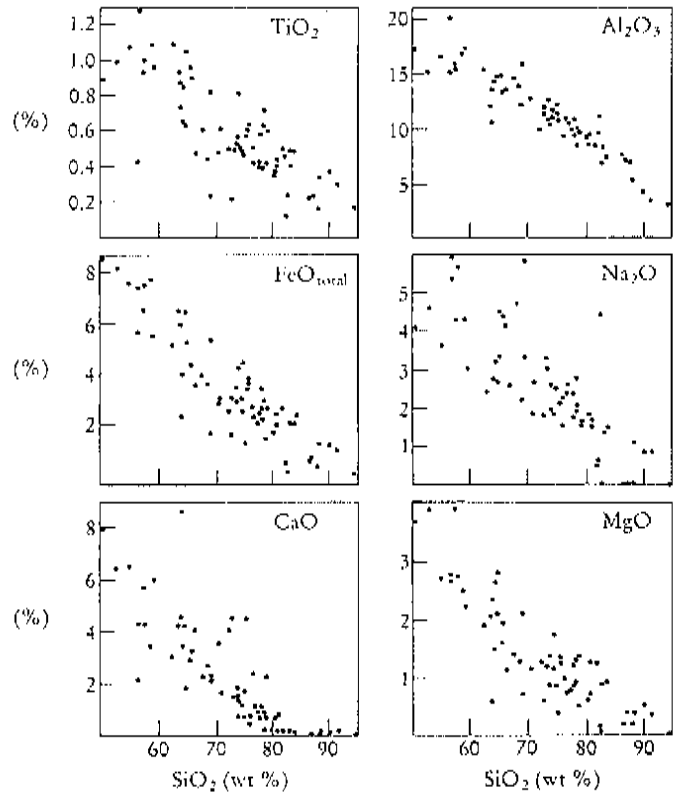

Figure 3.15 Harker variation diagrams for quartz-rich sandstone suites from eastern Australia (after Bhatia, 1983). The increase in SiO_2 reflects an increased mineralogical maturity, i.e. a greater quartz content and a smaller proportion of detrital grains.

The identification of former weathering conditions from sedimentary rocks

A good measure of the degree of chemical weathering can be obtained from the chemical index of alteration (CIA; Nesbitt and Young, 1982).

$$CIA = [Al_2O_3/(Al_2O_3 + CaO^* + Na_2O + K_2O)]$$

In addition, weathering trends can be displayed on a $(CaO^* + Na_2O) - Al_2O_3 - K_2O$ triangular plot (Nesbitt and Young, 1984, 1989). On a diagram of this type the initial stages of weathering form a trend parallel to the $(CaO + Na_2O) - Al_2O_3$ side of the diagram, whereas advanced weathering shows a marked loss in K_2O as compositions move towards the Al_2O_3 apex (Figure 3.16). The trends follow mixing lines representing the removal of alkalis and Ca in solution during the breakdown of first plagioclase and then potassium feldspar and ferromagnesian silicates.

The CIA and trends on triangular plots have been used in two different ways. Firstly, chemical changes in a recent weathering profile such as that illustrated in Figure 3.16 are used as a template against which the chemical history of an ancient profile can be read. Deviations from such trends can be used to infer chemical changes resulting from diagenesis or metasomatism (Nesbitt and Young, 1984, 1989). The second application is to mudstones. The major and trace element chemistry of modern muds reflects the degree of weathering in their source (Nesbitt

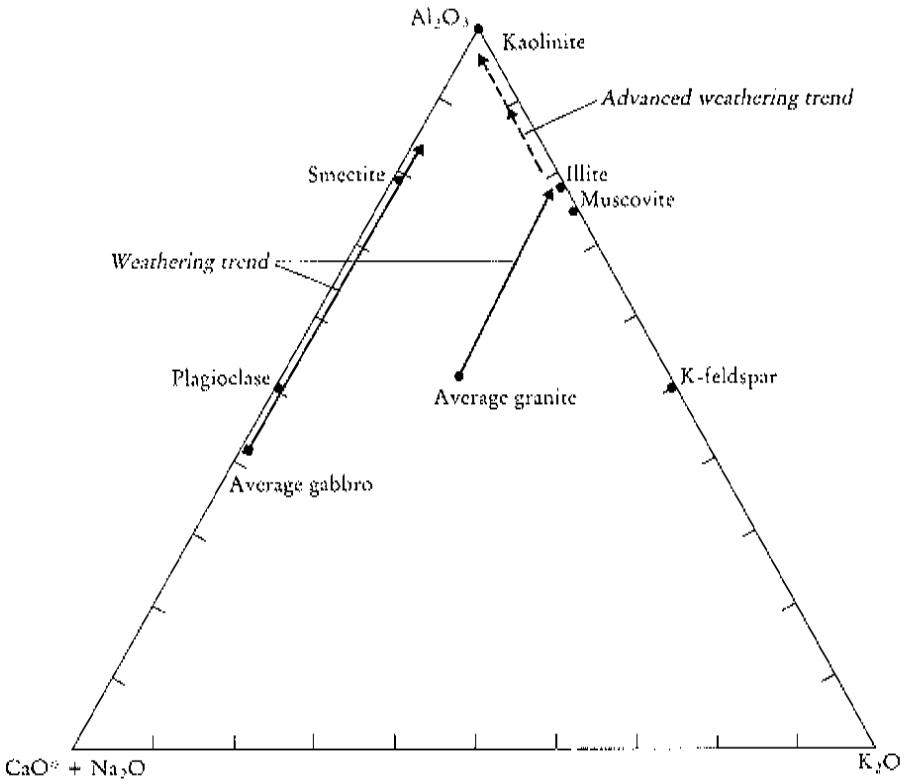

Figure 3.16 The $(Na_2O + CaO) - Al_2O_3 - K_2O$ diagram of Nesbitt and Young (1984, 1989) showing the weathering trends for average granite and average gabbro. The advanced weathering trend for granite is also shown. Compositions are plotted as molar proportions and the compositions of plagioclase, K-feldspar, muscovite and kaolinite are shown. CaO^* represents the CaO associated with the silicate fraction of the sample.

et al., 1990); thus the chemical composition of ancient muds may be used in a similar way to make inferences about past weathering conditions.

Mixing in metamorphic rocks

Banded gneisses from the Archaean Lewisian complex of northwest Scotland show linear trends on major element variation diagrams. There are two possible explanations of such trends. On the one hand the banded gneisses may be the product of the tectonic mixing of mafic and felsic end-members in the gneiss suite, in which case trends on the variation diagrams also reflect this mixing (Tarney, 1976). Alternatively, the trend could be pre-metamorphic and magmatic in origin and indicate the approximate igneous composition of the gneiss suite.

Element mobility

Element mobility describes the chemical changes which take place in rock after its formation, usually through interaction with a fluid. Most commonly, element mobility will take place during weathering, diagenesis and metamorphism or through interaction with a hydrothermal fluid. In metamorphic rocks, element mobility may also take place as a result of solid-state diffusion and melt generation. Here, however, we are chiefly concerned with fluid-controlled element mobility on

the scale of several centimetres or more. The mobility of major elements is controlled by three main factors — the stability and composition of the minerals in the unaltered rock, the stability and composition of the minerals in the alteration product and the composition, temperature and volume of the fluid phase.

Element mobility may be detected from mineralogical phase and compositional changes that have taken place in a rock as a result of metamorphism or hydrothermal activity and from the mineral assemblages present in associated veins. Scattered trends on variation diagrams are also a useful indicator, although chemical alteration can sometimes produce systematic changes which may mimic other mixing processes such as crystal fractionation. These apparent trends may result from volume changes arising from the removal or addition of a single component of the rock. Variation diagrams which can be used to identify element mobility are discussed in Section 4.9.3.

Table 3.4 summarizes the main mobile elements in a range of common rock

Table 3.4 Major element mobility in common rock types under a variety of hydrothermal conditions

Rock type		Si	Ti	Al	Fe	Mn	Mg	Ca	Na	K	P	Reference
Komatiite		×						×	×	×		Arndt (1983)
Basalt	Hydrothermal alteration	–			...	...	+	–	–	–		Mottl (1983)
Basalt	Hydrothermal alteration	+	–		–	–	–	–	+			MacGeehan and MacLean (1980)
Basalt	Submarine weathering	–			+		–	–	–	+		Pearce (1976)
Basalt	Weathering	–					–	–	–	–		Pearce (1976)
Basalt	Greenschist facies metamorphism				×		×		×	×		Pearce (1976), Gelinas *et al.* (1982)
Basalt	Amphibolite facies metamorphism	×						×	×			Rollinson (1983)
Granite	Weathering				×		×	×	–	×		Nesbitt and Young (1989)
Granite	Contact metamorphism			+	–		–	–	–	+		Vernon *et al.* (1987)
'Granite'	Granulite facies metamorphism						–			×		Allen *et al.* (1985)
Calcareous sediments	Medium grade metamorphism								–	–		Perry (1983)
Calcareous sediments	Contact metamorphism	×			×		×					Burcher-Nurminen (1981)
Sandstone–clay	Diagenesis	×			×		×	×		×		Boles and Franks (1979)

Key: ×, element mobile; –, element depleted; +, element enriched.

types under a variety of hydrothermal conditions. Basaltic rocks are well documented and most studies show that Ti, Al and P are generally immobile whereas Ca and Na are almost always mobilized. Similarly, in granites Ti, Al and P are generally immobile. Sediments are not so well studied although chemical changes during the diagenesis of a sandstone–clay sequence are well described and reflect the breakdown, with progressive burial of orthoclase and plagioclase and the conversion of smectite to illite. At higher metamorphic grades little is known except for a consensus that Al is immobile (Ferry, 1983).

Artificial trends

Sometimes trends on a variation diagram are artificially produced by the numerical processes used in plotting the data and do not automatically signify geochemical relationships. This is well documented by Chayes (1960) and Aitchison (1986), who have shown that correlations in compositional data can be forced as a result of the unit sum constraint (see Section 2.6). The most helpful way to circumvent this problem is to examine trends on variation diagrams in the light of a specific hypothesis to be tested. The closeness of fit between the model and the data can then be used to evaluate the hypothesis.

3.3.2 Selecting a variation diagram

The two main types of variation diagram currently used by geochemists are considered in this section — bivariate plots and triangular variation diagrams.

Bivariate plots

The principal aim of a bivariate plot, such as that illustrated in Figure 3.14, is to show variation between samples and to identify trends. Hence the element plotted along the *x*-axis of the diagram should be selected either to show the maximum variability between samples or to illustrate a particular geochemical process. Normally the oxide which shows the greatest range in the data-set would be selected; in many cases this would be SiO_2, but in basic igneous rocks it might be MgO and in clay-bearing sediments Al_2O_3.

In a reconnaisance geochemical study of a problem it might be necessary to prepare a very large number of variation diagrams in order to delimit the possible geological processes operating. In this case the initial screening of the data is best done by computer (see for example Barnes, 1988). If a correlation matrix is used, it is important to remember that good correlations may arise through a cluster of data points and a single outlier. Similarly, poor correlations can arise if the data-set contains several populations, each with a different trend.

More normally, and more fruitfully, however, most geochemical investigations are designed to solve a particular problem and to test a hypothesis — usually formulated from geological or other geochemical data. In this case the plotting parameter for a variation diagram should be selected as far as possible with the process to be tested in mind. For example, if in the case of igneous rocks a crystal fractionation mechanism is envisaged, then an element should be selected which is contained in the fractionating mineral and which will be enriched or depleted in the melt.

(a) Harker diagrams — bivariate plots using SiO_2 along the x*-axis* Variation diagrams in which oxides are plotted against SiO_2 are often called Harker

diagrams. They are the oldest form of variation diagram and are one of the most frequently used means of displaying major element data (see Figures 3.14, 3.15). SiO_2 is commonly chosen as the plotting parameter for many igneous rock series and for suites of sedimentary rocks with a variable quartz content because it is the major constituent of the rock and shows greater variability than any of the other oxides. However, the very fact that SiO_2 is the most abundant oxide means that there are a number of inherent problems of which the user must be aware. These are: (1) a negative tendency (see Figure 3.15), (2) spurious correlations and (3) a reduced scatter of values as SiO_2 increases (see the Al_2O_3–SiO_2 plot in Figure 3.15). These problems are fully discussed in Section 2.6.

(b) Bivariate plots which use MgO on the x*-axis* One of the most commonly used alternatives to the Harker diagram is the MgO plot. This is most appropriate for rock series which include abundant mafic members, for in this case the range of SiO_2 concentrations may be small. MgO, on the other hand, is an important component of the solid phases in equilibrium with mafic melts and shows a great deal of variation either as a consequence of the breakdown of magnesian phases during partial melting or their removal during fractional crystallization.

(c) Bivariate plots using cations It is sometimes simpler to display mineral compositions on a variation diagram if major element chemical data are plotted as cation %, that is the wt % oxide value divided by the molecular weight and multiplied by the number of cations in the oxide formula and then recast to 100 % (see Table 3.2, columns 1–4 and 6); see for example Francis (1985). An identical calculation with the result expressed as mol % cations instead of cation % is used by Hanson and Langmuir (1978) in their MgO–FeO cation diagram (see Section 3.3.4). Roedder and Emslie (1970) in a similar diagram use mol % of MgO and FeO (see Table 3.2, column 7).

(d) Bivariate plots using the magnesium number The older geochemical literature carries a large number of examples of complex, multi-element plotting parameters which were used as a measure of fractionation during the evolution of an igneous sequence. These are rather complicated to use and difficult to interpret and so have fallen into disuse. However, one which is useful, and so survives, is the **magnesium–iron ratio**, or **magnesium number** as it is sometimes called. The magnesium–iron ratio is particularly useful as an index of crystal fractionation in basaltic liquids (see Oskarsson *et al.*, 1982; Wilkinson, 1982) for here the Mg–Fe ratio changes markedly in the early stages of crystallization as a result of the higher Mg–Fe ratio of the liquidus ferromagnesian minerals than their host melts. The magnesium–iron ratio is expressed either in wt % form as $100[MgO/(MgO + FeO)]$ or $100[MgO/(MgO + FeO + Fe_2O_3)]$ or as an atomic fraction as $100[Mg^{2+}/(Mg^{2+} + Fe^{2+})]$. The inverse of this ratio is also used as a measure of iron enrichment.

Triangular variation diagrams

Triangular variation diagrams are used when it is necessary to show simultaneous change between three variables. However, this practice is not recommended and bivariate plots are to be preferred, since both the computation of the plotting parameters and the interpretation of the resultant trends raise a number of important problems (see Section 2.7).

The plotting procedure for triangular diagrams is illustrated in Figure 3.17. This is most conveniently done by microcomputer and Topley and Burwell (1984) give an example of a versatile interactive program written in BASIC.

(a) The AFM diagram The AFM diagram (Figure 3.18) is the most popular of triangular variation diagrams and takes its name from the oxides plotted at its apices — Alkalis ($Na_2O + K_2O$), Fe oxides ($FeO + Fe_2O_3$) and MgO. The igneous AFM diagram should not be confused with the metamorphic diagram of the same name which is used to show changing mineral compositions in Al_2O_3–FeO–MgO space. The plotting parameters are calculated by summing the oxides ($Na_2O + K_2O$) + [($FeO + Fe_2O_3$) recalculated as FeO] + MgO and then recalculating each as a percentage of the sum. There is some ambiguity over the way in which the Fe-oxides should be treated and the following alternatives are in current use:

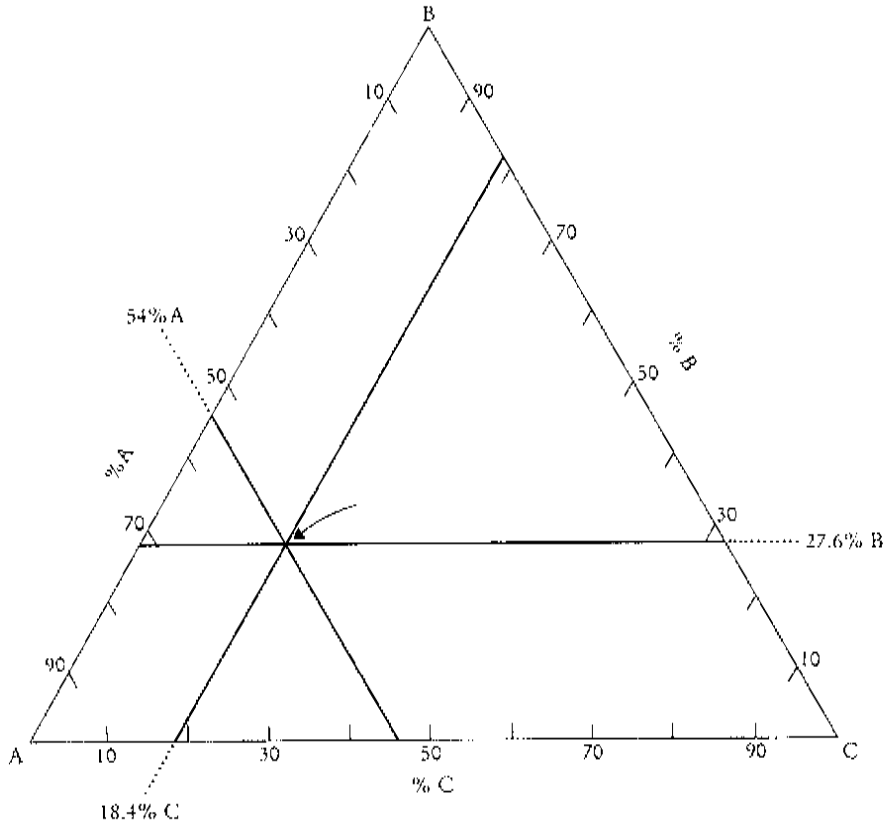

Figure 3.17 Construction lines for plotting the point A = 54 %, B = 27.6 % and C = 18.4 % on a triangular diagram. The values are plotted as follows: variable B is 100 % at the top of the plotting triangle and 0 % along the base of the triangle and so, counting upwards from the base (the concentrations are given on the right-hand side of the triangle), the horizontal line representing 27.6 % is located. In a similar way the line representing 54 % A is located, parallel to the right-hand side of the triangle. The point at which the two lines intersect is the plotting position. To check that it has been accurately located, the line for variable C should pass through the intersection of the two other lines.

F = ($FeO + 0.8998Fe_2O_3$), i.e. all Fe_2O_3 converted to FeO
is the same as
F = total ($FeO + Fe_2O_3$) expressed as FeO i.e. $FeO_{[total]}$
but different from
F = ($FeO + Fe_2O_3$) expressed as raw wt %

In addition some authors include MnO with the Fe-oxides. Rickwood (1989) has shown that the differences are minor and are unlikely to result in serious misplotting; nevertheless it is recommended that a standard procedure is adopted and that F is calculated as total Fe, i.e. ($FeO + Fe_2O_3$) recast as FeO. This then accommodates XRF analytical data in which the separate oxidation states of iron cannot be determined.

Most authors use oxide wt % when plotting data on an AFM diagram but in a few cases atomic proportions are used and it is not always clear which method has been adopted. The shape of the trend is similar in each case but the position of the atomic proportions plot is shifted away from the Fe apex relative to the position of the oxide plot for the same data (see Barker, 1978).

The AFM diagram is most commonly used to distinguish between tholeiitic and calc–alkaline differentiation trends in the subalkaline magma series. Kuno (1968) and Irvine and Baragar (1971) present dividing lines separating the rocks of the calc–alkaline series and rocks of the tholeiite series (Figure 3.18). Kuno's boundary line yields a smaller area for the tholeiitic suite. Both authors use wt % plots in which F is calculated as ($FeO + Fe_2O_3$) expressed as FeO. The coordinates for the boundary lines are given in the caption to Figure 3.18 (Rickwood, 1989).

Examples of the trends characteristic of the tholeiitic and calc–alkaline rock series are also plotted in Figure 3.18. The tholeiitic trend is illustrated by Thingmuli volcano in Iceland and the calc–alkaline trend is for the average compositions of the Cascades lavas (Carmichael, 1964).

(b) Problems in the use of the AFM diagram It is important to note that the AFM diagram is limited in the extent to which petrogenetic information may be extracted (Wright, 1974). This is chiefly a function of the trivariate plotting procedure, which does not use absolute values and only a part of the rock chemistry. In most rocks the A–F–M parameters make up less than 50 % of the oxide weight percentages and cannot therefore fully represent the rock chemistry. In addition, when plotting a rock series different proportions of each rock are normalized to 100 %. This distorts the plotted values. For example, in a series of volcanic rocks with a compositional range from basalt to dacite about 40 % of the basalt is used when plotting onto an AFM diagram whereas only about 15 % of the dacite is used. A further problem with the trivariate plotting procedure has been noted by Butler (1979), who argues that not only do trends on an AFM plot lead to non-quantitative expressions of mineralogical control but that the trends themselves could be an artefact of ternary percentage formation (see Section 2.7).

Barker (1978) advocated plotting mineral compositions on an AFM diagram in addition to rock compositions to assess mineralogical control of magmatic processes. However, this approach can only be semiquantitative since the lever rule (see below), which works well in bivariate plots, cannot be applied because of the disparate proportions of the compositions before projection. Thus AFM diagrams cannot be used in petrogenetic studies to extract quantitative information about

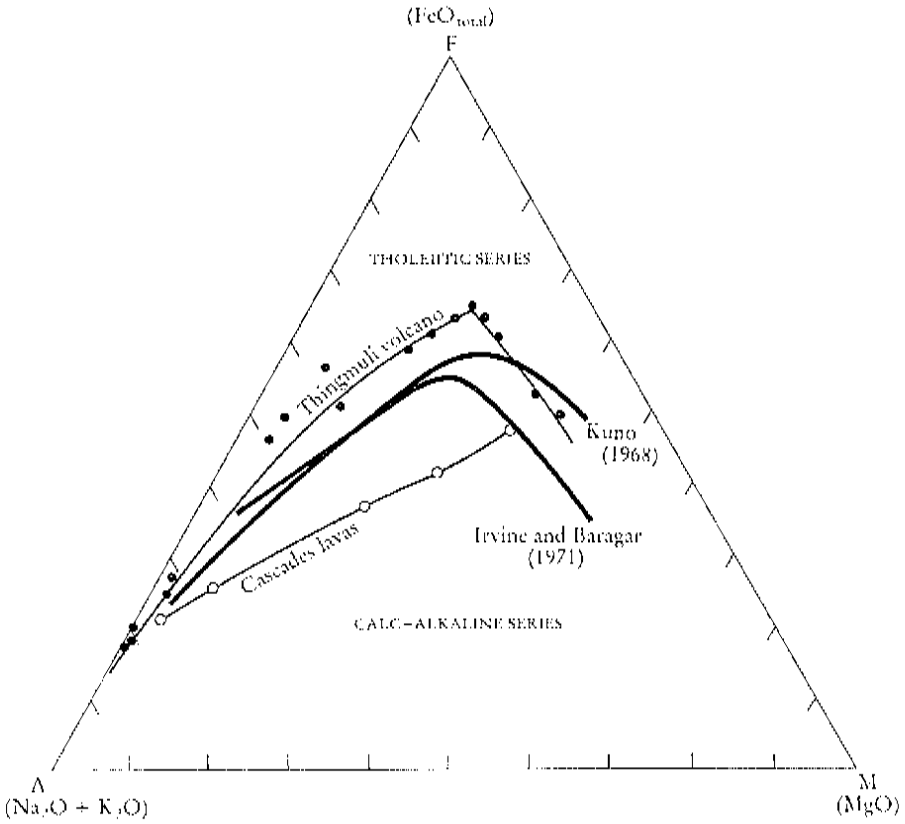

Figure 3.18 An AFM diagram showing the boundary between the calc–alkaline field and the tholeiitic field after Kuno (1968) and Irvine and Baragar (1971) (heavy lines). Also shown are lava compositions and trends (faint lines) for a typical tholeiitic sequence (Thingmuli volcano, Iceland — shown as filled circles — from Carmichael, 1964) and a typical calc alkaline trend (the average composition of Cascades lavas — shown as open rings — from Carmichael, 1964). The coordinates for points on the boundary lines of Kuno (1968) are A,F,M : 72.0,24.0,4.0; 50.0,39.5,10.5; 34.5,50.0,15.5; 21.5,57.0,21.5; 16.5,58.0,25.5; 12.5,55.5,32.0; 9.5,50.5,40.0; and for Irvine and Baragar (1971), A,F,M: 58.8,36.2,5.0; 47.6,42.4,10.0; 29.6,52.6,17.8; 25.4,54.6,20.0; 21.4,54.6,24.0; 19.4,52.8,27.8; 18.9,51.1,30.0; 16.6,43.4,40.0; 15.0,35.0,50.0 (from Rickwood, 1989).

processes. This must be done using bivariate oxide diagrams. The main usefulness of AFM diagrams, therefore, is to show trends which can be used to identify rock series as illustrated above.

Finally, however, it is worth noting that trends can be generated on an AFM diagram which have no geological meaning at all. Le Maitre (1976) plotted 26 000 samples of unrelated igneous rocks collected from around the world onto an AFM diagram and showed that they defined a marked calc–alkaline trend. He concluded that unrelated analyses taken at random can define trends on an AFM diagram and urged caution in interpreting such trends. A closer inspection of his data shows, however, that the samples are not entirely random since about 85 % of the rocks were collected from continents. Maybe these data have something to say about the composition and origin of the continental crust.

3.3.3 Interpreting trends on variation diagrams

It has been shown above that there are a variety of processes which can produce similar-looking trends on major element variation diagrams. It is important therefore to discover the extent to which these several processes might be distinguished from one another and identified.

Extract calculations

One approach is to try to calculate the composition of the materials added to or subtracted from a magma and to quantify the amount of material involved. This may be done using an extract calculation, a device described in some detail by Cox *et al.* (1979).

The method is illustrated in Figure 3.19(a), in which the chemical compositions (expressed in terms of variables A and B) of both minerals and rocks are plotted on the same variation diagram. Mineral X crystallized from liquid L_1 and the residual liquid follows the path to L_2. The distance from L_1 to L_2 will depend upon the amount of crystallization of mineral X.

This may be quantified as follows:

The amount of L_2 is proportional to the distance $X–L_1$
The amount of X is proportional to the distance $L_1–L_2$

Thus:

The percentage of $L_2 = 100 \times XL_1/XL_2$
Percentage of $X = 100 \times L_1L_2/XL_2$

This relationship is known as **the lever rule**.

If there are two or more minerals crystallizing simultaneously from liquid L_1 in such proportions that their average composition is C [Figure 3.19(b) and (c)], then the liquid path will move from C towards L_2. The proportion of solid to liquid will be given by the ratio L_1L_2:CL_1. The proportions of the minerals X and Y in Figure 3.19(b) is given by YC:XC. In the case of the variation diagrams shown above, the predicted trends are straight. However, this not always the case and minerals showing solid solution may produce curved trends during fractionation. This is more difficult to quantify.

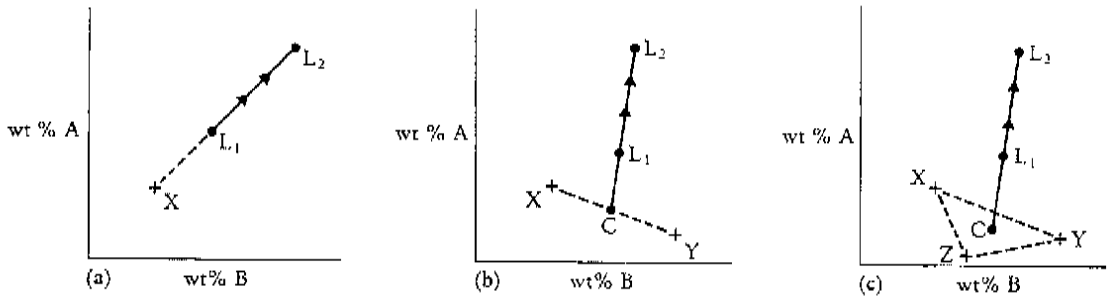

Figure 3.19 Bivariate plot showing extract calculations for crystal fractionation. (a) Mineral X is removed from liquid L_1 and the liquid composition moves from L_1 to L_2. (b) Mineral extract C (made up of minerals X and Y) is removed from liquid L_1 and drives the liquid composition to L_2. (c) Mineral extract C (made up of the minerals X, Y and Z) is removed from liquid L_1 and drives the resultant liquid composition to L_2.

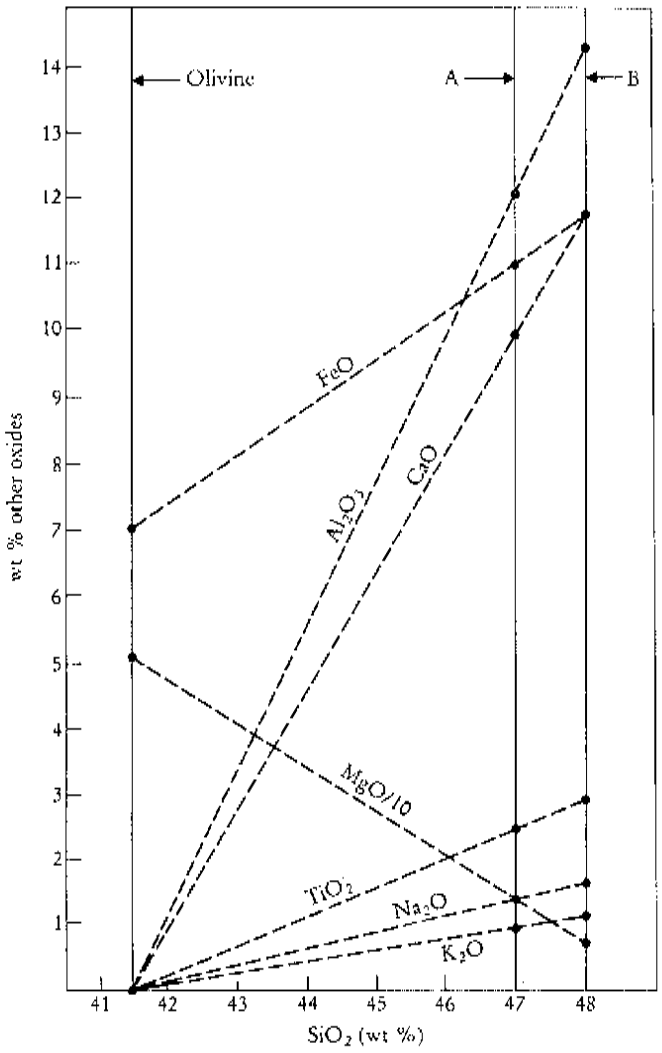

Figure 3.20 Addition–subtraction diagram for rocks A and B. The back-projection of trends for Al_2O_3, CaO, TiO_2, Na_2O and K_2O are reduced to zero and converge at SiO_2 41.5 %. MgO and FeO values at SiO_2 41.5 % indicate the composition of the olivine removed from rock A to produce composition B (after Cox *et al.*, 1979).

An extract calculation for a partial melting trend will not resolve into exact mineralogical constituents, whereas one based on a fractional crystallization trend should resolve exactly. Unfortunately these observations may not be as useful as they first appear, for Cox *et al.* (1979) point out that extract calculations are inexact when the minerals plotted show complex solid solution and that there are statistical uncertainties in fitting a straight line to a trend on a variation diagram. Thus in practice the differences between the effects of partial melting and fractional crystallization will be difficult to observe because of the imprecision of the method.

Addition–subtraction diagrams

An alternative approach to identifying the composition of the solid phase is to use an addition–subtraction diagram to calculate the composition of the phase(s). In this case, rather than just using two elements, the entire major element chemistry of two

or more rocks is used. The method is illustrated in Figure 3.20, in which the oxide concentrations of two rocks are plotted on a Harker diagram showing seven superimposed oxides. Back-projection shows that five of the elements converge and reduce to zero at 41.5 % SiO_2, consistent with olivine control. The composition of the olivine can be estimated from the diagram and a simple calculation shows that composition A can be converted to B by the removal of 15 % olivine. A similar explanation can be given to the data from Kilauea Iki lava lake in Figure 3.14.

In some volcanic rocks, particularly members of the calc–alkaline series, there may be a very large number of phenocrysts (olivine–clinopyroxene–biotite–plagioclase–K–feldspar–sphene–apatite–magnetite). In this case graphical methods may not easily produce a solution and the calculation is better handled by a computer. It is important to note, however, that there may not be a unique solution to more complex extract calculations. In andesites, for example, there is the ambiguity that the mineral assemblage (plagioclase–olivine or orthopyroxene–augite–magnetite) is chemically equivalent to hornblende (Gill, 1981).

Extract calculations may also be limited in their use if (1) the liquid line of descent is actually a mix of several lines; (2) solid solution changes the composition of the crystallizing phases during fractionation; (3) the phenocrysts present in magma are not representative of the fractionating phases.

Trends showing an inflection

Some variation diagrams show segmented trends. In this case the inflection is generally taken to indicate either the entry of a new phase during crystal fractionation or the loss of a phase during partial melting. Figure 3.21 shows a CaO–MgO variation diagram for Hawaiian lavas (Peterson and Moore, 1987). Below about 7 % MgO, CaO correlates positively with MgO, indicating the removal of CaO and MgO from the liquid in the coprecipitation of plagioclase and clinopyroxene. Above 7 % MgO, CaO and MgO correlate negatively because this part of the trend is controlled entirely by olivine. Inflections are not visible on all variation diagrams of a rock series and will only be apparent where the chemistry of the extract is reflected in the plotting parameters. However, when inflections are present they should be located at the same point in the rock series in each case. Inflections are most obvious where the number of fractionating minerals is small, such as in basaltic melts. In calc–alkaline volcanic rocks, where the number of fractionating minerals is large, the entry or exit of a single phase may not sufficiently affect the bulk chemistry of the melt to feature on a variation diagram.

Scattered trends

Variation diagrams sometimes show a cloud of data points rather than a neat linear trend. In the case of sedimentary rocks, this may be a function of the mixing processes leading to the formation of the sediment. In igneous rocks, however, where liquid–crystal equilibria are controlling compositions it is important to consider that some of the possible causes of scatter for this may throw further light on the processes. Similarly, in metamorphic rocks scattered trends may reflect the geochemical imprint of a metamorphic process on earlier igneous or sedimentary processes.

Some common reasons for scattered trends on varation diagrams for igneous rocks are:

(1) Not sampling liquid compositions. In highly porphyritic volcanic rocks much of the 'noise' in the data may be due to the accumulation of phenocrysts. In the case of many plutonic rocks it is very difficult to prove from field observations that the samples collected represent liquid compositions and in some cases it is highly improbable.

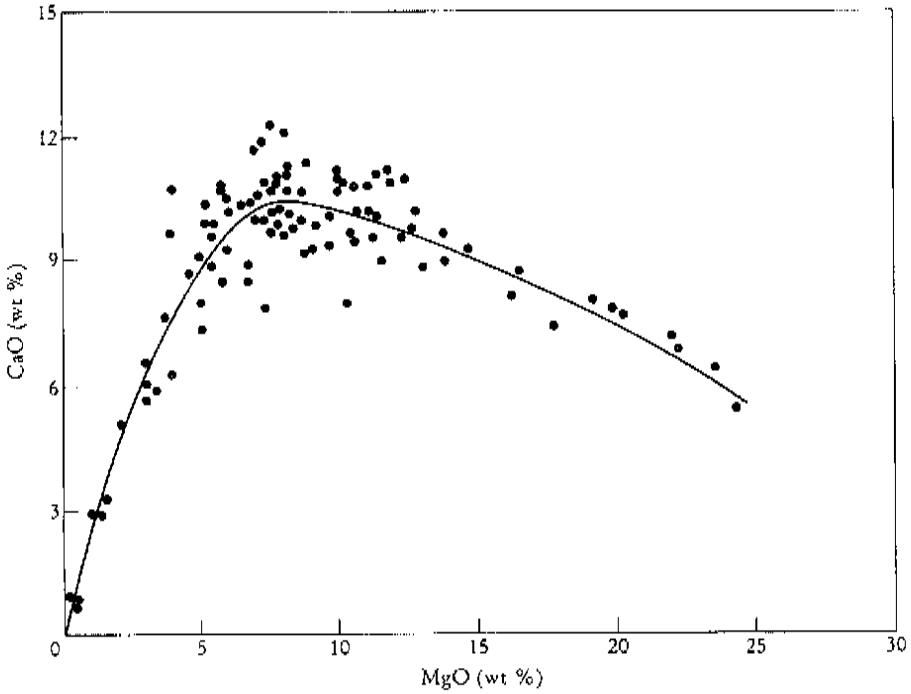

Figure 3.21 Bivariate plot of CaO vs MgO for basalts and related rocks from Hawaii. The change in slope at about MgO 7 % suggests a change in the fractionating phases at this point (after Peterson and Moore, 1987; courtesy of the US Geological Survey).

(2) The samples are not from a single magma. This can be true even for lavas from a single volcano.
(3) A changing fractionation assemblage during fractional crystallization.
(4) Sampling procedures; parameters such as sample size relative to the grain size of the rock, sample heterogeneity and the number of samples collected are all relevant in different contexts. The problem of sampling bias is well illustrated by Neilsen (1988), who emphasizes the necessity for detailed sampling if the process to be resolved takes place on a fine scale.
(5) Uncertainty in the analytical measurements. This may be due to the fact that analyses were made using different techniques or in different laboratories — both practices to be avoided if the data are to be plotted on the same diagram.

A computer-based approach to mixing calculations

There are a number of computer programs which can be used to interpret trends on variation diagrams and to solve mixing problems of the type described above. Fractional crystallization, for instance, may be expressed as:

rock A = rock B − (mineral X + mineral Y + mineral Z)

In this case a graphical solution will not yield a precise result whereas a computer-based, iterative mathematical procedure can estimate the proportions of the relative fractionating minerals. Similar formulations for mixing resulting from assimilation and partial melting may also be derived and these are equally amenable to computer solution.

Mixing programs of this type have been described by Stormer and Nicholls (1978) and Le Maitre (1981); these works include the computer source code in FORTRAN IV. Their aim is to minimize the difference between a measured rock composition and a composition calculated on the basis of a mixing hypothesis. The success of any model is estimated from the residuals of the calculation — the difference between the actual and calculated compositions. In Table 3.5 the results of a mixing calculation for the Columbia River basalts are presented (Wright, 1974). The hypothesis to be tested is whether the highly differentiated Umatilla 'basalt' is derived from the less evolved Lolo basalt. The differences between the calculated composition and the actual composition of the Lolo basalt, using the mixing program of Wright and Doherty (1970), suggest that the solution is acceptable. Examination of the residuals (the 'difference' in Table 3.5) confirms this, for they are small and the sum of the squares of the residuals is also very small.

Before accepting the results of such a calculation, however, they should be evaluated petrologically and the postulated fractionating phases (their relative proportions and their compositions) should be compared with the phenocrysts present in the lava suite. Where the rock has a complex history the mixing may be better formulated as a series of steps. Furthermore, it is important to stress that whilst a computer solution will produce a best-fit result, the result is not necessarily unique. Accordingly many workers seek to test mixing models initially proposed on the basis of major element chemistry with trace element data.

3.3.4 Modelling major element processes in igneous rocks

An alternative to the deductive use of variation diagrams in explaining petrological processes is an inverse approach in which the major element chemistry of an igneous suite is predicted from an initial starting composition. This type of major element modelling has been used chiefly to investigate fractional crystallization, although it also has other applications. The aim is to calculate, in a given silicate

Table 3.5 Differentiation of Columbia River basalt (Wright, 1974)

Lolo basalt = Umatilla basalt + olivine + augite + plagioclase + Fe–Ti oxides + apatite

	Proportion (%)	SiO_2	TiO_2	Al_2O_3	FeO	MnO	MgO	CaO	Na_2O	K_2O	P_2O_5
Umatilla basalt	44.76 %	54.94	2.64	13.87	12.58	0.22	2.70	6.27	3.24	2.60	1.02
Olivine	3.77 %	36.41	0.02	0.83	30.52	0.25	31.65	0.35	0.00	0.00	0.00
Augite	18.73 %	51.89	0.91	1.61	13.65	0.32	14.73	16.63	0.21	0.06	0.06
Plagioclase	25.16 %	54.57	0.00	28.95	0.00	0.00	0.00	11.16	5.14	0.21	0.00
Fe–Ti oxides	6.95 %	0.10	27.38	1.53	68.83	0.44	1.76	0.00	0.00	0.00	0.00
Apatite	0.67 %	0.00	0.00	0.00	0.00	0.00	0.00	56.00	0.00	0.00	44.00
Calculated composition		49.41	3.25	13.93	14.11	0.20	5.28	9.11	2.78	1.22	0.76
Lolo basalt		49.34	3.24	13.91	14.10	0.26	5.28	9.12	2.81	1.25	0.76
Difference (Lolo − calculated)		−0.07	−0.01	−0.02	−0.01	0.06	0.00	0.01	0.03	0.03	0.00
Sum of squares		0.011									

liquid, the nature of the first crystallizing phase, its composition and temperature of crystallization and the crystallization sequence of subsequent phases.

Three different approaches have been used. Firstly, the distribution of the major elements between mineral phases and a coexisting silicate melt may be calculated from experimental phase equilibrium data using regression techniques. Secondly, mineral–melt equilibria can be determined from mineral–melt distribution coefficients. A third, less empirical and more complex, approach is to use equilibrium thermodynamic models for magmatic systems. These require a thermodynamically valid mixing model for the liquid and an internally consistent set of solid–liquid thermochemical data.

The semi-empirical regression method was used by Nathan and Van Kirk (1978) to relate liquidus temperature to melt composition. From this relationship they were able to determine mineral compositions and the fractionating mineral assemblage at 1 atm pressure in both mafic and felsic liquids. Hostetler and Drake (1980) also used a regression technique but calculated solid–liquid distribution coefficients for eight major element oxides in the silicate melt. This permitted the calculation of phase equilibria for melts containing olivine, plagioclase and pyroxene from the melt composition but did not provide information on liquidus temperatures.

The alternative to the semi-empirical experimental approach to major element modelling is the thermodynamic modelling of silicate melts as described by Bottinga *et al.* (1981), Ghiorso (1985) and Ghiorso and Carmichael (1985). Ghiorso (1985) has developed an algorithm for chemical mass transfer in magmatic systems which predicts melt composition, mineral proportions and mineral compositions, and Ghiorso and Carmichael (1985) have demonstrated its usefulness when applied to fractional crystallization and assimilation in mafic melts at a range of pressures. Thermodynamic modelling, however, has an insatiable appetite for high-quality thermochemical data which do not exist for many minerals of interest in magmatic systems, thus severely limiting the applicability of this approach.

The chemical modelling of partial melting is even more difficult than the processes described above, for there is no general theory of melting which can cope with the multiphase, multicomponent nature of the Earth's crust and mantle at a range of pressures. Hanson and Langmuir (1978) and Langmuir and Hanson (1980) modelled basaltic systems from single-element and single-component mineral–melt distribution coefficients. These are combined with mass balance considerations and the stoichiometry of the mineral phases to calculate phase equilibria. Particularly interesting is their model for the partial melting of mantle pyrolite at 1 atmosphere pressure. Using the equations of Roeder and Emslie (1970) for the partitioning of magnesium and iron between olivine and melt, they calculated the abundances of MgO and FeO in the resultant melts and residual solids. These results are presented on an MgO–FeO cation % diagram which shows a field of melts and of residual solids, both contoured for percentage partial melting and temperature (Figure 3.22). Superimposed on the melt field are fractional crystallization trends for olivine in melts of differing composition. The diagram in Figure 3.22 cannot be used to define uniquely a partial melting trend from a given source, but it does delimit a field of permissible melts and for primary melt compositions can give information on the liquidus temperature and fraction of partial melting of the source. In addition, olivine fractional crystallization paths may be plotted for a given melt composition and the difference between equilibrium and fractional crystallization trends demonstrated (Langmuir and Hanson, 1980; Francis, 1985).

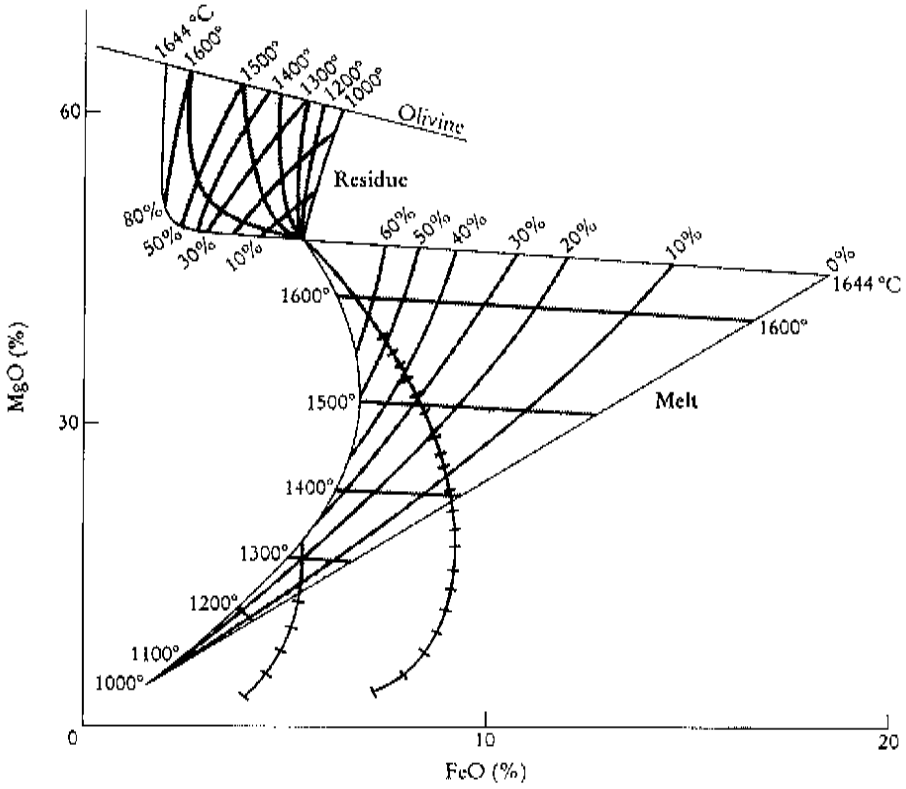

Figure 3.22 Fields of partial melt and residue, calibrated in liquidus temperature and percentage melting, for the partial melting of mantle pyrolite plotted on a FeO–MgO diagram expressed in cation mol % (calculated after the method of Hanson and Langmuir, 1978). The parent composition is where the two fields meet. The curved lines with small ticks show the trend of olivine fractional crystallization; the ticks are at 5 % intervals (from Langmuir and Hanson, 1980).

3.3.5 Discussion

Finally, it should be remembered that variation diagrams which utilize only the major elements have their limitations. Rarely can geological processes be uniquely identified from variation diagrams which use the major elements alone, and diagrams incorporating either trace elements or isotopes, as discussed in succeeding chapters, must also be employed.

3.4 Diagrams on which rock chemistry can be plotted together with experimentally determined phase boundaries

A number of igneous systems have been sufficiently well determined in the laboratory to allow the geochemist to interpret natural rock compositions in the

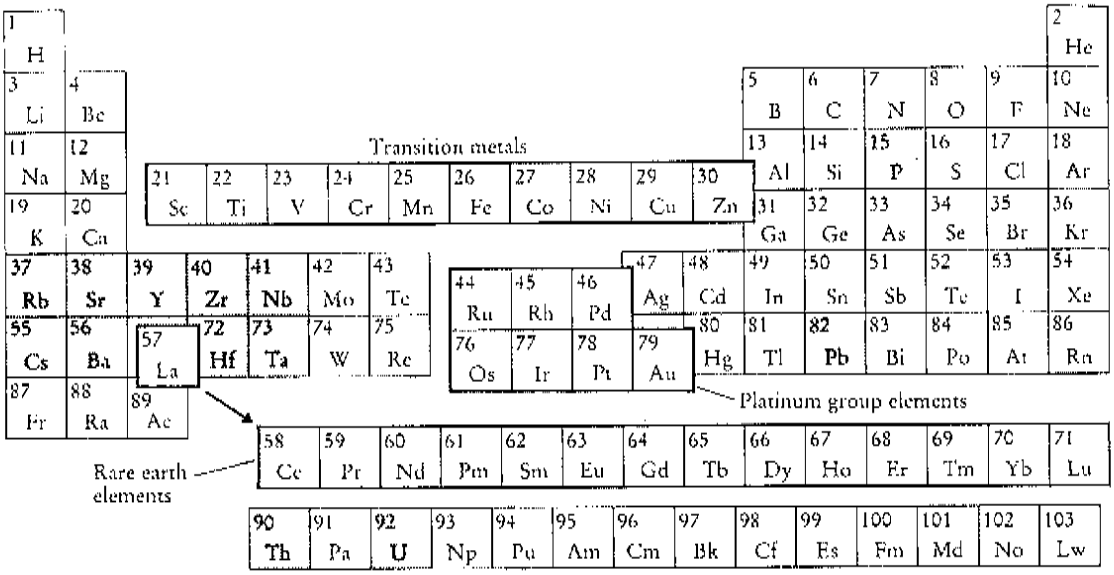

Figure 4.1 The periodic table of the elements, showing three main groups of trace elements, which are often treated together in geochemistry because of their relative positions in the table. These are the elements of the first transition series, the platinum group elements and the rare earth elements. The elements which are shaded are also important trace elements in geochemistry.

The elements in each of these respective groups have similar chemical properties and for this reason are expected to show similar geochemical behaviour. This is not always the case, however, because geological processes can take advantage of subtle chemical differences and fractionate elements of a group one from the other. Thus one of the tasks of trace element geochemistry is to discover which geological processes may have this effect and to quantify the extent of a particular process.

Trace element behaviour in magmatic systems

When the Earth's mantle is melted, trace elements display a preference either for the melt phase or the solid (mineral) phase. Trace elements whose preference is the mineral phase are described as **compatible**, whereas elements whose preference is the melt are described as **incompatible** — i.e. they are incompatible in the mineral structure and will leave at the first available opportunity. Incompatible elements have also been called **hygromagmatophile**, a term first introduced by Treuil and Varet (1973).

In detail there are degrees of compatibilty and incompatibility and trace elements will vary in their behaviour in melts of a different composition. For example, P is incompatible in a mantle mineralogy and during partial melting will be quickly concentrated in the melt. In granites, however, even though P is present as a trace element, it is compatible because it is accommodated in the structure of the minor phase apatite.

It is sometimes helpful to subdivide the incompatible elements on the basis of their charge/size ratio. This property is often described as field strength and may be thought of as the electrostatic charge per unit surface area of the cation. It is also described as the ionic potential of an element and is quantified as the ratio of the

valence to the ionic radius. Figure 4.2 shows a plot of ionic radius vs charge for most of the trace elements studied in geochemistry. Small highly charged cations are known as **high field strength (HFS)** cations (ionic potential > 2.0) and large cations of small charge are known as **low field strength** cations (ionic potential < 2.0). Low field strength cations are also known as **large ion lithophile elements (LILE)**. Elements with small ionic radius and a relatively low charge tend to be compatible. These include a number of the major elements and the transition metals. Figure 4.2 shows the main groupings of trace elements and highlights the similarity in ionic size and charge between some element groups. Elements with the same ionic charge and size are expected to show very similar geochemical behaviour.

High field strength cations include the lanthanides Sc and Y, and Th, U, Pb, Zr, Hf, Ti, Nb and Ta. The element pairs Hf and Zr, and Nb and Ta, are very similar in size and charge and show very similar geochemical behaviour. Low field strength, large ion lithophile cations include Cs, Rb, K and Ba. To these may be added Sr, divalent Eu and divalent Pb — three elements with almost identical ionic radii and charge.

4.2 Controls on trace element distribution

Most modern quantitative trace element geochemistry assumes that trace elements are present in a mineral in solid solution through substitution and that their concentrations can be described in terms of equilibrium thermodynamics. Trace elements may mix in either an ideal or a non-ideal way in their host mineral. Their very low concentrations, however, lead to relatively simple relationships between composition and activity. When mixing is ideal the relationship between activity and composition is given by **Raoult's Law**, i.e.

$$a_i = X_i \qquad [4.1]$$

where a_i is the activity of the trace element in the host mineral and X_i is its composition.

If the trace element interacts with the major components of the host mineral, the activity will depart from the ideal mixing relationship and at low concentrations the activity composition relations obey **Henry's Law**. This states that at equilibrium the activity of a trace element is directly proportional to its composition:

$$a_i^j = k_i^j X_i^j \qquad [4.2]$$

where k_i^j is the Henry's Law constant — a proportionality constant (or activity coefficient) for trace element i in mineral j. Henry's Law seems to apply to a wide range of trace element concentrations (Drake and Holloway, 1981) although at very low concentrations (< 10 ppm) there are deviations from Henry's Law behaviour (Harrison and Wood, 1980). Henry's Law also ceases to apply at very high concentrations, although the point at which this takes place cannot be easily predicted and must be determined for each individual system. In the case where trace elements form the essential structural constituent of a minor phase, such as Zr in zircon, Henry's Law behaviour does not strictly apply.

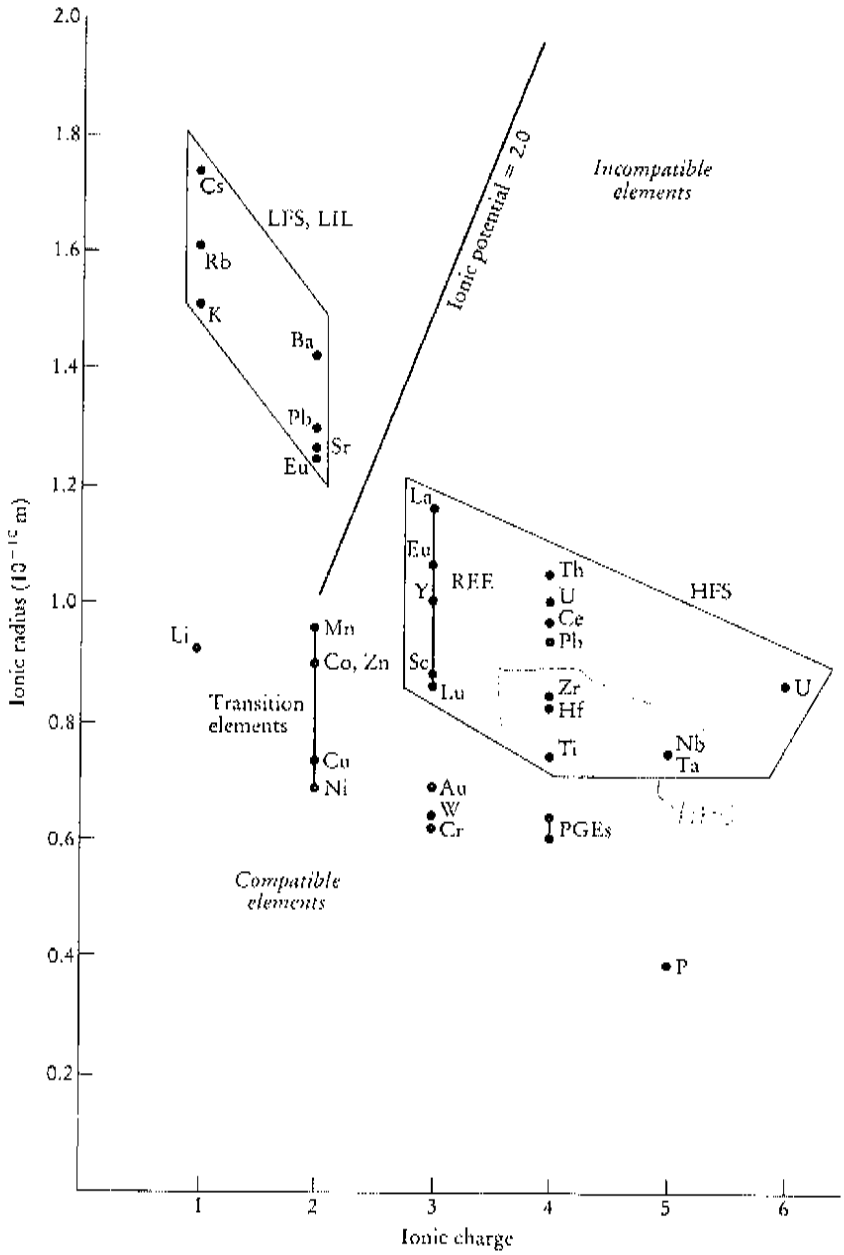

Figure 4.2 Plot of ionic radius vs ionic charge for trace elements of geological interest. An ionic potential (charge/size ratio) of 2.0 subdivides the incompatible elements into low field strength (LFS) elements, also known as large ion lithophile elements (LIL) and high field strength elements (HFS). Compatible elements are placed towards the bottom, left-hand corner of the diagram. The ionic radii are from Shannon (1976) and are quoted for eight-fold coordination to allow a comparison between elements. Some of the first transition series metals (transition elements) and the PGE elements, are quoted for six-fold coordination.

The relatively simple mixing relationships between trace elements and major elements in their host minerals mean that the distribution of trace elements between minerals and melt can be quantified in a simple way, as outlined below.

4.2.1 Partition coefficients

The distribution of trace elements between phases may be described by a **distribution coefficient** or **partition coefficient** (McIntire, 1963). The Nernst distribution coefficient is used extensively in trace element geochemistry and describes the equilibrium distribution of a trace element between a mineral and a melt. The Nernst distribution coefficient is defined by:

$$Kd = C^{\text{mineral}}_{\text{element}i} / C^{\text{melt}}_{\text{element}i} \qquad [4.3]$$

where Kd is the Nernst distribution coefficient, and C is the concentration of the trace element i in ppm or wt %. An example would be 500 ppm Sr in a plagioclase phenocryst and 125 ppm Sr in the glassy matrix of the lava giving a plagioclase/silicate melt Kd of 4 for Sr. The Nernst distribution coefficient as defined above includes the Henry's Law constants for trace element i in the mineral and in the melt and is a function of temperature, pressure and composition of the melt, but is controlled neither by the concentration of the trace element of interest nor by the concentration of other trace elements. Similar partition coefficients may be written for mineral–fluid or mineral–mineral distributions. A mineral/melt partition coefficient of 1.0 indicates that the element is equally distributed between the mineral and the melt. A value of greater than 1.0 implies that the trace element has a 'preference' for the mineral phase and in the mineral–melt system under investigation is a compatible element. A value of less than 1.0 implies that the trace element has a 'preference' for the melt and is an incompatible element.

An alternative mode of formulation of the partition coefficient (although not commonly used) is the **two-component partition coefficient**. This may be used when the trace element is replacing an identified major element in the host mineral. A good example would be Ni substitution for Mg in olivine. In this case the partition coefficient (K_D) is defined by the expression

$$K_D\,(i/j) = [X_i/X_j]^{\text{Solid}} / [X_i/X_j]^{\text{Liquid}} \qquad [4.4]$$

where i is the trace element and j is the element in the host mineral which is replaced by i, and X is concentration either in wt % or mol %.

Two-element partition coefficients have the advantage that they do not vary as extensively as single-element partition coefficients with changes in melt composition.

A **bulk partition coefficient** is a partition coefficient calculated for a rock for a specific element from the Nernst partition coefficients of the constituent minerals and weighted according to their proportions. It is defined by the expression

$$D_i = x_1 Kd_1 + x_2 Kd_2 + x_3 Kd_3 \ldots \qquad [4.5]$$

where D_i is the bulk partition coefficient for element i, and x_1 and Kd_1 etc. are the percentage proportion of mineral 1 in the rock and the Nernst partition coefficient for element i in mineral 1 respectively.

In a rock containing 50 % olivine, 30 % orthopyroxene and 20 % clinopyroxene, the bulk partition coefficient (D) for the trace element i would be

$$D_i = 0.5\ Kd_i^{\text{ol}} + 0.3\ Kd_i^{\text{opx}} + 0.2\ Kd_i^{\text{cpx}}$$

Measuring partition coefficients

Partition coefficients can be determined in natural systems from the analysis of minerals and their glassy matrix in rapidly cooled volcanic rocks. Provided sufficient care is given to obtaining a clean mineral separate from unzoned minerals and a sufficiently sensitive analytical technique is used, mineral/matrix or phenocryst/

matrix partition coefficients can be very reliable and are frequently used. Many of the early mineral/melt partition coefficient measurements are of this type (e.g. Philpotts and Schnetzler, 1970).

An alternative to using natural systems is to use experimental data in which synthetic or natural starting materials are doped with the element of interest. This approach has the advantage that variations in temperature and pressure can be more carefully monitored than in natural systems. However, it is important to attempt to establish Henry's Law behaviour when determining trace element partition coefficients, for this then allows the result to be extrapolated to other compositions and use to be made of the result in petrogenetic modelling (see e.g. Dunn, 1987). Irving (1978) gives an excellent review of experimental determinations of partition coefficients up until 1978.

Physical controls on the value of partition coefficients in mineral/melt systems

Many geochemistry texts contain compilations of mineral/melt partition coefficients for use in trace element modelling. However, great care must be taken in applying these data, for experimental studies have shown that the Nernst partition coefficient can vary extensively according to the temperature, pressure, composition and oxygen activity of the melt. Disentangling these separate effects in experimental studies and then taking full account of them in petrogenetic modelling can be a serious problem. In an elegant study based on a very large number of experiments, Green and Pearson (1986) showed how the partition coefficients for the REE in sphene vary according to temperature, pressure and rock composition (Figure 4.3). Their work illustrates how meaningless a single mean value for a partition coefficient can be, even when the melt composition has been specified. However, we are not always in the fortunate position of having as much information available as this and it is often necessary to 'make do' with the available data. Below we discuss the extent to which different variables may affect partition coefficients.

(a) Composition Without doubt, melt composition is the most important single factor controlling mineral/melt partition coefficients. This was demonstrated in studies by Watson (1976) and Ryerson and Hess (1978), who showed that elements partitioned between immiscible acid and basic melts show distinct preferences for one or other type of melt. It is for this reason that the partition coefficients listed in Tables 4.1 to 4.3 are grouped according to rock type and the silica content of the melt. The composition control of mineral/melt partition coefficients between the REE and hornblende is illustrated in Figure 4.4.

(b) Temperature A number of experimental studies show that partition coefficients are a function of temperature (Figure 4.3). For example, Dunn (1987) found that the partition coefficients for Lu between olivine and basalt, and Lu and Hf between clinopyroxene and basalt, all decrease with increasing temperature.

Sometimes unravelling the separate effects of temperature and composition can be difficult, especially where the liquidus temperature of a melt is a function of composition. Such is the problem with Ni partitioning between olivine and a basaltic melt. Two experimental studies, published at the same time, seem to show conflicting results. Leeman and Lindstrom (1978) showed that the prime control on the olivine partition coefficient for Ni in a natural basaltic melt was temperature whilst Hart and Davis (1978) showed that there is clear inverse correlation between the melt composition and partition coefficient. To resolve the apparent conflict

Table 4.1 Mineral/melt partition coefficients for basaltic and basaltic andesite liquids

	Olivine		Ortho-pyroxene	Clinopyroxene		Hornblende			Phlog-opite	Plagioclase			Garnet			Mag-netite	Sphene
Rb	0.0098		0.022	0.031		0.29			3.06	0.071			0.042				
Sr	0.0140		0.040	0.060		0.46			0.081	1.830			0.012				
Ba	0.0099		0.013	0.026		0.42			1.090	0.230			0.023				
K	0.0068		0.014	0.038		0.96				0.170			0.015				
(Ref)								(6)				(6)		(7)	(8)		
Y	0.010		0.18	0.900		1.00			0.03	0.030			9.00			0.20	
Ti	0.020		0.10	0.400		1.50			0.90	0.040			0.30			7.50	
Zr	0.012		0.18	0.100		0.50		1.5640	0.60	0.048		0.0121	0.65			0.10	
Hf	0.013			0.263		0.50		1.5335		0.051		0.0115	0.45	0.140	0.250	2.0–4.0	
Nb	0.010		0.15	0.005		0.80			1.00	0.010			0.02			0.40	4.65
Ta				0.013									0.06			1.0–10	13
Th				0.030		0.50				0.010							
U	0.002			0.040		0.10				0.010							
(Ref)	(1)	(2)	(1)	(1)	(2)	(3)	(4)	(6)	(1)	(1)	(2)	(6)	(1)	(7)	(8)	(5)	
La		0.0067			0.056		0.25	0.5442			0.190	0.1477		0.001	0.026	1.5–3.0	
Ce	0.0069	0.0060	0.02	0.15	0.092	0.20	0.32	0.8430	0.034	0.120	0.111	0.0815	0.03	0.007	0.051	1.3–3.0	
Pr																	
Nd	0.0066	0.0059	0.03	0.31	0.230	0.33		1.3395	0.032	0.081	0.090	0.0551	0.07	0.026		1.0 3.0	
Sm	0.0066	0.0070	0.05	0.50	0.445	0.52	1.40	1.8035	0.031	0.067	0.072	0.0394	0.29	0.102	0.600	1.1–2.2	
Eu	0.0068	0.0074	0.05	0.51	0.474	0.40	1.20	1.5565	0.030	0.340	0.443	1.1255	0.49	0.243	1.000	0.6–1.5	
Gd	0.0077	0.0100	0.09	0.61	0.556	0.63		2.0165	0.03	0.063	0.071	0.0310	0.97	0.680	2.100		
Tb					0.570		1.30							0.705		1.0–2.0	
Dy	0.0096	0.0130	0.15	0.68	0.582	0.64		2.0235	0.030	0.055	0.063	0.0228	3.17	1.940	4.100		
Ho														1.675	13.200		
Er	0.0110	0.0256	0.23	0.65	0.583	0.55		1.7400	0.034	0.063	0.057	0.0202	6.56	4.700			
Tm																1.0–2.0	
Yb	0.0140	0.0491	0.34	0.62	0.542	0.49	1.20	1.6420	0.042	0.067	0.056	0.0232	11.50	6.167	35.60	0.9–1.8	
Lu	0.0160	0.0454	0.42	0.56	0.506	0.43	1.10	1.5625	0.046	0.06	0.053	0.0187	11.90	6.950	41.00		
Ni	5.9–29		5	1.5–14		6.8										29.0	
Co	6.60		2–4	0.5–2.0		2.00							0.7–1.8	0.955	0.660	7.4	
V	0.06		0.6	1.35		3.40										26.0	
Cr	0.70		10	3+		12.5							0.6–2.9	1.345	0.060	153.0	
Sc	0.17		1.2	1.7–3.2		2.2–4.2								8.500	2.600		
Mn	1.45		1.4	0.3–1.2													

Data from compilation of Arth (1976); compilation of Pearce and Norry (1979); Green *et al.* (1989); Schock (1979); Fujimaki *et al.* (1984); Dostal *et al.* (1983); compilation of Henderson (1982); Leeman and Lindstrom (1978); Lindstrom and Weill (1978); Green and Pearson (1987). REE data: (1) compilation of Arth (1976); (2) Fujimaki *et al.* (1984); (3) basaltic compositions (Arth, 1976), Eu from Green and Pearson (1985a); (4) basaltic andesite (Dostal *et al.*, 1983); (5) Schock (1979); (6) mean of two basaltic andesites SiO_2 = 55 % and 57 % from Fujimaki *et al.* (1984); (7) mean of 2 basalts + 1 basanite + 1 alkali olivine basalt (Irving and Frey, 1978); (8) hawaiite (SiO_2 = 48.7 %) (Irving and Frey, 1978).

Table 4.2 Mineral/melt partition coefficients for andesitic liquids

	Olivine	Orthopyroxene			Clinopyroxene			Hornblende	Plagioclase				Garnet	Magnetite	Sphene
(Ref.)				(8)		(7)	(8)	(3,8)		(5)	(8)	(7)	(7)	(7)	(4)
Rb				0.022		0.020	0.013	0.040			0.053	0.070	0.010	0.010	
Sr				0.032		0.080	0.033	0.2–0.4		2.82	1.600	1.800		0.010	0.060
Ba				0.013		0.020	0.040	0.100		0.503	0.155	0.160		0.010	
K				0.014		0.020	0.011	0.33			0.117	0.110	0.010	0.010	
(Ref.)	(6,7)	(6)	(7)		(6)	(7)		(6,7)	(6)	(5)		(7)	(2,6)	(6,7)	(4)
Y	0.010	0.450			1.500			2.500	0.060	0.013			11.00	0.500	
Ti	0.03	0.250			0.400			3.00	0.050				0.500	9.000	
Zr	0.010	0.046	0.100		0.162	0.270		1.400	0.013			0.010	0.500	0.200	
Hf		0.051	0.100		0.173	0.250			0.015				0.570		
Nb	0.010	0.350			0.300			1.300	0.025					1.000	6.100
Ta															17.000
Th	0.010		0.050			0.010		0.150				0.010		0.100	
(Ref.)		(1)	(7)	(8)	(1)	(7)	(8)	(3)	(1)	(5)	(8)	(7)	(2)	(7)	(4)
La		0.031			0.047			0.500	0.302	0.228			0.076		2.00
Ce		0.028	0.050	0.030	0.084	0.250	0.508		0.221	0.136	0.186	0.200		0.200	
Pr															
Nd		0.028		0.047	0.183		0.645		0.149	0.115	0.143				
Sm		0.028	0.100	0.082	0.377	0.750	0.954	1.2–3.0	0.102	0.077	0.117	0.110	1.250	0.300	10.000
Eu		0.028	0.120	0.069		0.800	0.681		1.214	0.079	0.376	0.310	1.520	0.250	
Gd		0.039		0.132	0.583		1.350		0.067	0.056	0.050		5.200		
Tb													7.100		
Dy		0.076		0.212	0.774		1.460		0.050	0.045	0.126				
Ho								1.5–3.0					23.800		10.000
Er		0.153		0.314	0.708		1.330		0.045	0.040	0.034				
Tm															
Yb		0.254	0.460	0.438	0.633	0.900	1.300	1.2–2.1	0.041		0.029	0.050	53.000	0.250	
Lu		0.323		0.646	0.665				0.039	0.046	0.031		57.000		6.000
(Ref.)	(7)		(7)			(7)		(7)				(7)	(2,7)	(7)	
Ni	58.000		8.000			6.000		10.000				0.010	0.600	10.000	
Co			6.000			3.000		13.000				0.010	1.800	8.00	
V	0.080		1.100			1.100		32.000				0.010	8.000	30.000	
Cr	34.000		13.000			30.000		30.000				0.010	22.000	32.000	
Sc	0.300		3.000			3.000		10.000				0.010	3.900	2.000	

(1) Fujikami *et al.* (1984): sample No. 8.

(2) Irving and Frey (1978): andesite, SiO_2= 60.79 wt%.

(3) Green and Pearson (1985a): interpolated from Figure 3.

(4) REE: Green and Pearson (1983): at 7.5 kb; values increase with pressure. Nb,Ta: Green *et al.* (1989).

(5) Drake and Weill (1975): Eu value for Eu^{3+}.

(6) Pearce and Norry (1979): intermediate compositions.

(7) Compilation of Gill (1981): Zr in Cpx: Watson and Ryerson (1986).

(8) Philpotts and Schnetzler (1970): and Schnetzler and Philpotts (1970).

Table 4.3 Mineral/melt partition coefficients for dacitic and rhyolitic melts

	Orthopyroxene				Clinopyroxene				Hornblende		Biotite				Garnet	
(Ref.)	(2)	(3)	(4)	(7)	(2)	(3)	(4)	(7)	(1)	(2)	(1)	(2)	(3)	(4)	(1)	(5)
Rb	0.003				0.032					0.014	3.260	2.240	3.200	4.200	0.009	
Sr	0.009				0.516					0.022	0.120		0.447		0.015	
Ba	0.003		(1.10)		0.131		(1.40)			0.044	6.360	9.700	23.533	5.367	0.017	
K	0.002	0.605			0.037					0.081					0.200	
Cs													3.000	2.300		
Pb													0.767			
Y	1.000		<1.1		4.000		3.100			6.000		0.030	1.233		35.000	
Ti	0.400				0.700					7.000					1.200	
Zr	0.200			0.033	0.600			0.184	0.310	4.000			1.197		1.200	
Hf		0.200	(0.00)	0.031		0.633	(0.00)	0.247					0.703	0.600		3.300
Nb	0.800				0.800					4.000			6.367			
Ta		0.165	(1.14)			0.263	(0.75)						1.567	1.340		
Th		0.130	(6.53)			0.150	(5.99)						0.997	1.227		
U		0.145	(0.28)				(0.21)						0.773	0.167		
La		0.780	<0.4	0.015		1.110	0.600	0.015					5.713	3.180		0.390
Ce	0.150	0.930	<0.4	0.016	0.500	1.833	1.000	0.044	0.899	1.520	0.037	0.320	4.357	2.803	0.350	0.690
Pr																
Nd	0.220	1.250	<0.9	0.016	1.110	3.300	2.100	0.166	2.890	4.260	0.044	0.290	2.560	2.233	0.530	0.603
Sm	0.270	1.600	(7.87)	0.017	1.670	5.233	(10.65)	0.457	3.990	7.770	0.058	0.260	2.117	1.550	2.660	2.035
Eu	0.170	0.825	(2.85)		1.560	4.100	(5.00)	0.411	3.440	5.140	0.145	0.240	2.020	0.867	1.500	0.515
Gd	0.340			0.027	1.850			0.703	5.480	10.000	0.082	0.280			10.500	6.975
Tb		1.850	(5.50)			7.533	(9.25)						1.957	1.053		11.900
Dy	0.460	1.800	(3.85)	0.041	1.930	7.300	(8.90)	0.776	6.200	13.000	0.097	0.290	1.720	0.823	28.600	
Ho																28.050
Er	0.650			0.072	1.800			0.699	5.940	12.000	0.162	0.350			42.800	
Tm																
Yb	0.860	2.200	(2.35)	0.115	1.580	6.367	(4.55)	0.640	4.890	8.380	0.179	0.440	1.473	0.537	39.900	43.475
Lu	0.900	2.250	(2.70)	0.154	1.540	5.933	(4.30)	0.683	4.530	5.500	0.185	0.330	1.617	0.613	29.600	39.775
Ni																
Co			(140)				(72)							88.667		2.625
V																
Cr													19.650	5.233		3.700
Sc		18.000	(22.0)			53.000	(89.50)						13.633	15.567		15.950
Mn		45.500	(57.0)			32.667	(28.35)						124.530	10.367		

(1) Rb–K and REE: Arth (1976), dacites; Hbl Zr value from Watson and Harrison (1983).

(2) Rb–K and REE: Arth (1976), rhyolites. Y–Nb: Pearce and Norry (1979), acid magmas.

(3) Nash and Crecraft (1985), rhyolites — SiO_2 71.9–76.2 wt %.

(4) Mahood and Hildreth (1983), high-silica rhyolites — SiO_2 75–77.5 wt %. For pyroxenes, values in parentheses (Mahood & Hildreth, 1983); other values: Michael (1988).

(5) Irving and Frey (1978), dacites and rhyolites — SiO_2 62.89–70.15 wt %.

(6) Fujimaki (1986), dacites — SiO_2 63.21–64.86 wt %.

(7) Fujimaki *et al.* (1984), dacite No. 7 — SiO_2 70.81 wt %.

(8) Nb,Ta: Green and Pearson (1987), trachyte. REE interpolated from Figure 3 of Green *et al.* (1989).

(9) Brooks *et al.* (1981).

Magnetite	Ilmenite		Quartz	Plagioclase			K feldspar			Apatite		Zircon		Sphene	Allanite		
(2)	(3)	(3)	(3)	(1)	(2)	(3)	(2)	(3)	(4)	(2)	(6)	(4)	(6)	(8)	(4)	(9)	(Ref.)
			0.041	0.048	0.041	0.105	0.340	1.750	0.487								Rb
				2.840	4.400	15.633	3.870	5.400	3.760								Sr
			0.022	0.360	0.308	1.515	6.120	11.450	4.300								Ba
			0.013	0.263	0.100												K
			0.029			0.105		0.195	0.032			3.15					Cs
						0.972		2.473									Pb
2.000					0.100	0.130				40							Y
12.500			0.038		0.050					0.1							Ti
0.800					0.100	0.135		0.030		0.1	0.64						Zr
	1.883	3.100	0.030			0.148		0.033	0.017		0.73	3193.5	977.50		18.9		Hf
2.500					0.060					0.1				6.3			Nb
	3.167	106.000	0.008			0.035		0.010	0.019			47.50		16.5	3.1		Ta
	0.463	7.500	0.009			0.048		0.023	0.018			76.80			484.0	168.0	Th
	0.517	3.200	0.025			0.093		0.048	0.021			340.50			15.5	<6.7	U
	1.223	7.100	0.015			0.380		0.080	0.072		14.50	16.90	4.18	4.0	2594.5	820.0	La
	1.640	7.800	0.014	0.240	0.270	0.267	0.044	0.037	0.046	34.7	21.10	16.75	4.31		2278.5	635.0	Ce
																	Pr
	2.267	7.600	0.016	0.170	0.210	0.203	0.025	0.035	0.038	57.1	32.80	13.30	4.29		1620.0	463.0	Nd
	2.833	6.900	0.014	0.130	0.013	0.165	0.018	0.025	0.025	62.8	46.00	14.40	4.94	21.0	866.5	205.0	Sm
	1.013	2.500	0.056	2.110	2.150	5.417	1.130	4.450	2.600	30.4	25.50	16.00	3.31		111.0	81.0	Eu
				0.900	0.097	0.125	0.011			56.3	43.90	12.00	6.59			130.0	Gd
	3.267	6.500	0.017					0.025	0.033			37.00			273.0	71.0	Tb
	2.633	4.900	0.015	0.086	0.064	0.112	0.006	0.055	0.052	50.7	34.80	101.50	47.40		136.5		Dy
														19.0			Ho
				0.084	0.055		0.006			37.2	22.70	135.00	99.80				Er
																	Tm
	1.467	4.100	0.017	0.077	0.049	0.090	0.012	0.030	0.015	23.9	15.40	527.00	191.0		30.8	8.9	Yb
	1.203	3.600	0.014	0.062	0.046	0.092	0.006	0.033	0.031	20.2	13.80	641.50	264.5	10.0	33.0	7.7	Lu
																	Ni
									0.240			16.00			42.5		Co
																	V
	109.00	3.000										189.50			380.0		Cr
	10.633	5.900	0.012			0.053		0.023	0.040			68.65			55.9		Sc
	32.000	115.000	0.039			0.365			0.022			1.52			18.1		Mn

Leeman and Lindstrom (1978) formulated a complex partition coefficient that included the composition effect. They showed that Ni partitioning between olivine and basalt is temperature-dependent and concluded that, in this case, composition is less important than temperature in determining the partition coefficient.

(c) Pressure One of the most convincing demonstrations of the effect of pressure on partition coefficients is the work of Green and Pearson (1983, 1986) on the

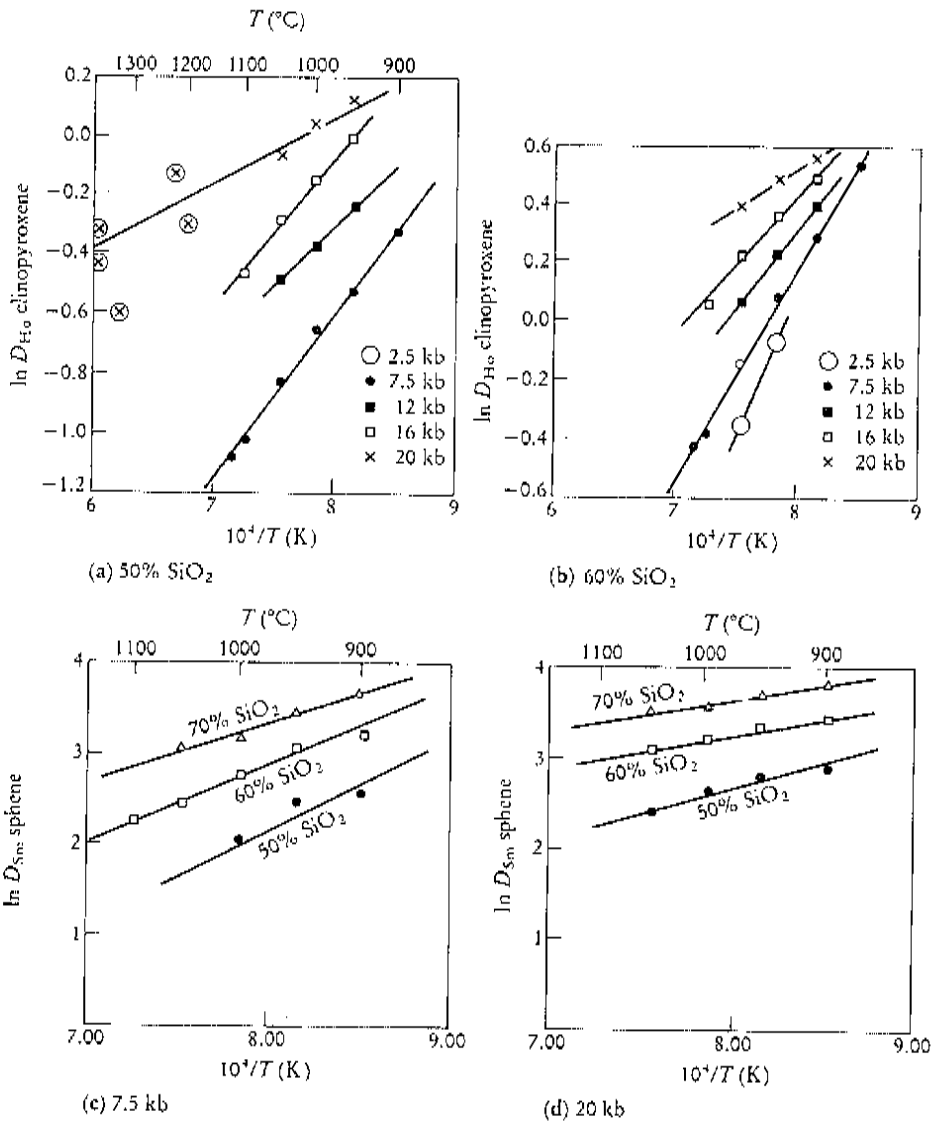

Figure 4.3 The combined effects of pressure, temperature and rock composition on a partition coefficient. (a) and (b) The partition coefficient for the REE Ho in clinopyroxene as a function of temperature, for pressures of 2.5, 7.5, 12, 16 and 20 kb in liquids with 50 wt % SiO_2 and 60 wt % SiO_2 (after Green and Pearson, 1985b). (c) and (d) The partition coefficient for Sm in sphene as a function of temperature for liquids with 50, 60 and 70 wt % SiO_2 at 7.5 kb and 20 kb pressure (after Green and Pearson, 1986). Both these diagrams may be used to interpolate a value for the partition coefficient for any pressure, temperature and composition within the experimental range. These values may then be extrapolated to other members of the REE series.

partitioning of REE between sphene and an intermediate silicic liquid. Within a small compositional range (56–61 wt % SiO_2) at 1000°C Green and Pearson showed that there is a measurable increase in partition coefficient with increasing pressure from 7.5 to 30 kb (Figure 4.5). One important aspect of this pressure effect is that

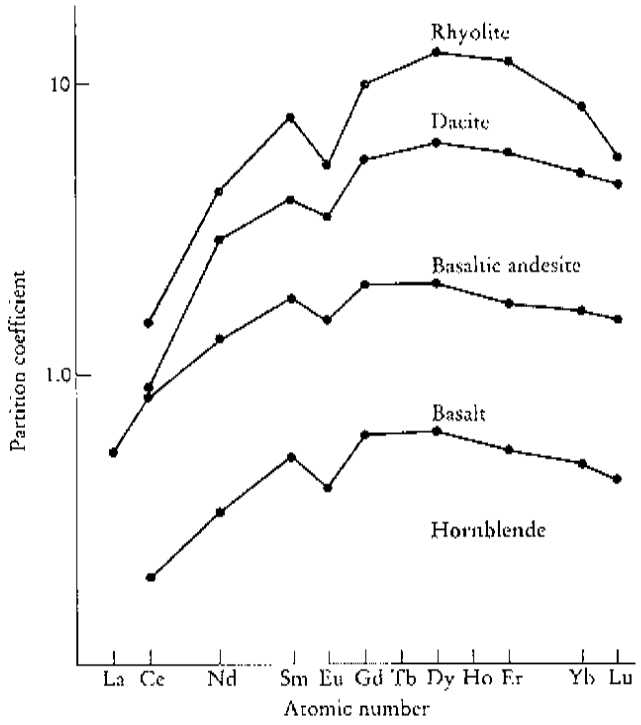

Figure 4.4 A plot of the partition coefficients for the rare earth elements between hornblende and melt (log scale) vs atomic number (normal scale) in basalt, basaltic andesite, dacite and rhyolite. There is a clear increase in partition coefficient with increasing silica content of the melt, amounting to an order of magnitude difference between basaltic and rhyolitic melts. Data from Tables 4.1 to 4.3.

high-level phenocryst/matrix pair partition coefficients may not be suitable for geochemical modelling of deep crustal and mantle processes. However, the effect of increased pressure and increased temperature are generally in an opposite sense and may to some extent cancel each other out.

(d) Oxygen activity The most widely quoted example of the control of oxygen activity on a partition coefficient is that of the partitioning of Eu^{2+} between plagioclase and a basaltic melt (Drake and Weill, 1975). There is an order of magnitude difference in the partition coefficient for Eu between atmospheric conditions and the relatively reducing conditions found in natural basalts (Figure 4.6). This is because europium forms Eu^{2+} at low oxygen activities and Eu^{3+} at high oxygen activities. Eu^{2+} and Eu^{3+} behave very differently in their partitioning between plagioclase and a basaltic melt, for Eu^{2+} is much more compatible than Eu^{3+} in plagioclase. Thus at low oxygen activities partition coefficients for Eu between plagioclase and basaltic melts are high (generally > 1.0) and anomalous relative to the other REE (Figure 4.6), whereas at high oxygen activities partition coefficients for Eu are low and Eu behaves in a similar way to the other REE.

(e) Crystal chemistry Onuma *et al.* (1968), Matsui *et al.* (1977) and Philpotts (1978) have shown that crystal structure exerts a major influence on trace element partitioning. Using a plot of partition coefficient (expressed as log to the base 10,

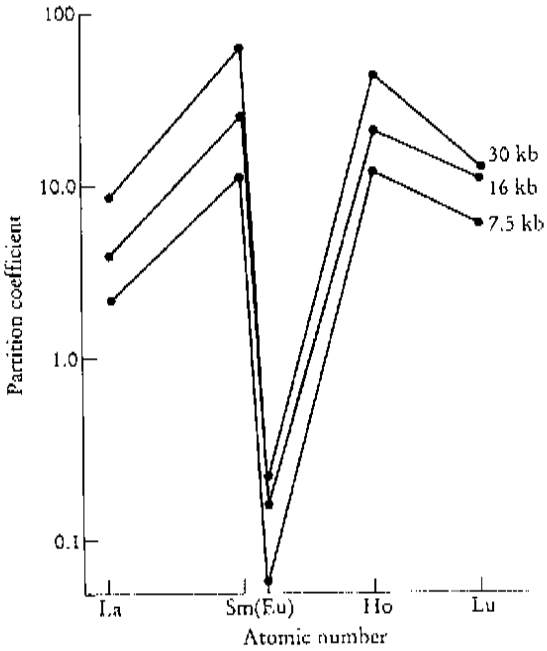

Figure 4.5 The partition coefficents for selected REE between sphene and a silicic melt of intermediate composition, plotted as a function of pressure. There is an increase in partition coefficient with increasing pressure in the range 7.5 to 30 kb (after Green and Pearson, 1983).

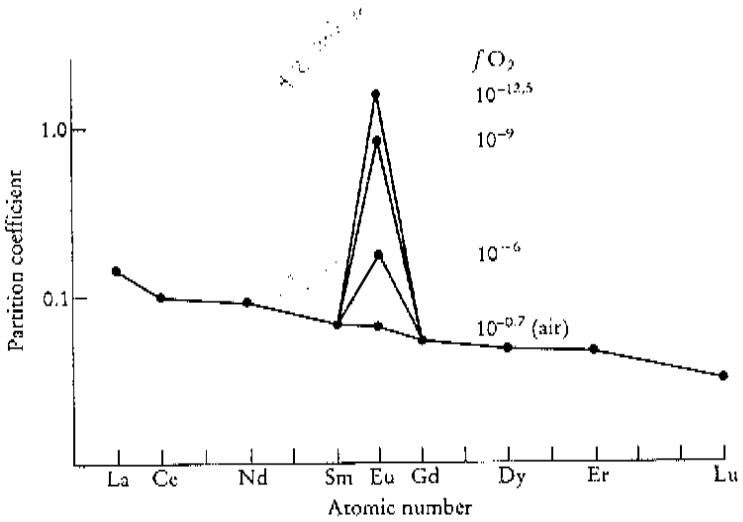

Figure 4.6 The partition coefficient for Eu between plagioclase and a basaltic melt plotted as function of oxygen activity (fO_2) compared with other REE (after Drake and Weill, 1975)

i.e. $\log_{10}$) vs ionic radius (in Ångstroms; 1 Å = 10^{-10} m), they showed that the partition coefficients of elements carrying the same ionic charge in the same mineral/melt system exhibit a smooth curve (Figure 4.7). Curves for different ionic charge tend to be parallel to each other for the same mineral/melt system. Such

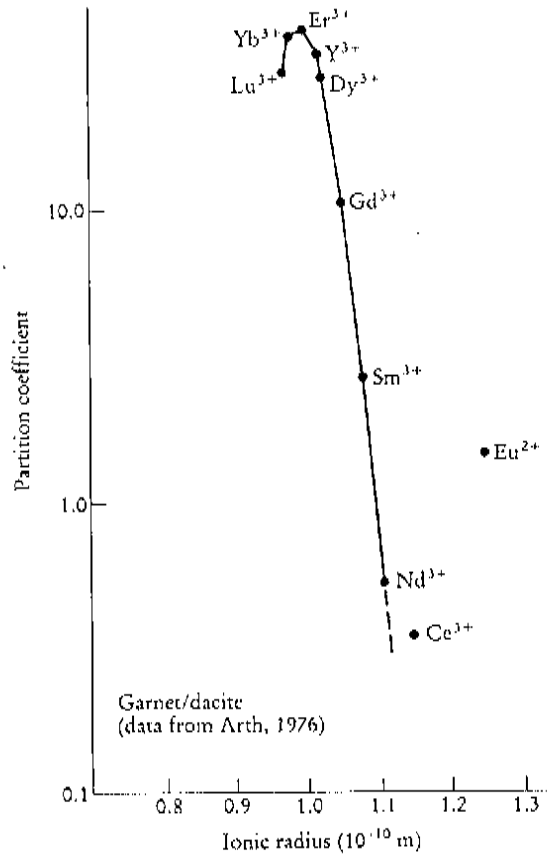

Figure 4.7 A plot of partition coefficient vs ionic radius (from Shannon, 1976) on an Onuma diagram, for the REE between garnet and dacite (data from Arth, 1976). The trivalent REE and Y (with the exception of Ce) define a smooth curve.

diagrams have become known as **Onuma diagrams**. Deviations from anticipated patterns may reveal controls on trace element partitioning other than those of the size and charge of the cation. Onuma diagrams can also be used to estimate the size of a distribution coefficient when measurements have been made for a similar element.

(f) Water content of the melt Few studies have been carried out to examine explicitly the effects of the water content of a melt on trace element partitioning behaviour. However, Green and Pearson (1986) showed that in the case of the partitioning of the REE between sphene and silicate liquids the water content of the melt (0.9–29 mol % water) has no significant effect on measured partition coefficients.

(g) Selecting a partition coefficient Clearly, the most important parameter controlling the partitioning of a trace element between a mineral and melt is the composition of the melt itself. Once this is established, a partition coefficient should be used whose pressure and temperature conditions of determination most closely match those of the system being investigated.

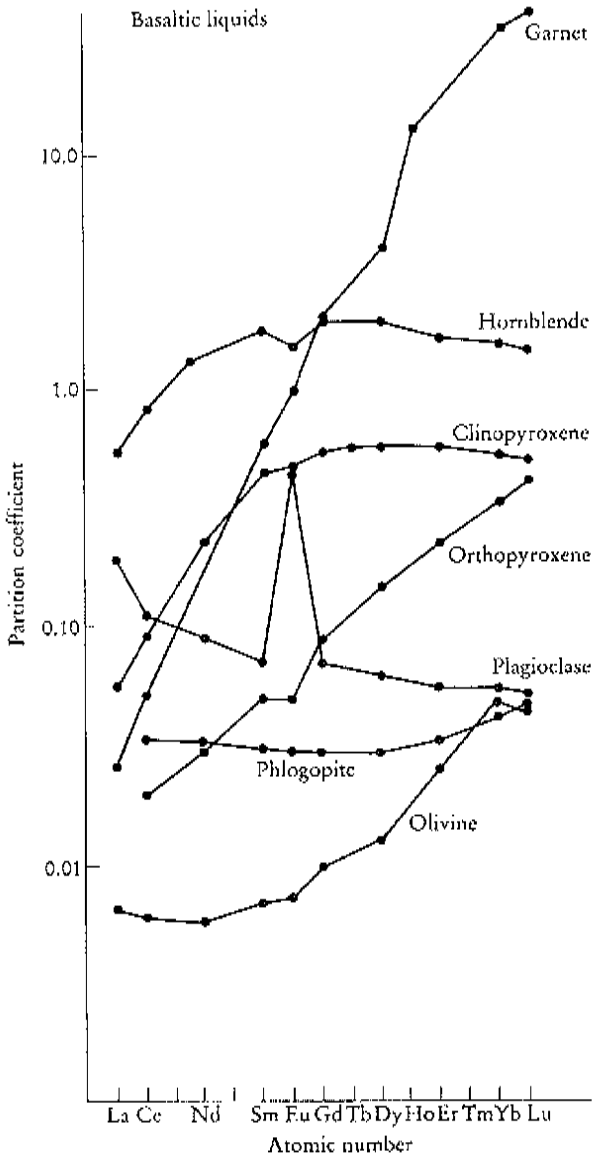

Figure 4.8 A plot of partition coefficient vs atomic number for the REE in common minerals in basaltic melts. Data from Table 4.1. (The hornblende data are for a basaltic andesite.)

Partition coefficients in basalts and basaltic andesites

In Table 4.1 partition coefficients are listed for trace elements in minerals in equilibrium with basaltic and basaltic andesite liquids. Following the TAS classification these are liquids with silica contents in the range 45–57 wt % . A summary of the REE partition coefficients is presented in Figure 4.8 as a plot of partition coefficient vs atomic number. The compilation in Table 4.1 is based upon a variety of published sources from experimental and phenocryst/matrix data. Averages are arithmetic means.

The several sets of REE data shown are generally in good agreement with each other. There is however a strong compositional effect on the *Kd* for the REE in

hornblende (Green and Pearson, 1985a) and so the differences in published values for basalts (Arth, 1976) and basaltic andesites (Dostal *et al.*, 1983; Fujimaki *et al.*, 1984) may reflect a real difference in the partition coeficients. There may be a similar explanation for the differences in partition coefficient in garnet.

Colson *et al.* (1988) in a detailed study of trace element partitioning between olivine and silicic melt, and orthopyroxene and silicic melt, have shown that many partition coefficients are strongly dependent upon temperature and melt composition. They show that these partition coefficients vary according to ionic size and they have modelled temperature and composition dependence as a function of these variables. On the basis of their equations it is possible to predict partition coefficients between olivine and melt, and orthopyroxene and melt, for a wide range of tri- and di-valent cations under a variety of magmatic conditions.

Partition coefficients in andesites

Table 4.2 lists partition coefficients for trace elements between a range of rock-forming minerals and andesitic liquids (57–63 wt % SiO_2 in the TAS classification). A summary of the REE values is given in Figure 4.9. Many published sources of partition coefficients treat andesites and basalts together and a comparison of Figures 4.1 and 4.2 shows that the partition coefficients for the REE are similar in basaltic and andesitic liquids. Values for garnet, the pyroxenes and the value for Eu in plagioclase, however, are higher in andesites than in basalts. REE partition coefficients for hornblende are higher in andesites than basalts, but are comparable between andesites and basaltic andesites. Values for the REE in the pyroxenes vary between published sources; this may in part be due to compositional effects.

Partition coefficients in dacites and rhyolites

The compilation in Table 4.3 compares partition coefficients from a number of published sources for dacites, rhyodacites, rhyolites and high-silica rhyolites. These are rocks which have > 63 wt % SiO_2 in the TAS classification. A summary of the REE values is presented in Figure 4.10.

A comparison between the REE in rhyolites and in basaltic and andesitic liquids (Figures 4.8 to 4.10) shows that values for pyroxenes and hornblende are an order of magnitude higher in the rhyolites and that these minerals now show a small but measurable negative europium anomaly. The values for the light REE in garnet are also higher and the Eu anomaly in plagioclase is much increased.

Partition coefficients for the REE in any one of the ferromagnesian minerals are variable. This may in part be a function of changing melt composition although there are a number of other possible explanations. Firstly, the presence of mineral inclusions gives rise to very high partition coefficients in rhyolites with very high silica contents (SiO_2 > 75 %). This may also account for some of the differences in the sets of values for biotite. Secondly, it is possible that the changing iron/magnesium ratio of ferromagnesian minerals may also explain differences in partition coefficients, although there are currently insufficient data with which to evaluate this possibility. In the case of pyroxenes the light REE values of Mahood and Hildreth (1983) are probably in error and the alternative values of Michael (1988) are used here. Values for the feldspars are in reasonable agreement between the different published results although the LIL elements Sr, Ba, Rb, Eu and Pb^{2+} show very erratic results in the original data-sets and this is still apparent in the mean values in this compilation. This may in part be a temperature effect (Irving, 1978; Long, 1978) but may also be compositionally controlled, for Long (1978)

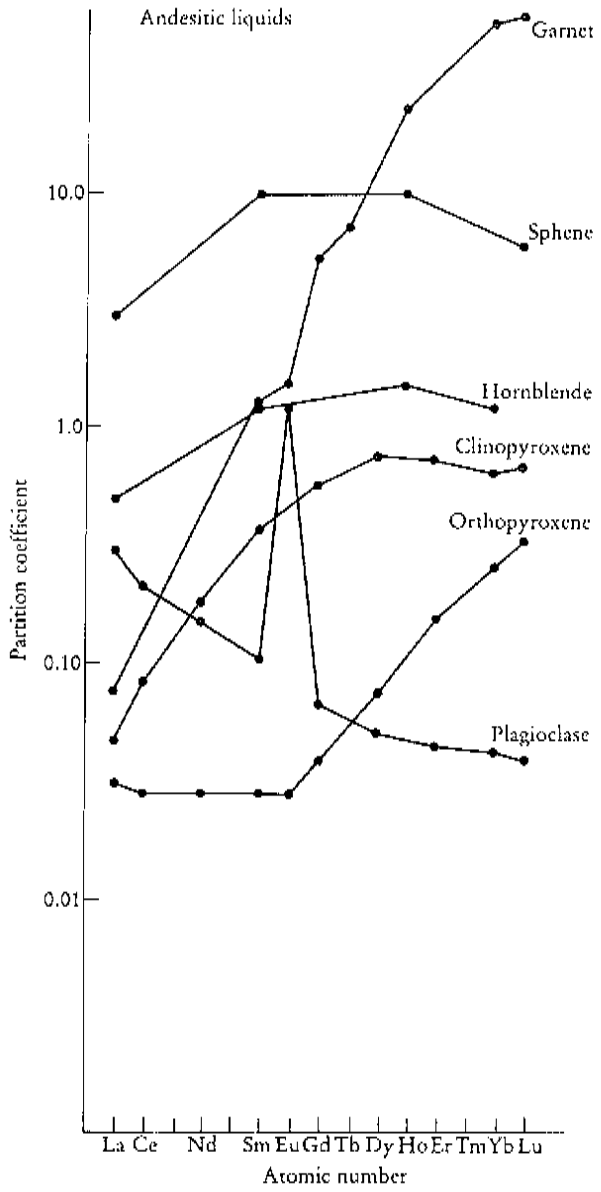

Figure 4.9 A plot of partition coefficient vs atomic number for the REE in common minerals in andesitic melts. Data from Table 4.2.

noted that the partitioning of Sr between alkali feldspar and a granitic melt is sensitive to the concentration of Ba in the melt. Partition coefficients for Eu in plagioclase increase with decreasing oxygen activity (Figure 4.6).

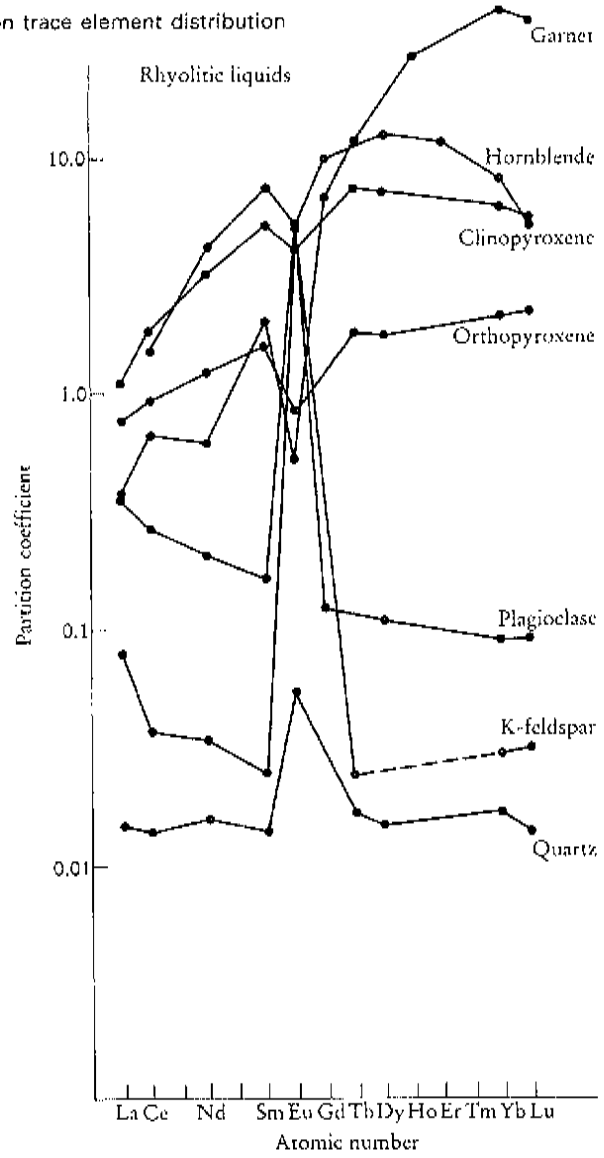

Figure 4.10 A plot of partition coefficient vs atomic number for the REE in common minerals in rhyolitic melts. Data from Table 4.3.

4.2.2 Geological controls on the distribution of trace elements

Clearly, a geochemical study of trace elements is only of use if we have some understanding of the way in which geological processes control their distribution. At present our knowledge is patchy, for some processes are well understood and there are mathematical models available to describe them. In these areas, principally those involving mineral/melt equilibria, trace element geochemistry has had a profound impact on geological thinking. Other areas, equally important but less amenable to the quantitative approach, are understood qualitatively. In this section we review a wide range of geological processes and discuss the way they control trace element distributions. Where there are appropriate mathematical models the equations are given and the terms used are defined in Box 4.1.

Box 4.1

Definition of terms used in equations for trace element partitioning between solid and melt (Section 4.2.2)

C_L	Weight concentration of a trace element in the liquid
$\bar{C}_L$	Average weight concentration of a trace element in a mixed melt
C_0	In partial melting, the weight concentration of a trace element in the original unmelted solid; in fractional crystallization, the weight concentration in the parental liquid
C_R	Weight concentration of a trace element in the residual solid during crystal fractionation
C_S	Weight concentration of a trace element in the residual solid after melt extraction
$_{ss}S_B$	Weight concentration of a trace element in a steady-state liquid after a large number of RTF cycles
C_A	Concentration of a trace element in the wallrock being assimilated during AFC processes
D_{RS}	Bulk distribution coefficient of the residual solids (see Eqn [4.5])
D_0	Bulk distribution coefficient of the original solids (see Eqn [4.5])
D	Bulk distribution coefficient of the fractionating assemblage during crystal fractionation
F	Weight fraction of melt produced in partial melting; in fractional crystallization, the fraction of melt remaining
f	Fraction of melt allocated to the solidification zone in *in situ* crystallization which is returned to the magma chamber
f'	A function of F, the fraction of melt remaining in AFC processes
Kd	Mineral/melt partition coefficient
M_L	Mass of the liquid in *in situ* crystallization
M_0	Total mass of the magma chamber *in situ* crystallization
n	Number of rock volumes processed during zone refining
P	Bulk distribution coefficient of minerals which make up a melt (see Eqn [4.9])
r	Ratio of the assimilation rate to the fractionation rate in AFC processes
x	Mass fraction of the liquid crystallized in each RTF cycle
y	Mass fraction of the liquid escaping in each RTF cycle

Element mobility

Any suite of rocks which has been subjected to hydrothermal alteration or metamorphism is likely to suffer element mobility. It is essential, therefore, in any trace element study to demonstrate first that element concentrations are undisturbed and original before inferences can be made about the petrogenesis of the rock group.

Trace element mobility is controlled by the mineralogical changes which take place during alteration and the nature of the fluid phase. As a generalization, incompatible elements which belong to the LFS group (Cs, Sr, K, Rb, Ba — Figure 4.2) are mobile, whereas the HFS elements are immobile. This latter group includes the REE, Sc, Y, Th, Zr, Hf, Ti, Nb, Ta and P (Pearce, 1983). In addition the transition metals Mn, Zn and Cu tend to be mobile, particularly at high temperatures (see Seewald and Seyfried, 1990), whilst Co, Ni, V and Cr are immobile. Such generalizations are normally valid, although many exceptions are documented. This may be illustrated with reference to the traditionally immobile REE. Humphries (1984) shows that there is no simple relationship between the degree of mobility of the REE and rock type or metamorphic grade, and emphasizes

the mineralogical and fluid controls. For example, the REE may be more easily released from a glassy basalt during alteration than from a rock with the same composition but which is crystalline. Again the REE may be mobilized by halogen-rich or carbonate-rich mineralizing fluids in a rock in which they would otherwise be stable with respect to the movement of an aqueous fluid.

A special case of trace element mobilization is in the dehydration of subducted ocean floor, a process thought to be pertinent to the generation of calc-alkali magmas. Pearce (1983) has suggested that the elements Sr, K, Rb, Ba, Th, Ce, P and Sm may be mobile in such circumstances.

Partial melting

Two types of partial melting process are commonly described in the geological literature and represent end-member models of natural processes. **Batch melting**, also known as equilibrium fusion and equilibrium partial melting, describes the formation of a partial melt in which the melt is continually reacting and re-equilibrating with the solid residue at the site of melting until mechanical conditions allow it to escape as a single 'batch' of magma. In **fractional melting**, also known as Rayleigh melting, only a small amount of liquid is produced and instantly isolated from the source. Equilibrium is therefore only achieved between the melt and the surfaces of mineral grains in the source region.

Which partial melting process is appropriate in a particular situation depends upon the ability of a magma to segregate from its source region, which in turn depends upon the permeability threshold of the source. The problem is discussed in some detail by Wilson (1989). Fractional melting may be an appropriate model for some basaltic melts, for recent physical models of melt extraction from the mantle indicate that very small melt fractions can be removed from their source region (McKenzie, 1985; O'Nions and McKenzie, 1988). More viscous, felsic melts have a higher permeability threshold and probably behave according to the batch melting equation. It is worth noting in passing that physical models of melt extraction describe melt fractions in terms of their *volume* whereas chemical models describe melt fractions in terms of their *mass*.

(a) Batch melting The concentration of a trace element in the melt C_L is related to its concentration in the unmelted source C_0 by the expression

$$C_L/C_0 = 1/[D_{RS} + F(1 - D_{RS})] \quad [4.6]$$

and the concentration of a trace element in the unmelted residue C_S relative to the unmelted source C_0 is

$$C_S/C_0 = D_{RS}/[D_{RS} + F(1 - D_{RS})] \quad [4.7]$$

where D_{RS} is the bulk partition coefficient (see Eqn [4.5]) of the **residual solid** and F is the weight fraction of melt produced. It should be noted that the bulk partition coefficient is calculated for the residual solids present at the instant the liquid is removed, so that solid phases that were present but are now melted out do not influence the trace element concentration in the liquid (Hanson, 1978). This formulation of the batch melting equation is very straightforward to use. If, however, a more complex formulation is sought, then the batch melting equation is

expressed in terms of the original mineralogy of the source and the relative contributions each phase makes to the melt:

$$C_L/C_0 = 1/[D_0 + F(1 - P)] \quad [4.8]$$

where D_0 is the bulk distribution coefficient at the onset of melting and P is the bulk distribution coefficient of the minerals which make up the melt. P is calculated from

$$P = p_1\ Kd_1 + p_2\ Kd_2 + p_3\ Kd_3 + \ldots \quad [4.9]$$

where p_1 etc. is the normative weight fraction of mineral 1 in the melt and Kd_1 is the mineral–melt distribution coefficient for a given trace element for mineral 1.

In the case of modal melting (i.e. where the minerals contribute to the melt in proportion to their concentration in the rock), Eqn [4.8], simplifies to

$$C_L/C_0 = 1/[D_0 + F(1 - D_0)] \ldots \quad [4.10]$$

Even more complex formulations, which allow a phase to be consumed during melting, melt proportions to vary during partial melting and variations in partition coefficients, are given by Hertogen and Gijbels (1976) and Apted and Roy (1981).

Taking the simple case where D is calculated for the unmelted residue Eqn [4.6], the degree of enrichment or depletion relative to the original liquid (C_L/C_0) for different values of F is illustrated in Figure 4.11(a) for seven different values of D, the bulk distribution coefficient. When D is small, expression [4.6] reduces to $1/F$ and marks the limit to trace element enrichment for any given degree of batch melting (see shaded area on Figure 4.11a). When F is small, Eqn [4.6] reduces to $1/D$ and marks the maximum possible enrichment of an incompatible element and the maximum depletion of a compatible element relative to the original source. Small degrees of melting can cause significant changes in the ratio of two incompatible elements where one has a bulk partition coefficient of, say, 0.1 and the other 0.01, but at smaller values of D (0.01–0.0001) the discrimination is not possible.

Enrichment and depletion in the solid residue in equilibrium with the melt (Eqn [4.7]) is shown in Figure 4.11(b) for different values of F and D. Even small degrees of melting will deplete the residue significantly in incompatible elements. Compatible elements, however, at small degrees of melting remain very close to their initial concentrations. Cox *et al.* (1979) used this relationship to estimate the average content of compatible elements such as Ni and Cr in the upper mantle from the composition of ultramafic nodules from which a melt may have already been extracted.

(b) Fractional melting There are two versions of the fractional melting equation. One considers the formation of only a single melt increment whilst the other considers the aggregated liquid formed by the collection of a large number of small melt increments. If it is assumed that during fractional melting the mineral phases enter the melt in the proportions in which they are present in the source, then the concentration of a trace element in the liquid relative to the parent rock *for a given melt increment* is given by the expression

$$C_L/C_0 = \frac{1}{D_0}(1 - F)^{(1/D_0 - 1)} \quad [4.11]$$

where F is the fraction of melt already removed from the source and D_0 is the bulk

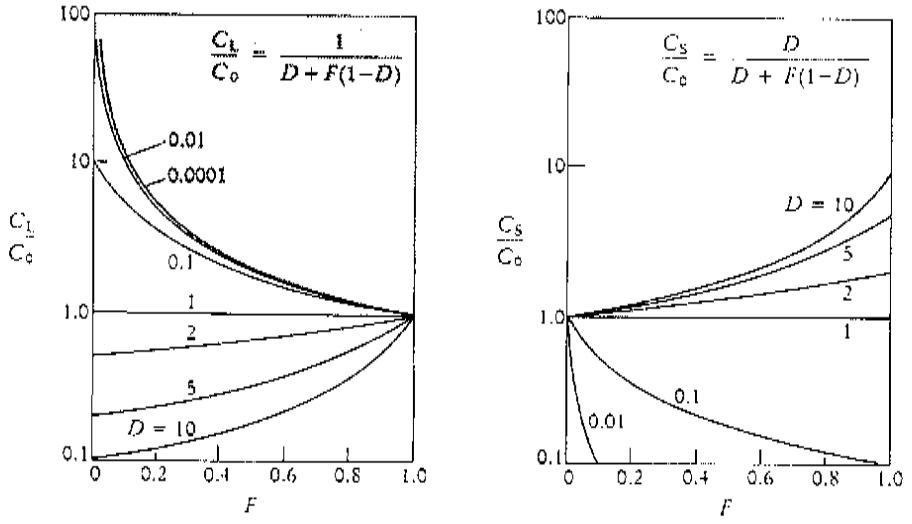

(a) Batch melting—liquids (b) Batch melting—residue

Figure 4.11 (a) The enrichment of a trace element in a partial melt relative to its concentration in the source (C_L/C_0) during batch partial melting with changing degrees of melting (F). The numbered curves are for different values of the bulk partition coefficient D. At small degrees of melting, compatible elements are greatly depleted relative to the source whereas incompatible elements are greatly enriched to a maximum of $1/F$. The shaded region is the area in which enrichment is impossible. (b) Enrichment and depletion of a trace element in the residue relative to the original source (C_S/C_0) with changing degrees of melting (F) for different values of bulk partition coefficient (D).

partition coefficient for the original solid phases prior to the onset of melting. The equation for the residual solid is

$$C_S/C_0 = (1 - F)^{(1/D_0 - 1)} \qquad [4.12]$$

The general expressions for the more probable case where minerals do not enter the melt in their modal proportions are given by

$$C_L/C_0 = \frac{1}{D_0}(1 - PF/D_0)^{(1/P-1)} \qquad [4.13]$$

and

$$C_S/C_0 = \frac{1}{(1 - F)}(1 - PF/D_0)^{1/P} \qquad [4.14]$$

where P is the bulk distribution coefficient of the minerals which make up the melt and is calculated from Eqn [4.9].

The variation in trace element concentrations relative to the original liquid (C_L/C_0) during fractional melting for a single melt increment at different degrees of melting and for different values of D is shown for modal melting (Eqn [4.11]) in Figure 4.12(a). An enlargement of the region of interest (F = 0–0.1) is given in Figure 4.12(c). In the range 0–10 % melting, the changes in element concentrations relative to the original source are more extreme than in batch melting, although the limiting value of 1/D is the same.

Trace element concentrations in the original solid, momentarily in equilibrium with the liquid (Eqn [4.12]) are shown for small melt fractions in Figure 4.12(d). Incompatible elements are even more strongly depleted than in batch melting although compatible element concentrations are unchanged relative to the source.

Where *several melt increments have collected together* the general expression is

$$\bar{C}_L/C_0 = \frac{1}{F}\left[1 - (1 - PF/D_0)^{1/P}\right] \qquad [4.15]$$

where $\bar{C}_L$ is the averaged concentration of a trace element in a mixed melt. In the case of modal melting Eqn [4.15] simplifies to

$$\bar{C}_L/C_0 = \frac{1}{F}\left[1 - (1 - F)^{1/D_0}\right] \qquad [4.16]$$

The numerical consequences of fractional melting where the melt increments are collected together in a common reservoir are illustrated in Figure 4.12(b). This type of fractional melting is indistinguishable from batch melting except for compatible elements at very large degrees of melting (cf. Figure 4.11a).

Crystal fractionation

Three types of fractional crystallization are considered here — equilibrium crystallization, Rayleigh fractionation and *in situ* crystallization.

(a) Equilibrium crystallization The process of equilibrium crystallization describes complete equilibrium between all solid phases and the melt during crystallization. This is not thought to be a common process although the presence of unzoned crystals in some mafic rocks suggests that it may be applicable on a local scale in some mafic magmas. The distribution of trace elements during equilibrium crystallization is the reverse of equilibrium melting (page 121), and the equation therefore is

$$C_L/C_0 = 1/[D + F(1 - D)] \qquad [4.17]$$

In this case C_0 is redefined as the initial concentration of a trace element in the primary magma, F is the fraction of melt remaining and D is the bulk partition coefficient of the fractionating assemblage. The enrichment and depletion of trace elements relative to the orginal liquid may be deduced from Figure 4.11(a), the batch melting diagram, but in this case the diagram should be read from right to left.

(b) Fractional crystallization/Rayleigh fractionation More commonly crystals are thought to be removed from the site of formation after crystallization and the distribution of trace elements is not an equilibrium process. At best, surface equilibrium may be attained. Thus, fractional crystallization is better described by the Rayleigh Law. Rayleigh fractionation describes the extreme case where crystals are effectively removed from the melt the instant they have formed. The equation for Rayleigh fractionation is

$$C_L/C_0 = F^{(D-1)} \qquad [4.18]$$

and the equation for the enrichment of a trace element relative to the original liquid in the crystals as they crystallize (the instantaneous solid) C_R is given by

$$C_R/C_0 = DF^{(D-1)} \qquad [4.19]$$

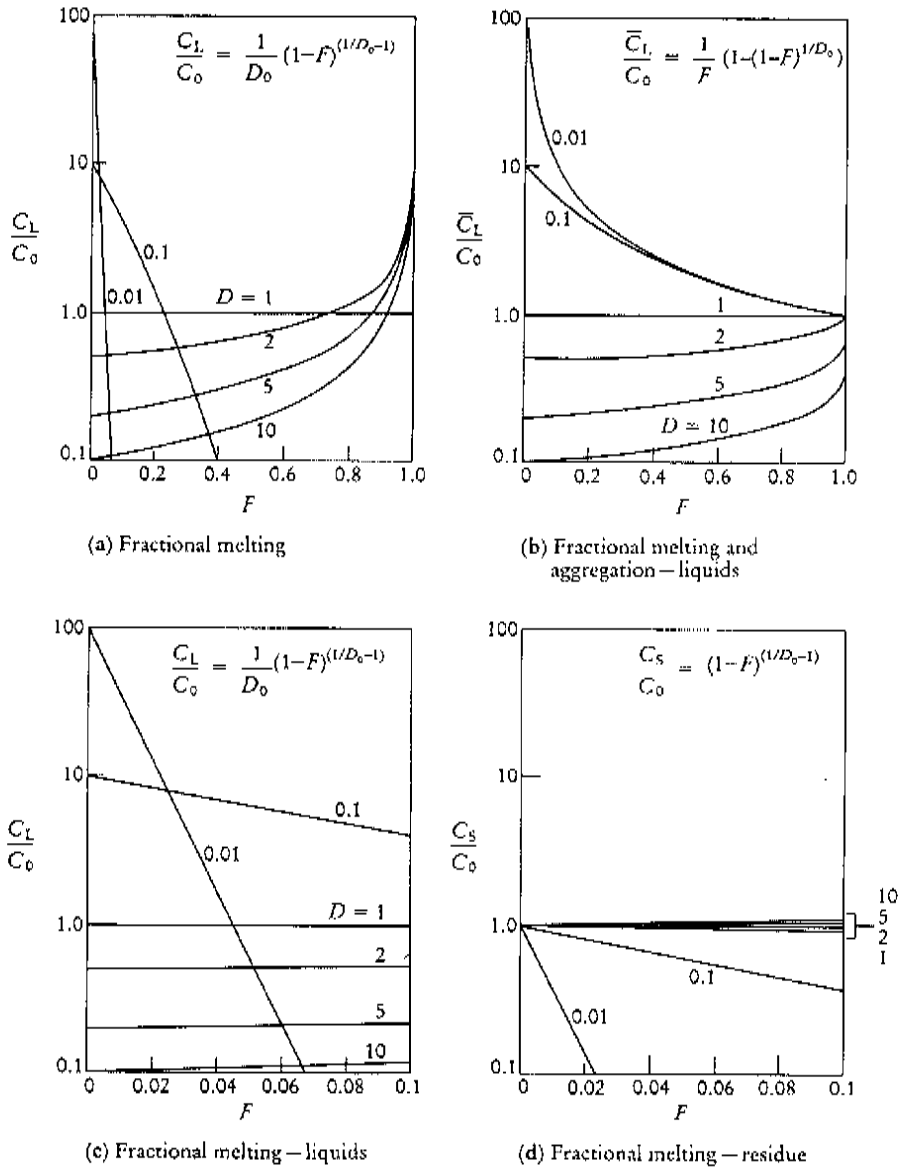

Figure 4.12 (a) The enrichment of a trace element in a melt relative to its source (C_L/C_0) as a function of the fraction of melting (F), during fractional melting for different values of bulk partition coefficient (D). During fractional melting only a very small melt fraction is produced and it is instantly removed from the source. (b) The enrichment of a trace element in a melt relative to its source ($\bar{C}_L/C_0$) as a function of fraction of melting (F) and bulk partition coefficient (D) during fractional melting. In this case small melt fractions are removed instantly from the source but aggregate together. This process produces very similar results to that of batch melting. (c) An enlargement of (a) between values of F of 0 and 0.1. (d) The enrichment of a trace element in the residual solid relative to the concentration in the original source (C_s/C_0) as a function of F between values of 0 and 0.1.

The equation for the mean enrichment of a trace element in the cumulate relative to the original liquid, i.e. the total residual solid C_R, is

$$C_R/C_0 = (1 - F)^{(D-1)} \qquad [4.20]$$

Rayleigh fractionation is illustrated in Figure 4.13(a), which shows the concentration of a trace element relative to its initial concentration in the liquid at differing values of F – the proportion of liquid remaining — for different values of D. For incompatible elements there is little difference between Rayleigh fractionation and equilibrium crystallization until more than about 75 % of the magma has crystallized, at which point the efficient separation of crystals and liquid becomes physically difficult. The limiting case for incompatible elements is where $D=0$, in which case $C_L/C_O = 1/F$, the same as for equilibrium crystallization. It is therefore impossible to enrich a liquid beyond this point by fractional crystallization. Rayleigh fractionation is less effective than batch melting in changing the ratio of two incompatible elements, for the curves for 0.1 and 0.01 are very close together (Figure 4.13a). Compatible elements are removed from the melt more rapidly than in the case of equilibrium crystallization.

The concentration of trace elements in the instantaneous solid residue of Rayleigh fractionation is illustrated in Figure 4.13(b). More relevant, however, is

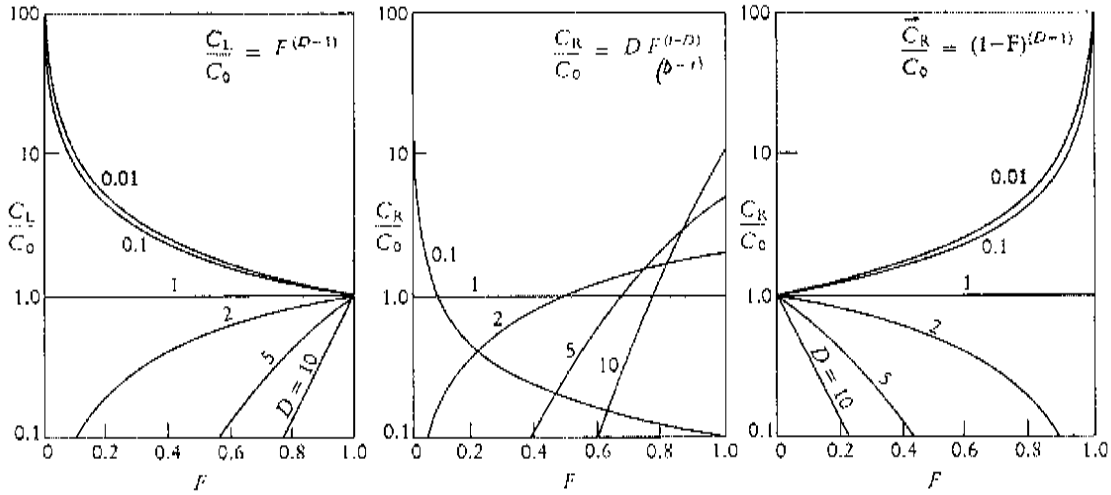

(a) Rayleigh fractionation — liquids

(b) Rayleigh fractionation — residue, instantaneous solid

(c) Rayleigh fractionation — residue, mean concentration in cumulate

Figure 4.13 (a) The enrichment of a trace element in a melt relative to its concentration in the parental melt (C_L/C_0) as a function of the fraction of remaining liquid (F) during Rayleigh fractionation for different values of bulk partition coefficient (D). The limiting value of C_L/C_0 is $1/F$ and the shaded area is the region of impossible values. (b) The enrichment of a trace element in the instantaneous solid, i.e. the solid which is produced and then immediately removed during crystal fractionation, relative to the parental liquid (C_R/C_0) as a function of the fraction of remaining liquid and bulk partition coefficient. (c) The enrichment of a trace element in the residue, i.e. the mean concentration in the cumulate, relative to the parental liquid (C_R/C_0) as a function of the fraction of remaining liquid and bulk partition coefficient (D). Diagrams (a) to (c) are read from right to left, as the value of F decreases with fractional crystallization.

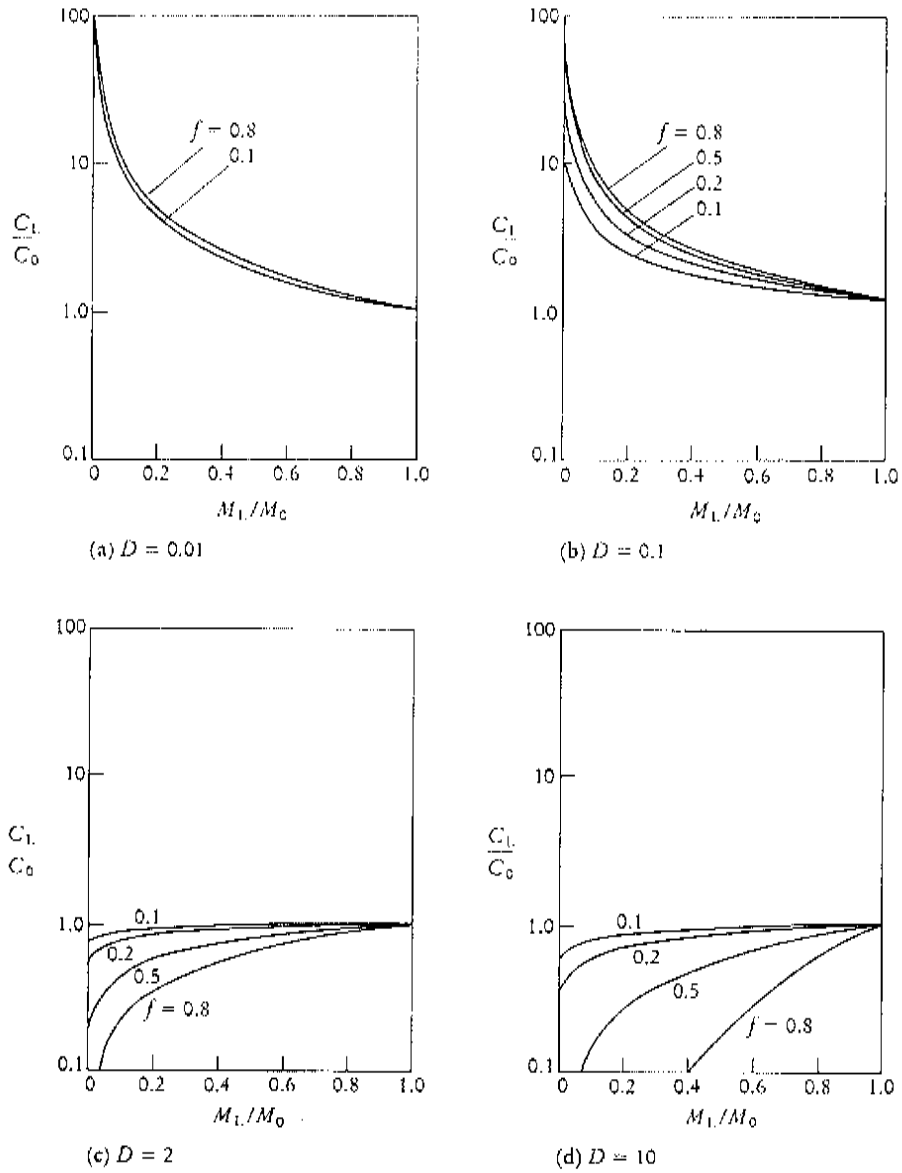

Figure 4.14 (a)–(d) The enrichment of a trace element in a melt relative to the parent melt (C_L/C_0) as a function of the fraction of remaining melt (M_L/M_0 — the ratio of the mass of the liquid to the mass of the magma chamber), bulk partition coefficient ($D = 0.01, 0.1, 2, 10$) and the fraction of magma in the solidification zone which is returned to the magma chamber ($f = 0.1, 0.2, 0.5, 0.8$) during *in situ* crystallization.

where r is the ratio of the assimilation rate to the fractional crystallization rate, C_A is the concentration of the trace element in the assimilated wallrock and f' is described by the relation

$$f' = F^{-(r-1+D)/(r-1)}$$

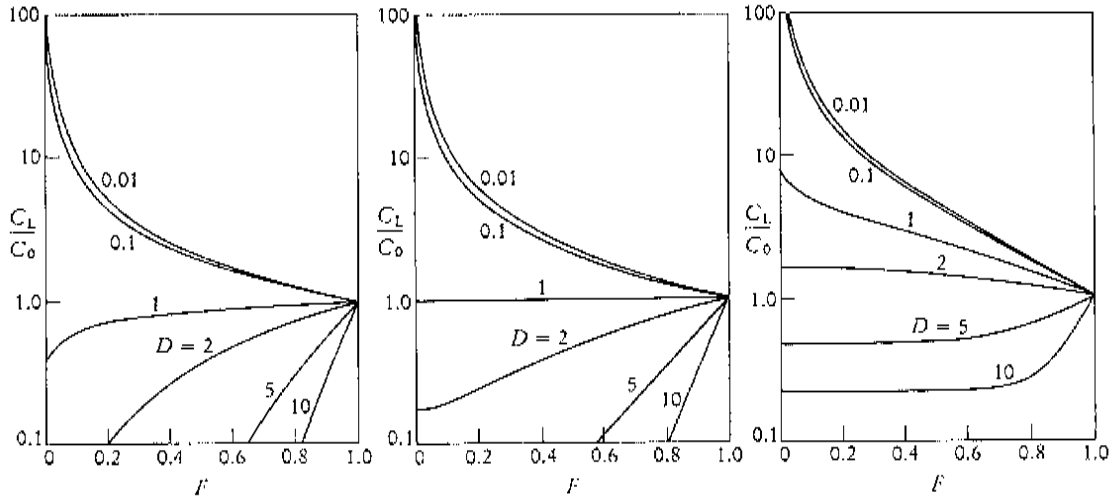

(a) $C_A/C_0 = 0.1$ (b) $C_A/C_0 = 1.0$ (c) $C_A/C_0 = 10$

Figure 4.15 (a)–(c) The enrichment of a trace element in a melt relative to the parental melt (C_L/C_0) as a function of the fraction of the remaining liquid (F) and the ratio of the concentration of the trace element in the assimilated country rock to the concentration in the parental liquid (C_A/C_0 = 0.1, 1, 10) and the bulk partition coefficient (D = 0.01, 0.1, 1, 2, 5, 10) during assimilation and fractional crystallization (AFC). The calculated curves are for the case where the ratio of the rate of assimilation to fractional crystallization (r) is 0.2.

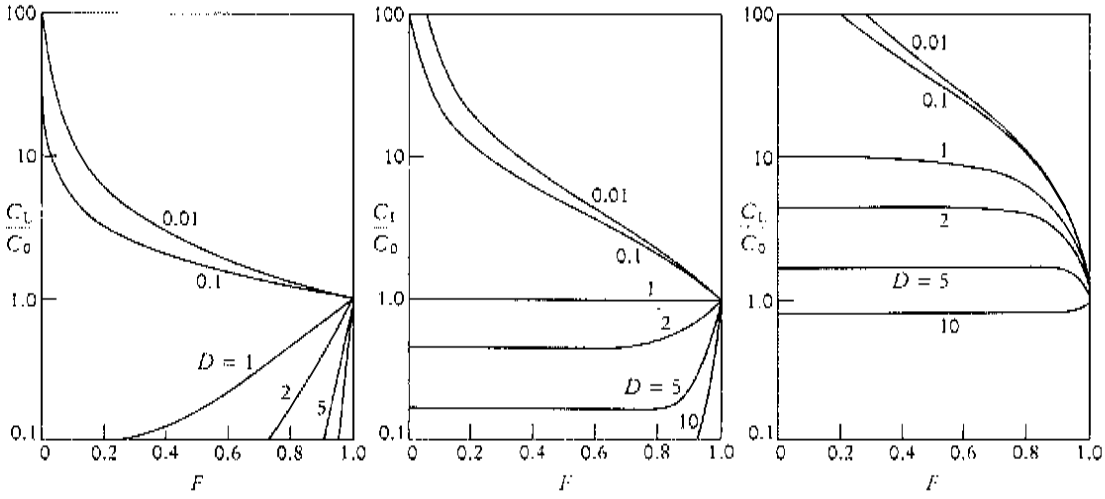

(a) $C_A/C_0 = 0.1$ (b) $C_A/C_0 = 1.0$ (c) $C_A/C_0 = 10$

Figure 4.16 (a)–(c) The enrichment of a trace element in a melt relative to the parental melt (C_L/C_0) as a function of the fraction of the remaining liquid (F) and the ratio of the concentration of the trace element in the assimilated country rock to the concentration in the parental liquid (C_A/C_0) and the bulk partition coefficient (D) during assimilation and fractional crystallization (AFC). The calculated curves are for the case where the ratio of the rate of assimilation to fractional crystallization (r) is 0.8.

where F is the fraction of magma remaining and D is the bulk distribution coefficient.

Figures 4.15 and 4.16 depict the enrichment of a trace element relative to its concentration in the parental magma with varying amounts of remaining melt for two different rates of assimilation relative to fractional crystallization (r = 0.2 and 0.8) and three different concentrations of the trace element in the assimilant relative to the parental magma (C_A/C_O), and different values of D.

Where the rate of assimilation to fractional crystallization is small (r = 0.2) incompatible elements behave in a similar manner to Rayleigh fractionation. Depletion in compatible elements is less dramatic, particularly when the concentration of the trace element in the assimilant is higher than in the primary magma (Figure 4.15c), although for very compatible elements concentrations level off after a small degree of fractionation.

Where the rate of assimilation is high (r = 0.8) and the concentration of the trace element relative to the parental magma is small (Figure 4.16a), incompatible elements are enriched and there is some separation between incompatible and strongly incompatible elements. Compatible elements are strongly depeleted. As the trace element concentration in the assimilant increases relative to the parental melt, enrichment increases and even compatible elements are enriched (Figure 4.16c).

(b) Zone refining In the section above on partial melting, it was suggested that batch melting and Rayleigh melting represent end-member models of natural melting processes. In reality it is likely that melts are neither instantaneously removed from the source nor do they remain totally immobile in their source. Rather they migrate at a finite rate and continuously react with the matrix through which they pass (Richter, 1986). During its passage through unmelted matrix it is possible that a melt will become further enriched in trace elements.

One possible mechanism for such a process is that of zone refining (Harris, 1974), analogous to a metallurgical industrial process, in which superheated magma consumes several times its own volume during melt migration and thus becomes enriched in incompatible elements. The equation for the enrichment of a trace element by zone refining is

$$C_L/C_0 = \frac{1}{D} - \left[\frac{1}{D} - 1\right]e^{-nD} \qquad [4.23]$$

where n is the number of equivalent rock volumes that have reacted with the liquid. Where n is very large the right-hand side reduces to $1/D$. The extent to which zone refining occurs in nature is the subject of debate, however, for a continual supply of superheated liquid is unlikely to occur on a large scale.

The numerical effects of zone refining are illustrated in Figure 4.17, which shows the enrichment of a trace element relative to its original concentration for the number of rock volumes consumed (n). For a compatible element with D = 2.0 the maximum enrichment ($1/D$) is reached when n is about 200, but for incompatible elements (0.1–0.01) the maximum enrichment is not reached even after 1000 rock volumes.

Dynamic models

(a) Dynamic melting To improve upon earlier 'static' models of partial melting, Langmuir *et al.* (1977) proposed a model of partial melting in which a number of melting processes take place continuously and simultaneously. The main feature of

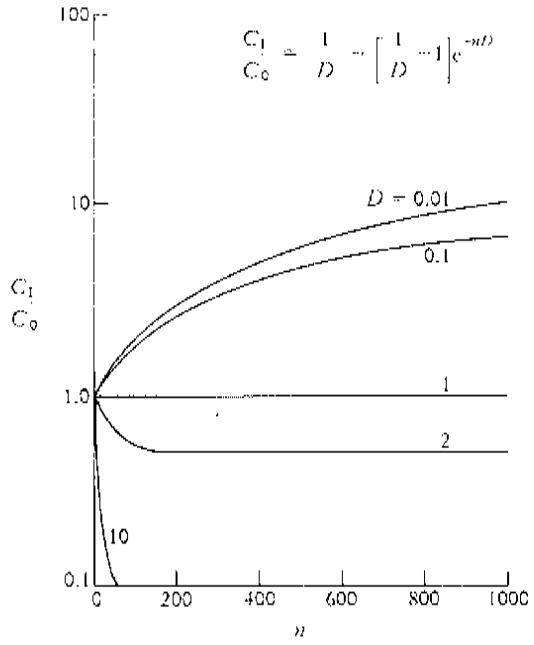

Figure 4.17 The enrichment of a trace element in a melt relative to the source (C_l/C_0) as a function of the number of rock volumes (n) and bulk partition coefficient (D) during zone refining.

the model is that there is incomplete melt extraction from the source which means that the source, always contains a mixture of melt and residue. Langmuir *et al.* (1977) used this approach to explain the variability of REE patterns from the Famous region of the Mid-Atlantic Ridge.

(b) The RTF magma chamber In an attempt to view magma chamber processes in a more dynamic way O'Hara (1977) and O'Hara and Matthews (1981) proposed a model to describe the behaviour of trace elements in a periodically Replenished, periodically Tapped, continuously Fractionated magma chamber (abbreviated to RTF). They proposed that the life of a magma chamber comprises a series of cycles each of which has four stages — fractional crystallization, magma eruption, wallrock contamination and replenishment. The concentration of a trace element in a steady-state liquid produced after a large number of cycles relative to the concentration in the replenishing magma batch ($_{SS}C_B/C_0$) is given by the expression

$$_{SS}C_B/C_0 = \frac{(x + y)(1 - x)^{D-1}}{1 - (1 - x - y)(1 - x)} \qquad [4.24]$$

where x is the mass fraction of the liquid crystallized in each cycle, y is the mass fraction of the liquid escaping in each cycle and D is the bulk distribution coefficient, and where x, y and D do not vary in the life of the magma chamber.

The degree of enrichment $_{SS}C_B/C_0$ is plotted against x in Figure 4.18 for y = 0.1 and for several different values of D.

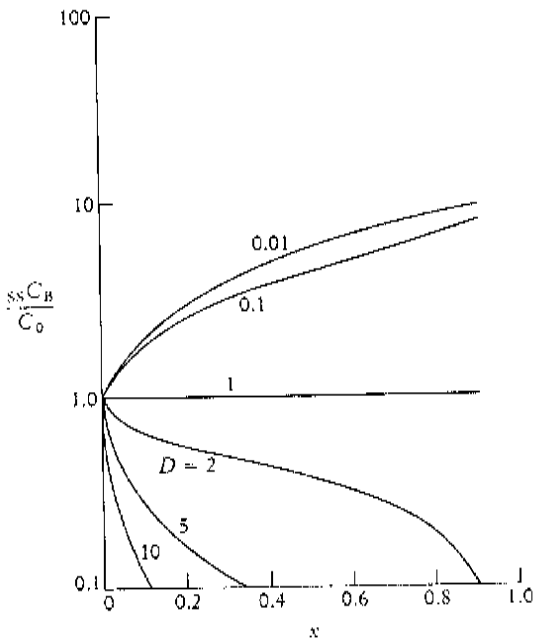

Figure 4.18 The enrichment of a trace element in a steady-state liquid relative to the concentration in the replenishing magma batch ${}_{ss}C_B/C_0$ as a function of the mass fraction of the liquid crystallized in each cycle (x) and the bulk partition coefficient (D) after a large number of cycles in a RTF magma chamber. The curves shown here are for the condition $y = 0.1$, i.e. the mass fraction of the liquid escaping in each cycle is 0.1. At higher values of y the degree of enrichment of incompatible elements is reduced.

In the special case where $x + y = 1$, i.e. when the magma chamber is emptied then

$${}_{ss}C_B/C_0 = (1 - x)^{D-1} \qquad [4.25]$$

which is the Rayleigh fractionation equation.

When $D = 0$, i.e. in the case of a totally incompatible trace element,

$${}_{ss}C_B/C_0 = 1 + \frac{x}{y} \qquad [4.26]$$

and is a measure of the maximum enrichment attainable.

Hagen and Neumann (1990) proposed that RTF processes are continuous rather than a series of cycles as suggested by O'Hara and Matthews (1981) and their paper usefully includes the FORTRAN 77 code to implement the two models.

Sedimentary processes

Trace element concentrations in sediments result from the competing influences of the provenance, weathering, diagenesis, sediment sorting and the aqueous geochemistry of the individual elements. The highest concentrations of trace elements are found in clay-rich sediments and most geochemical studies have concentrated on these lithologies. Selected trace elements may be used to identify

particular geochemical processes and to identify the sedimentary provenance. The most important elements in this respect are the REE, Th, Sc and to a lesser extent Cr and Co. These elements have very low concentrations in sea and river waters, low residence times in the ocean and element ratios which are unaffected by diagenesis and metamorphism. Thus they are transported exclusively in the terrigenous component of a sediment and reflect the chemistry of their source.

Other elements are more soluble. For example, Fe, Mn, Pb and sometimes Cr are mobile during diagenesis. Cs, Rb and Ba are fixed during weathering but Sr is leached. Immobile elements such as Zr, Hf and Sn may be mechanically distributed according to grain size and may be controlled by the concentration of heavy minerals.

4.3 Rare earth elements (REE)

The rare earth elements (REE) are the most useful of all trace elements and REE studies have important applications in igneous, sedimentary and metamorphic petrology. The REE comprise the series of metals with atomic numbers 57 to 71 — La to Lu (Table 4.4). In addition, the element Y with an ionic radius similar to that of the REE Ho is sometimes included. Typically the low-atomic-number members of the series are termed the light rare earths (LREE), those with the higher atomic

Table 4.4 The rare earth elements

Atomic number	Name	Symbol	Ionic radius for eight-fold coordination *	
57	Lanthanum	La	La^{3+}	1.160
58	Cerium	Ce	Ce^{3+}	1.143
			Ce^{4+}	0.970
59	Praesodymium	Pr	Pr^{3+}	1.126
60	Neodymium	Nd	Nd^{3+}	1.109
61	Promethium	Pm	Not naturally occurring	
62	Samarium	Sm	Sm^{3+}	1.079
63	Europium	Eu	Eu^{3+}	1.066
			Eu^{2+}	1.250
64	Gadolinium	Gd	Gd^{3+}	1.053
65	Terbium	Tb	Tb^{3+}	1.040
66	Dysprosium	Dy	Dy^{3+}	1.027
67	Holmium	Ho	Ho^{3+}	1.015
68	Erbium	Er	Er^{3+}	1.004
69	Thulium	Tm	Tm^{3+}	0.994
70	Ytterbium	Yb	Yb^{3+}	0.985
71	Lutetium	Lu	Lu^{3+}	0.977
39	Yttrium	Y	Y^{3+}	1.019

* From Shannon (1976), in Ångstroms (10^{-10} m).

numbers the heavy rare earths (HREE) and less commonly the middle members of the group, Sm to Ho, are known as the middle REE (MREE).

4.3.1 The chemistry of the REE

The REE all have very similar chemical and physical properties. This arises from the fact that they all form stable 3+ ions of similar size. Such differences as there are in chemical behaviour are a consequence of the small but steady decrease in ionic size with increasing atomic number. This is illustrated for ions in eight-fold coordination state in Table 4.4. These small differences in size and behaviour are exploited by a number of petrological processes causing the REE series to become fractionated relative to each other. It is this phenomenon which is used in geochemistry to probe into the genesis of rock suites and unravel petrological processes.

A small number of the REE also exist in oxidation states other than 3+ but the only ions of geological importance are Ce^{4+} and Eu^{2+}. These form a smaller and a larger ion respectively, relative to the 3+ oxidation state.

Table 4.5 Chondrite values used in normalizing REE (concentrations in ppm)

Analytical method	Wakita NAA	Haskin NAA	Masuda IDMS	Nakamura IDMS	Evensen IDMS	Boynton IDMS	T & M IDMS	Primitive mantle value
Chondrite(s) analysed: (Ref.)	Composite (1)	Composite (2)	Leedey (3)	Composite (4)	Avg.CI (5)	Avg.CI (6)	Avg. CI (7)	(8)
La	0.340	0.330	0.3780	0.3290	0.244 60	0.3100	0.3670	0.7080
Ce	0.910	0.880	0.9760	0.8650	0.637 90	0.8080	0.9570	1.8330
Pr	0.121	0.112			0.096 37	0.1220	0.1370	0.2780
Nd	0.640	0.600	0.7160	0.6300	0.473 80	0.6000	0.7110	1.3660
Sm	0.195	0.181	0.2300	0.2030	0.154 00	0.1950	0.2310	0.4440
Eu	0.073	0.069	0.0866	0.0770	0.058 02	0.0735	0.0870	0.1680
Gd	0.260	0.249	0.3110	0.2760	0.204 30	0.2590	0.3060	0.5950
Tb	0.047	0.047			0.037 45	0.0474	0.0580	0.1080
Dy	0.300		0.3900	0.3430	0.254 10	0.3220	0.3810	0.7370
Ho	0.078	0.070			0.056 70	0.0718	0.0851	0.1630
Er	0.020	0.200	0.2550	0.2250	0.166 00	0.2100	0.2490	0.4790
Tm	0.032	0.030			0.025 61	0.0324	0.0356	0.0740
Yb	0.220	0.200	0.2490	0.2200	0.016 51	0.2090	0.2480	0.0480
Lu	0.034	0.034	0.0387	0.0339	0.025 39	0.0322	0.0381	0.0737
Y							2.1000	

(1) Wakita *et al.* (1971): composite of 12 chondrites.
(2) Haskin *et al.* (1968): composite of nine chondrites.
(3) Masuda *et al.* (1973): Leedey chondrite.
(4) Nakamura (1974).
(5) Evensen *et al.* (1978): average of CI chondrites.
(6) Boynton (1984).
(7) Taylor and McLennan (1985): 1.5 x values of Evensen [column (5)].
(8) McDonough *et al.* (1991).

4.3.2 Presenting REE data

Rare earth element concentrations in rocks are usually normalized to a common reference standard, which most commonly comprises the values for chondritic meteorites. Chondritic meteorites were chosen because they are thought to be relatively unfractionated samples of the solar system dating from the original nucleosynthesis. However, the concentrations of the REE in the solar system are very variable because of the different stabilities of the atomic nuclei. REE with even atomic numbers are more stable (and therefore more abundant) than REE with odd atomic numbers, producing a zig-zag pattern on a composition–abundance diagram (Figure 4.19). This pattern of abundances is also found in natural samples. Chondritic normalization therefore has two important functions. Firstly it eliminates the abundance variation between odd and even atomic number elements and secondly it allows any fractionation of the REE group relative to chondritic meteorites to be identified. Normalized values and ratios of normalized values are denoted with the subscript N — hence for example Ce_N, $(La/Ce)_N$.

The REE are normally presented on a concentration vs atomic number diagram on which concentrations are normalized to the chondritic reference value, expressed as the logarithm to the base 10 of the value. Concentrations at individual points on the graph are joined by straight lines (Figure 4.20). This is sometimes referred to as the Masuda–Coryell diagram after the original proponents of the diagram (Masuda, 1962; Coryell *et al.*, 1963). Trends on REE diagrams are usually referred to as REE 'patterns' and the shape of an REE pattern is of considerable petrological interest.

Not infrequently the plotted position of Eu lies off the general trend defined by the other elements on an REE diagram (Figure 4.20) and may define a **europium anomaly**. If the plotted composition lies above the general trend then the anomaly is described as positive and if it lies below the trend then the anomaly is said to be negative. Europium anomalies may be quantified by comparing the measured concentration (Eu) with an expected concentration obtained by interpolating between the normalized values of Sm and Gd (Eu^*). Thus the ratio Eu/Eu^* is a measure of the europium anomaly and a value of greater than 1.0 indicates a positive anomaly whilst a value of less than 1.0 is a negative anomaly. Taylor and McLennan (1985) recommend using the geometric mean; in this case $Eu/Eu^* = Eu_N/\sqrt{[(Sm_N).(Gd_N)]}$.

(a) Difficulties with chondrite normalization Unfortunately it has become apparent that chondritic meteorites are actually quite variable in composition and 'chondrites with "chondritic" REE abundances are the exception rather than the rule' (Boynton, 1984). This variability in chondritic composition has given rise to a large number of sets of normalizing vales for the REE (Table 4.5) and to date no standardized value has been adopted. The variability may be reduced to two factors — the analytical method and the precise type of chondrites analysed. Some authors use 'average chondrite' whilst others selected C1 chondrites as the most representative of the composition of the original solar nebula.

(b) Choosing a set of normalizing values Figure 4.20 shows flat rare earth patterns typical of an Archaean tholeiite normalized to the range of chondritic values listed in Table 4.5. The patterns show both variety in shape and in concentration range. The consensus seems to favour values based upon average chondrite rather than C1

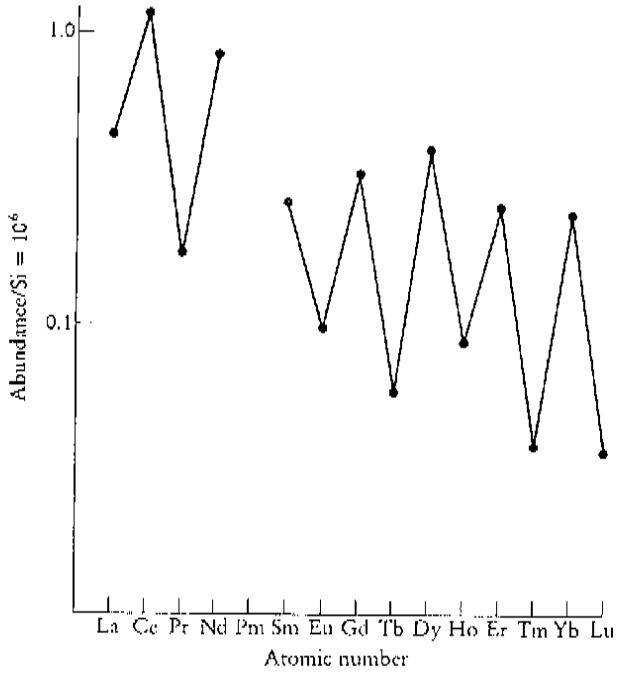

Figure 4.19 Rare earth element abundances (log scale) in the solar system plotted against atomic number. Data from Anders and Ebihara (1982), normalized to Si = 10^6 atoms. Elements with even atomic numbers have higher abundances than those with odd atomic numbers.

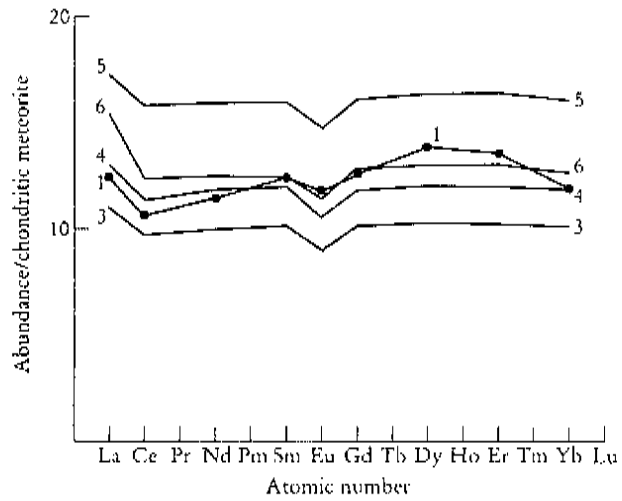

Figure 4.20 Rare earth element abundances normalized to chondritic meteorite values plotted against atomic number for an Archaean tholeiitic basalt (sample 11 — Rollinson, 1983). The same sample has been normalized using five different sets of values; the numbers refer to the columns of normalizing values listed in Table 4.5.

chondrites and either the values of Boynton (1984) based upon Evensen *et al.* (1978), or the values of Nakamura (1974), with additions from Haskin *et al.* (1968), seem to be satisfactory. In fact the two sets of values are very similar and lie in the middle of the range of values currently in use.

REE ratio diagrams

The degree of fractionation of a REE pattern can be expressed by the concentration of a light REE (La or Ce) ratioed to the concentration of a heavy REE (Yb or Y). Both elements are chondrite-normalized. The ratio $(La/Yb)_N$ is often plotted against either Ce_N or Yb_N on a bivariate graph and is a measure of the degree of REE fractionation with changing REE content. Similar diagrams may be constructed to measure the degree of light REE fractionation [$(La/Sm)_N$ vs Sm_N], heavy REE fractionation [$(Gd/Yb)_N$ vs Yb_N] and Eu anomaly [$(La/Sm)_N$ vs (Eu/Eu^*)] in individual REE patterns.

NASC normalization for sediments

It has been observed that the concentration of many elements in fine-grained sedimentary rocks in continental platforms around the world is similar as a consequence of mixing through repeated cycles of erosion. This 'average sediment' is often used as the normalizing value for REE concentrations in sedimentary rocks. A frequently used composition is that of the North American Shale Composite (NASC) and the recommended values of Gromet *et al.* (1984) are given in Table 4.6 (column 5). Alternatives to NASC in current use are a composite European shale (Haskin and Haskin, 1966) and the post Archaean average Australian sedimentary rock (McLennan, 1989). Some authors have taken the average abundance of REE in sedimentary rocks as a measure of the REE content of the upper continental crust. This assumes that sedimentary processes homogenize the REE previously fractionated during the formation of igneous rocks. Thus an alternative to shale normalization is to use values for average upper continental crust (Table 4.6, column 8).

Relative to chondritic meteorites, NASC has about 100 times the light REE and about 10 times the heavy REE content and a small negative Eu anomaly (Figure 4.21). Normalization against NASC is a measure of how typical a sediment is, and may identify subtle enrichments and deficiencies in certain elements.

Rock normalization

Less commonly some authors normalize REE concentrations to a particular sample in a rock suite as a measure of relative change. This is also useful when the REE concentrations of the individual minerals in the rock have also been determined, for then they can be expressed relative to the concentration in the whole rock. A similar form of normalization is to express the concentration in a mineral relative to the composition of the groundmass; this is frequently used to display mineral/melt partition coefficients (Section 4.2.1).

4.3.3 Interpreting REE patterns

The REE are regarded as amongst the least soluble trace elements and are relatively immobile during low-grade metamorphism, weathering and hydrothermal alteration. Michard (1989), for example, shows that hydrothermal solutions have between 5×10^2 and 10^6 times less REE than the reservoir rock through which they have passed and therefore hydrothermal activity is not expected to have a major effect on

Table 4.6 Standard sedimentary compositions used for normalizing the REE concentrations in sedimentary rocks (concentrations in ppm)

(Ref.)	NASC (1)	NASC (2)	NASC (3)	NASC (4)	NASC (5)	ES (6)	PAAS (7)	Upper crust (8)	Typical seawater (9) (10^{-12} mol kg^{-1})	River water (10)
La	39.000	32.000	32.000	31.100	31.100	41.100	38.200	30.000	20.800	425.0
Ce	76.000	70.000	73.000	66.700	67.033	81.300	79.600	64.000	9.640	601.0
Pr	10.300	7.900	7.900			10.400	8.830	7.100		
Nd	37.000	31.000	33.000	27.400	30.400	40.100	33.900	26.000	21.100	365.0
Sm	7.000	5.700	5.700	5.590	5.980	7.300	5.550	4.500	4.320	80.4
Eu	2.000	1.240	1.240	1.180	1.253	1.520	1.080	0.880	0.823	20.7
Gd	6.100	5.210	5.200		5.500	6.030	4.660	3.800	5.200	83.5
Tb	1.300	0.850	0.850	0.850	0.850	1.050	0.774	0.640		
Dy					5.540		4.680	3.500	5.610	97.9
Ho	1.400	1.040	1.040			1.200	0.991	0.800		
Er	4.000	3.400	3.400		3.275	3.550	2.850	2.300	4.940	64.6
Tm	0.580	0.500	0.500			0.560	0.405	0.330		
Yb	3.400	3.100	3.100	3.060	3.113	3.290	2.820	2.200	4.660	51.7
Lu	0.600	0.480	0.480	0.456	0.456	0.580	0.433	0.320		
Y		27.000				31.800	27.000	22.000		

(1) North American shale composite (Haskin and Frey, 1966).
(2) North American shale composite (Haskin and Haskin, 1966).
(3) North American shale composite (Haskin *et al.*, 1968).
(4) North American shale composite (Gromet *et al.*, 1984) — INAA.
(5) North American shale composite (Gromet *et al.*, 1984) — recommended.
(6) Average European shale (Haskin and Haskin, 1966).
(7) Post-Archaean average Australian sedimentary rock (McLennan, 1989).
(8) Average upper continental crust (Taylor and McLennan, 1981).
(9) Elderfield and Greaves (1982), Table 1, 900 m sample.
(10) Hoyle *et al.* (1984): River Luce, Scotland; 0.7 μm filter.

rock chemistry unless the water/rock ratio is very high. However, the REE are not totally immobile, as is emphasized in the review by Humphries (1984), and the reader should be cautious in interpreting the REE patterns of heavily altered or highly metamorphosed rocks. Nevertheless REE patterns, even in slightly altered rocks, can faithfully represent the original composition of the unaltered parent and a fair degree of confidence can be placed in the significance of peaks and troughs and the slope of an REE pattern.

REE patterns in igneous rocks

The REE pattern of an igneous rock is controlled by the REE chemistry of its source and the crystal–melt equilibria which have taken place during its evolution. Here we describe in a qualitative manner the way in which the roles of individual minerals may be identified during magmatic evolution, either during partial melting in the source region or in subsequent crystal fractionation. In Section 4.9 the quantitative aspects of this approach are considered and applied to trace elements in general. The reasoning here is based upon the partition coefficients for the REE in the major rock-forming minerals listed in Tables 4.1 to 4.3 and depicted in Figures 4.8 to 4.10.

Europium anomalies are chiefly controlled by feldspars, particularly in felsic magmas, for Eu (present in the divalent state) is compatible in plagioclase and

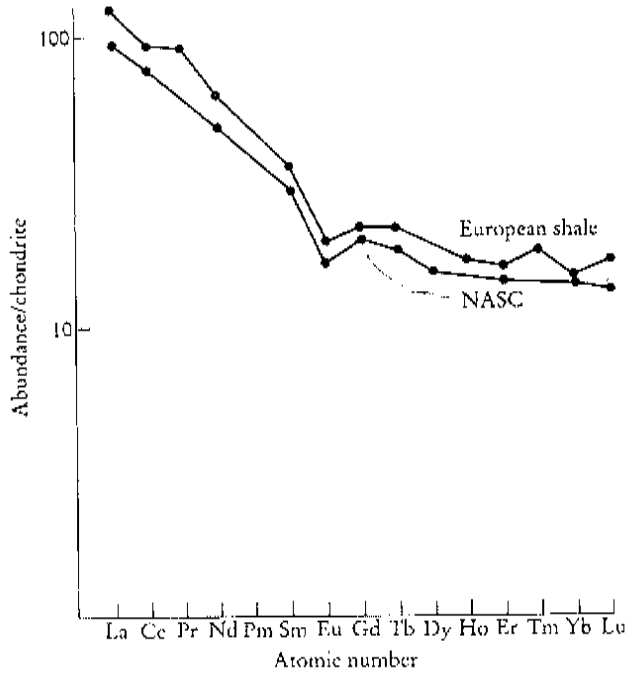

Figure 4.21 Rare earth element abundances in North American Shale Composite (NASC) and European shale, normalized to chondritic values. Data from Table 4.7, columns 5 and 6; normalizing values from Table 4.5, column 4.

potassium feldspar, in contrast to the trivalent REE which are incompatible. Thus the removal of feldspar from a felsic melt by crystal fractionation or the partial melting of a rock in which feldspar is retained in the source will give rise to a negative Eu anomaly in the melt. To a lesser extent hornblende, sphene, clinopyroxene, orthopyroxene and garnet may also contribute to a Eu anomaly in felsic melts, although in the opposite sense to that of the feldspars.

Enrichment in the middle REE relative to the light and heavy REE is chiefly controlled by hornblende. This is evident from the partition coefficients plotted in Figure 4.4. The REE are compatible in hornblende in felsic and intermediate liquids and the highest partition coefficients are between Dy and Er. Such large partition coefficients mean that even a moderate amount of hornblende (20–30 %) may dominate the bulk partition coefficient for this range of elements and influence the shape of the REE pattern. The same effect can also be observed with clinopyroxene, although the partition coefficients are not so high. Sphene also may also affect an REE pattern in a similar way although, because it is present usually in low concentrations, the effect may be masked by other phases.

Fractionation of the light REE relative to the heavy ones may be caused by the presence of olivine, orthopyroxene and clinopyroxene, for the partition coefficients increase by an order of magnitude from La to Lu in these minerals. In basaltic and andesitic liquids, however, the REE are all incompatible in each of these minerals and are only slightly fractionated.

Extreme depletion of the heavy REE relative to the light is most likely to indicate the presence of garnet in the source, for there is a large variation in the partition coefficients of the REE. In basaltic liquids the partition coefficient for Lu is more than 1000 times greater than that for La. The effect is less extreme, although still large, in felsic liquids. Hornblende in felsic liquids may also account for extreme enrichment of light REE relative to heavy, although the range of partition coeffients is not as great as in the case of garnet.

In felsic liquids accessory phases such as sphene, zircon, allanite, apatite and monazite may strongly influence an REE pattern for although they may be present in only small quantities (often much less than 1 % of the rock) their very high partition coefficients mean that they have a disproportionate influence on the REE pattern. Zircon will have an effect similar to that of garnet and will deplete in the heavy REE; sphene and apatite partition the middle REE relative to the light and heavy, and monazite and allanite cause depletion in the light REE.

REE patterns in sea and river water

The aqueous geochemistry of the REE is a function of the type of complexes that the REE may form, the length of time the REE remain in solution in the oceans (their residence time), and to a lesser extent the oxidizing potential of the water. The topic is well reviewed by Brookins (1989). The REE contents of rivers and seawater are extremely low (Table 4.6), for they are chiefly transported as particulate material. When normalized to a shale composite (Section 4.3.2), REE concentrations in seawater are between six and seven orders of magnitude smaller that the shale value. River waters are about an order of magnitude higher.

The REE in ocean waters provide information about oceanic input from rivers, hydrothermal vents and from aeolian sources (Elderfield, 1988). On a shale-normalized plot (Figure 4.22) seawater tends to show a gradual enrichment in REE concentrations from the light to heavy REE and often shows a prominent negative Ce anomaly (Elderfield and Greaves, 1982). This anomaly is expressed as Ce/Ce^* where Ce^* is an interpolated value for Ce based upon the concentrations of La and Pr or La and Nd. The Ce anomaly occurs in response to the oxidation of Ce^{3+} to Ce^{4+} and the precipitation of Ce^{4+} from solution as CeO_2. Eu anomalies in seawater reflect either aeolian or hydrothermal input. River water also shows a small negative Ce anomaly and an increase in REE concentrations from the light to heavy REE (Hoyle *et al.*, 1984) similar to that observed in seawater (Figure 4.22).

REE patterns in sediments

REE concentrations in sedimentary rocks are usually normalized to a sedimentary standard such as NASC, although this practice is not universal and some authors use chondritic normalization.

(a) Clastic sediments The single most important factor contributing to the REE content of a clastic sediment is its provenance (Fleet, 1984; McLennan, 1989). This is because the REE are insoluble and present in very low concentrations in sea and river water; thus the REE present in a sediment are chiefly transported as particulate matter and reflect the chemistry of their source. In comparison, the effects of weathering and diagenesis are minor. Studies such as those by Nesbitt (1979) show that whilst the REE are mobilized during weathering, they are reprecipitated at the site of weathering. A more recent study shows, however, that in the case of extreme weathering the degree of weathering of the source can be recognized in the REE chemistry of the derivative sediment (Nesbitt *et al.*, 1990).

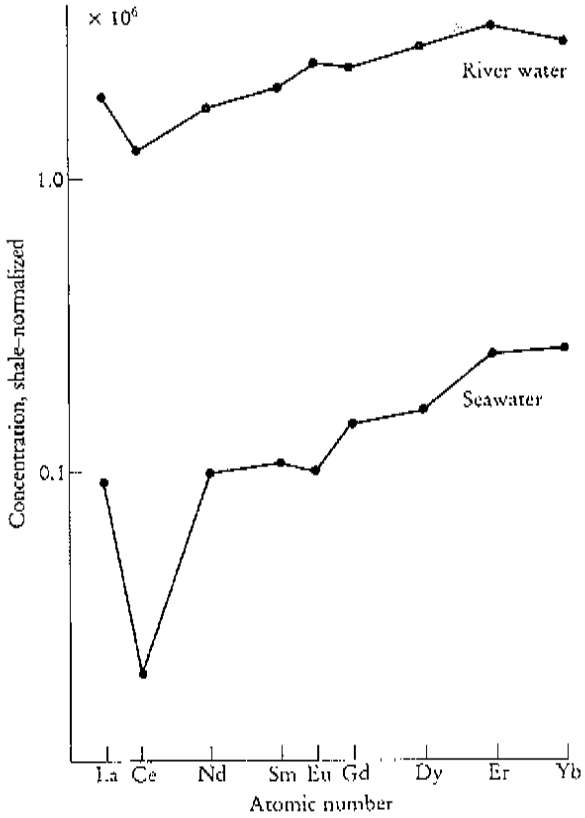

Figure 4.22 Concentrations of rare earth elements in average seawater and average river water normalized to NASC. The data are given in Table 4.6, columns 9 and 10. Normalizing values are from Table 4.6 column 5. Note that the concentrations in seawater and river water are quoted in mol kg^{-1} and must in this case be multiplied by the atomic weight. Concentrations shown are $\times 10^{-6}$.

Diagenesis has little influence on the redistribution of the REE, for very large water/rock ratios are required to effect any change in sediment chemistry.

An important study by Cullers *et al.* (1987), on the effect of sedimentary sorting on REE concentrations, found that the REE pattern of the source was most faithfully represented in the clay-sized fraction of the sediment. Clay-bearing rocks also have a much higher concentration of total REE than other sediments. It is for this reason that many authors have used the REE content of the clay portion of a sediment or clay-rich sediments in order to establish the sedimentary processes and to identify the provenance. The presence of quartz has a diluting effect on REE concentrations, as does carbonate. The presence of heavy minerals, particularly zircon, monazite and allanite, may have a significant but erratic effect on the REE pattern of an individual sample.

(b) Chemical sediments Chemical sediments are most likely to reflect the composition of the seawater from which they were precipitated. This is seen in ferromanganese nodules which show REE patterns that are the inverse of a typical

seawater pattern, i.e. they are enriched in light relative to heavy REE and show a positive Ce anomaly. This is not a universal feature of ferromanganese nodules, however, for the composition of chemical sediments also reflects local redox conditions and is strongly influenced by post-depositional changes (Elderfield and Greaves, 1981).

4.4 Normalized multi-element diagrams or incompatible element diagrams (spider diagrams)

Normalized multi-element diagrams are based upon a grouping of elements incompatible with respect to a typical mantle mineralogy. They are an extension of the more familiar chondrite-normalized REE diagrams in which other trace elements are added to the traditional REE diagram. They are a particularly useful way of depicting basalt chemistry although their use has been extended to all igneous and some sedimentary rocks. Mantle values or those of chondritic meteorites are used for normalization and they measure deviations from a primitive composition. The terms 'mantle (or chondrite)-normalized multi-element diagram' or 'incompatible element diagram' do not roll off the tongue with ease and the more colloquial '**spider diagram**' (or 'spidergram' for an individual pattern) is used here.

4.4.1 Multi-element diagrams for igneous rocks

There are three popular ways of normalizing trace element data for presentation as a spider diagram. These include an estimated primitive mantle composition and chondritic meteorites — two 'views' of the primitive undifferentiated earth. Others normalize their data to primitive MORB. Each version of the spider diagram has a slightly different array of elements with a slightly different order. In detail there are innumerable variations on each particular theme, usually dictated by the number of trace elements and the quality of their determinations in a particular data-set. This state of affairs is not satisfactory and some standardization is desirable. First, however, we consider the present 'state of the art'.

Primordial (primitive) mantle-normalized spider diagrams

The primitive mantle is the composition of the mantle before the continental crust formed. One of the most frequently used estimates of its composition is that of Wood *et al.* (1979a), who employed it as a means of comparing compositional variations between basic lavas. Nineteen elements are arranged in order of increasing compatibility with respect to a small percentage melt of the mantle. The values are given in Table 4.7, column 1. Element concentrations are plotted on a logarithmic scale (Figure 4.23) and average N-type MORB plots as a relatively smooth curve, depleted at the most incompatible end (Figure 4.23b).

There are a number of variations in the list of elements plotted. The most common alternative is a 13-element plot reflecting those elements whose concentrations are relatively high in basic igneous rocks and which are readily analysed by X-ray fluorescence. Normalizing values currently in use are given in Table 4.7, columns 1 to 5. Of these five sets of values, those of McDonough *et al.* (1992) (a slight revision of Sun and McDonough, 1989) — Table 4.7, column 4 — are becoming increasingly popular.

Chondrite-normalized spider diagrams

Thompson (1982) proposed that normalization to chondritic values may be preferable to the primordial mantle composition since chondritic values are directly measured rather than estimated. The order of elements (Figure 4.24) is slightly different from that of Wood *et al.* (1979a) and is to some extent arbitrary but was chosen to give the smoothest overall fit to data for Icelandic lavas and North Atlantic ocean-floor basalts; it approximates to one of increasing compatibility from left to right. As a rule of thumb, concentrations below about ten times chondrite

Table 4.7 Normalizing values (in ppm) used in the calculation of 'spider diagrams' and listed in their plotting order

Primordial mantle						Chondrite								MORB normalization			
(Ref.)	(1)	(2)	(3)	(4)	(5)	(6)		(7)		(8)	(9)			(10)			(11)
Cs	0.019	0.017		0.023	0.018				Cs	0.012	0.188						
Rb	0.860	0.660	0.810	0.635	0.550	Ba	6.900	Rb	1.880	Pb	0.120	2.470	Sr	120	Rb	1.00	
Ba	7.560		6.900	6.990	5.100	Rb	0.350	K	850	Rb	0.350	2.320	K_2O (%)	0.15	Ba	12.00	
Th	0.096		0.094	0.084	0.064	Th	0.042	Th	0.040	Ba	3.800	2.410	Rb	2.00	K_2O (%)	0.15	
U	0.027		0.026	0.021	0.018	K	120	Ta	0.022	Th	0.050	0.029	Ba	20.00	Th	0.20	
K	252.0	230.0	260.0	240.0	180	Nb	0.350	Nb	0.560	U	0.013	0.008	Th	0.20	Ta	0.17	
Ta	0.043		0.040	0.041	0.040	Ta	0.020	Ba	3.600	Ta	0.020	0.014	Ta	0.18	Sr	136	
Nb	0.620		0.900	0.713	0.560	La	0.329	La	0.328	Nb	0.350	0.246	Nb	3.50	La	3.00	
La	0.710		0.630	0.708	0.551	Ce	0.865	Ce	0.865	K	120	545	Ce	10.00	Ce	10.00	
Ce	1.900			1.833	1.436	Sr	11.800	Sr	10.500	La	0.315	0.237	P_2O_5 (%)	0.12	Nb	2.50	
Sr	23.000		28.000	21.100	17.800	Nd	0.630	Hf	0.190	Ce	0.813	0.612	Zr	90.00	Nd	8.00	
Nd	1.290			1.366	1.067	P	46.000	Zr	9.000	Sr	11.000	7.260	Hf	2.40	P_2O_5 (%)	0.12	
P	90.400	92.000				Sm	0.203	P	500	Nd	0.597	0.467	Sm	3.30	Hf	2.50	
Hf	0.350		0.350	0.309	0.270	Zr	6.840	Ti	610	P	46.000	1220	TiO_2 (%)	1.50	Zr	88.00	
Zr	11.000		11.000	11.200	8.300	Hf	0.200	Sm	0.203	Sm	0.192	0.153	Y	30.00	Eu	1.20	
Sm	0.385		0.380	0.444	0.347	Ti	620	Y	2.000	Zr	5.600	3.870	Yb	3.40	TiO_2 (%)	1.50	
Ti	1200	1300	1300	1280	960	Tb	0.052	Lu	0.034	Ti	620	445	Sc	40.00	Tb	0.71	
Tb	0.099			0.108	0.087	Y	2.000	Sc	5.210	Y	2.000	1.570	Cr	250.0	Y	35.00	
Y	4.870		4.600	4.550	3.400	Tm	0.034	V	49.000						Yb	3.50	
Pb				0.071		Yb	0.220	Mn	1720						Ni	138	
								Fe	265000						Cr	290	
								Cr	2300								
								Co	470								
								Ni	9500								

(1) Wood *et al.* (1979a); Ti from Wood *et al.* (1981).
(2) Sun (1980); Cs 0.017–0.008.
(3) Jagoutz *et al.* (1979).
(4) McDonough *et al.* (1992).
(5) Taylor and McLennan (1985).
(6) Thompson (1982); alternative value for Ba=3.85 (Hawkesworth *et al.*, 1984); Rb,K,P from primitive mantle values of Sun (1980).
(7) Wood *et al.* (1979b).
(8) Sun (1980); chondrite and undepleted mantle data.
(9) Sun and McDonough (1989): C1 chondrite.
(10) Pearce (1983); Sc and Cr from Pearce (1982).
(11) Bevins *et al.* (1984).

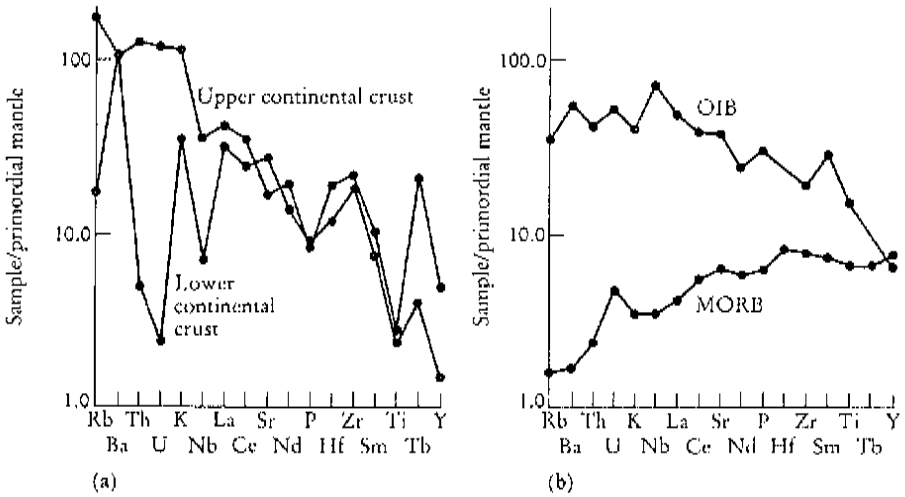

Figure 4.23 Trace element concentrations normalized to the composition of the primordial mantle and plotted from left to right in order of increasing compatibility in a small fraction melt of the mantle. The normalizing values are those of McDonough *et al.* (1992) — Table 4.7, column 4. (a) Upper and lower continental crust from Weaver and Tarney (1984) — data in Table 4.8; (b) Average N-type MORB from Saunders and Tarney (1984) and OIB from Sun (1980) — data in Table 4.8.

Table 4.8 Trace element data used in spider diagrams (Figures 4.23, 4.24, 4.26)

(Ref.)	Upper crust (1)	Lower crust (2)	Average crust (3)	MORB (4)	OIB (5)
Rb	110.00	11.00	61.00	1.00	22.00
Ba	700.00	757.00	707.00	12.00	380.00
Th	10.50	0.42	5.70	0.20	3.40
U	2.50	0.05	1.30	0.10	1.10
K	27393	8301	17430	830	9600
Nb	25.00	5.00	13.00	2.50	53.00
Ta				0.16	3.00
La	30.00	22.00	28.00	3.00	35.00
Ce	64.00	44.00	57.00	10.00	72.00
Sr	350.00	569.00	503.00	136.00	800.00
Nd	26.00	18.50	23.00	8.00	35.00
P	742.22	785.88	829.54	570.00	2760.00
Hf	5.80	3.60	4.70	2.50	
Zr	240.00	202.00	210.00	88.00	220.00
Sm	4.50	3.30	4.10	3.30	13.00
Ti	3597.00	2997.50	3597.00	8400.00	20000.00
Tb	2.20	0.43	0.24	0.71	
Y	22.00	7.00	14.00	35.00	30.00
Tm	0.33	0.19	0.24		
Yb	2.20	1.20	1.53		

(1) Upper continental crust (Taylor and McLennan, 1981).
(2) Lower continental crust (Weaver and Tarney, 1984).
(3) Average continental crust (Weaver and Tarney, 1984).
(4) Average N-type MORB (Saunders and Tarney, 1984; Sun, 1980).
(5) Average OIB (Sun, 1980).

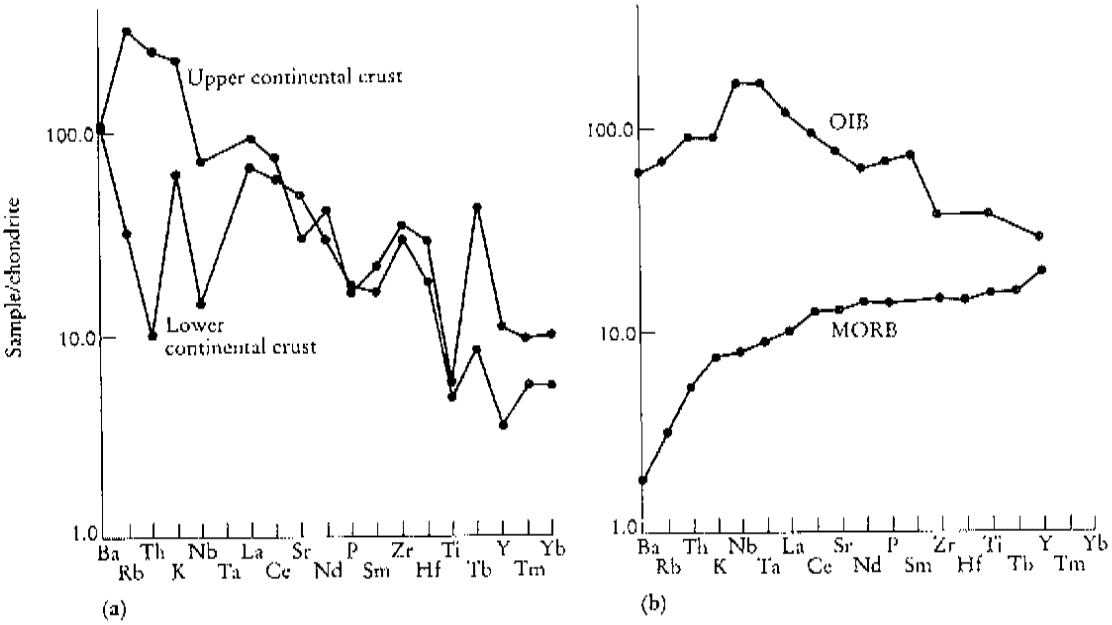

Figure 4.24 Trace element concentrations normalized to the composition of chondritic meteorites and plotted from left to right in order of increasing compatibility in a small fraction melt of the mantle. The normalizing values are those of Thompson (1982) — Table 4.7, column 6. (a) Upper and lower continental crust from Weaver and Tarney (1984) — data in Table 4.8; (b) Average N-type MORB from Saunders and Tarney (1984) and OIB from Sun (1980) — data in Table 4.8.

approach the detection limit for most techniques and so should be treated with caution (Thompson *et al.*, 1983). Thompson *et al.* (1983) point out that when basalts of varying MgO contents are compared on spider diagrams, there may be a very erratic set of patterns arising from the variable effects of fractional crystallization. To avoid this confusion they suggest the recalculation of the normalized data to make $(Yb)_N = 10.0$. This slight oversimplification of the data is justified because Yb values in lavas with the same MgO value vary only by a factor of about two and the net result is a much clearer set of patterns. Normalization values are given in Table 4.7, columns 6 to 9. The more obvious discrepancies between values in this list arise because some authors have used a mixture of chondritic and primordial mantle values.

MORB-normalized spider diagrams

MORB-normalized spidergrams are most appropriate for evolved basalts, andesites and crustal rocks — rocks to which MORB rather than primitive mantle could be parental. This form of spider diagram was proposed by Pearce (1983) and is based upon two parameters (Figure 4.25). Firstly, ionic potential (ionic charge for the element in its normal oxidation state, divided by ionic radius) is used as a measure of the mobility of an element in aqueous fluids. Elements with low (<3) and high (>12) ionic potentials are mobile and those with intermediate values are generally

immobile. Secondly, the bulk distribution coefficient for the element between garnet lherzolite and melt is used as a measure of the incompatibility of an element in small-degree partial melts. The elements are ordered so that the most mobile elements (Sr, K, Rb and Ba) are placed at the left of the diagram and in order of increasing incompatibility. The immobile elements are arranged from right to left in order of increasing incompatibility (Figures 4.25 and 4.26). A slightly different version of this diagram is used by Saunders and Tarney (1984), who arrange the elements into a LIL-group (Rb, Ba, K, Th, Sr, La, Ce), followed by an HFS-group (Nb, Ta, Nd, P, Hf, Zr, Eu, Ti, Tb, Y, Yb), followed by the transition metals Ni and Cr. These authors proposed that data should be normalized to Zr = 10.0 in order to eliminate concentration differences arising from low-pressure crystal fractionation.

The normalizing values used by Pearce (1983) are taken from the average MORB of Pearce *et al.* (1981) and are given in Table 4.7, column 10. A longer list of elements arranged in a slightly different order is used by Bevins *et al.* (1984)

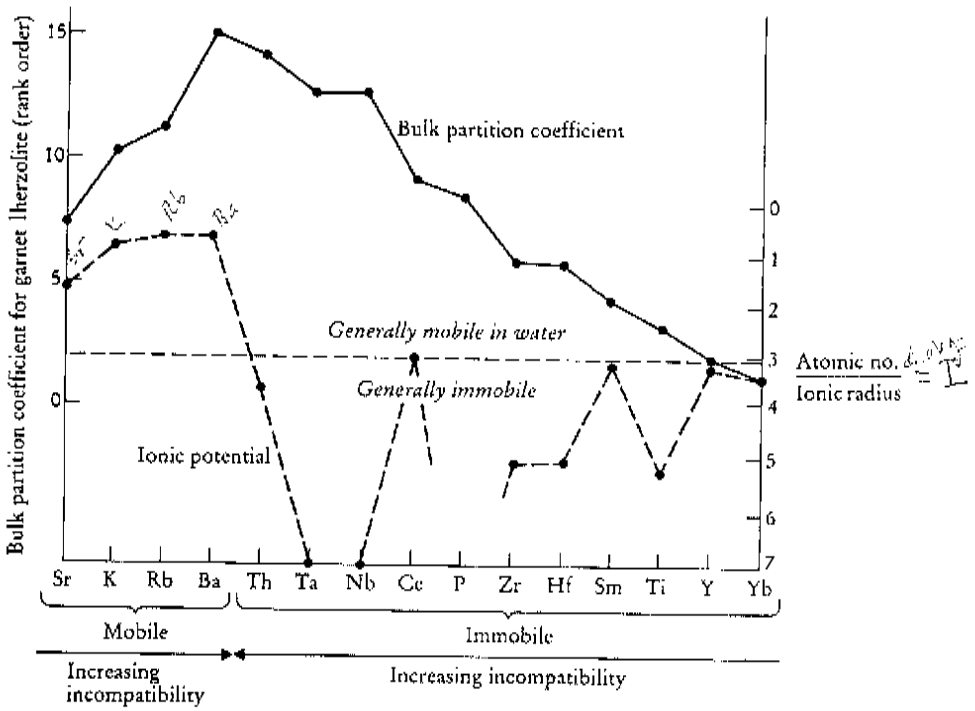

Figure 4.25 The petrogenetic variables that determine the order of elements in the MORB-normalized spider diagram of Pearce (1983). The ionic potential (broken line and right-hand scale) is the ratio of the atomic number to ionic radius and is a measure of the mobility of an element in aqueous fluids. Elements with a low ionic potential (<3, i.e. above the dotted line) are generally mobile in water whereas those with a higher ionic potential are generally immobile. (Note that P has an ionic potential which plots off-scale.) The bulk partition coefficient for an element between garnet lherzolite and a small percentage melt is a measure of incompatibility (left-hand scale). The immobile elements are plotted in rank order starting with the most compatible element (on the right). The mobile elements are ordered in a similar way so that element incompatibility increases from the edge to the centre of the diagram.

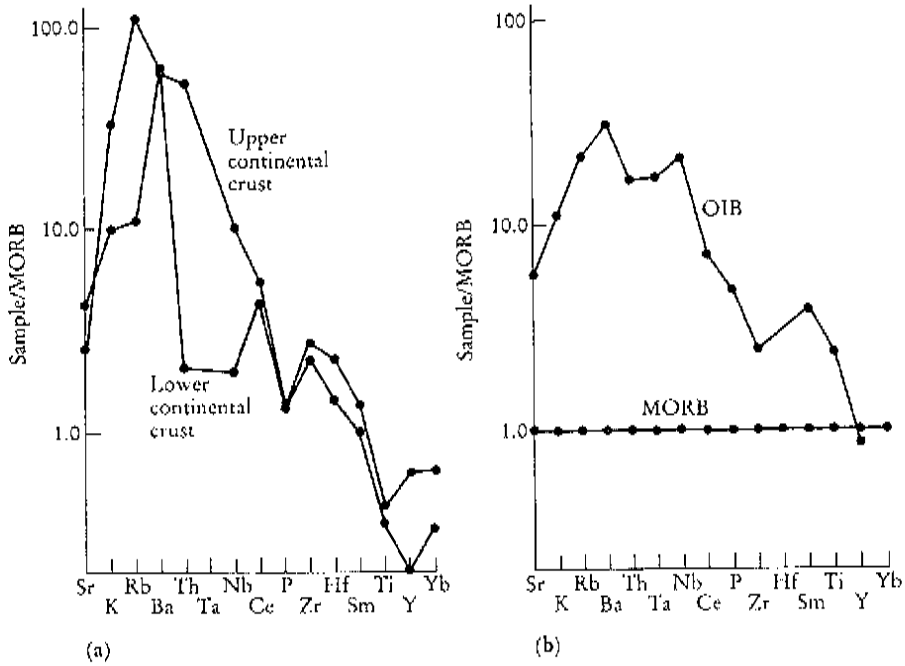

Figure 4.26 Trace element concentrations normalized to the composition of average MORB and plotted as in Figure 4.25. The normalizing values are those of Saunders and Tarney (1984) with additions from Sun (1980) — Table 4.7, column 11. (a) Upper and lower continental crust from Weaver and Tarney (1984) — data in Table 4.8; (b) Average N-type MORB from Saunders and Tarney (1984) and OIB from Sun (1980) — data in Table 4.8.

using values from Pearce *et al.* (1981) and Saunders and Tarney (1984) (Table 4.7, column 11).

Which spider diagrams do we use?

There is a pressing need for the standardization of multi-element diagrams. Current practice is chaotic, some authors not even quoting the source of their normalizing values. This has led to a situation where it is impossible to compare one spidergram with another. Rock (1987b) has argued for a set of standard multi-element diagrams with a universal set of consistent normalizing values — not necessarily 'perfect values', but ones which are universally accepted. The price of standardization is that some authors may have to sacrifice some elements of personal preference from their private version of a multi-element diagram. For igneous rocks two multi-element diagrams are sufficient: one to compare rock chemistry with a 'mantle source' and another to compare rock chemistry with 'the most abundant volcanic rock' — MORB. To maintain consistency with REE plots and to avoid a measure of subjectivity implicit in models of the primordial mantle, the chondrite model is recommended and the element order and normalizing values of Thompson (1982) (Table 4.7, column 6) should be adopted. These values utilize the REE data of Nakamura (1974) and thus provide some consistency with REE plots. A condensed version of the diagram is permissible if the full range of trace elements have not been determined, although the reader should be aware of the possibility of induced anomalies resulting from missing elements. The standard diagram and normalizing

values for the MORB source should be those of Pearce (1983) (Table 4.7, column 10), since this is the most widely used and the most objectively based (Rock, 1987b).

Interpreting multi-element diagrams for igneous rocks

Multi-element diagrams contain a more heterogeneous mix of trace elements than do REE diagrams. Consequently they often show a greater number of peaks and troughs reflecting the different behaviour of different groups of trace elements. For example, contrast the behaviour of the more mobile LIL elements (Cs, Rb, K, Ba, Sr, Eu) with the less mobile HFS elements (Y, Hf, Zr, Ti, Nb, Ta). On the one hand the LIL element concentrations may be a function of the behaviour of a fluid phase, whilst the HFS element concentrations are controlled by the chemistry of the source and the crystal/melt processes which have taken place during the evolution of the rock. Partition coefficients for the HFS elements in the major rock-forming minerals in a range of melt compositions are summarized in Tables 4.1 to 4.3.

Of the less mobile elements, mineralogical controls on the distribution of the REE have already been discussed. Other elements are often strongly controlled by individual minerals. For example, Zr concentrations may be controlled by zircon, P by apatite, Sr by plagioclase, Ti, Nb and Ta by ilmenite, rutile or sphene. Negative Nb anomalies are also characteristic of the continental crust and may be an indicator of crustal involvement in magma processes.

More mobile LIL element concentrations may be controlled by aqueous fluids but these elements are concentrated in the continental crust and can also be used as an indicator of crustal contamination of magmas.

4.4.2 Multi-element diagrams for sediments

The processes controlling the trace element composition of sedimentary rocks may be investigated using normalization diagrams similar to those for spidergrams discussed above, although they are not as widely used as their equivalents in igneous petrology. Different normalization values are employed for different types of sediment, each representing average Phanerozoic values for the particular sediment (see Table 4.9). The most commonly used normalizing values are those for average shale such as average post-Archaean shale and the North American shale composite (NASC), representing 'average crustal material', although average upper continental crust is also used. Wronkiewicz and Condie (1987), in a study of Archaean shales, plot 15 elements representing the LIL, HFS and transition metals, normalized to NASC. In clays which contain a variable amount of carbonate material, samples are better normalized against the most clay-rich, carbonate-free sample in the suite in order to emphasize the difference in trace element chemistry between the clay and carbonate-rich components (Norman and De Deckker, 1990).

The average trace element concentration in a Phanerozoic quartzite is given by Boryta and Condie (1990) for 18 elements; these values may be used in quartzite normalization (Table 4.9). Trace elements in marbles and calc-silicate rocks were normalized to average Phanerozoic limestone (Condie *et al.*, 1991). The normalizing values are listed in Table 4.9. To minimize the effect of varying amounts of carbonate, Condie *et al.* (1991) also normalized their elemental concentrations to Al_2O_3.

Table 4.9 Normalizing values for multi-element diagrams for sedimentary rocks (values in ppm)

(Ref.)	NASC (1)	Average upper crust (2)	Average Phanerozoic limestone (3)	Average Phanerozoic quartz arenite (4)
Na	7479	28200		
Al	89471	84700	5294	2647
K	31546	27400		
Ca	24303	25000		
Sc	14.90	10.00		1.00
Ti	4676	3600	1199	1499
V		60.00		10.00
Cr	124.50	35.00	15.00	30.00
Mn	4646	600	651	
Fe	39565	35000	3777	3777
Co	25.70	10.00		1.50
Ni	58.00	20.00	15.00	5.00
As	28.40			
Br	0.69			
Rb	125.00	110.00	20.00	
Sr	142.00	350.00	400.00	40.00
Y		22.00	5.00	5.00
Zr	200.00	240.00	20.00	200.00
Nb		25.00	1.50	20.00
Sb	2.09			
Cs	5.16	3.70		
Ba	636.00	700.00	85.00	350.00
La	31.10	30.00	5.00	4.00
Ce	66.70	64.00	10.00	
Nd	27.40	26.00		
Sm	5.59	4.50		
Eu	1.18	0.88	0.20	
Tb	0.85	0.64		
Yb	3.06	2.20		0.50
Lu	0.46	0.32		
Hf	6.30	5.80		3.50
Ta	1.12			2.00
W	2.10			
Pb		15.00	7.00	
Th	12.30	10.50		3.00
U	2.66	2.50		

(1) Gromet *et al.* (1984).
(2) Taylor and McLennan (1981).
(3) Condie *et al.* (1991).
(4) Boryta and Condie (1990).

Interpreting multi-element diagrams for sediments

Cullers (1988) showed that the silt fraction of a sediment most closely reflects the provenance of the sediment. The feldspars and sphene control concentrations of Ba, Na, Rb and Cs; ferromagnesian minerals control the concentrations of Ta, Fe, Co, Sc and Cr; Hf is controlled by zircon; and the REE and Th are controlled by sphene. The ratios La/Sc, Th/Sc, La/Co, Th/Co, Eu/Sm and La/Lu are also good indicators of provenance.

The effects of the extent of weathering and its influence on sediment

composition were assessed by Wronkiewicz and Condie (1987) using the alkali and alkaline earth element content of sediments. They showed that large cations (Cs, Rb and Ba) are fixed in a weathering profile whilst smaller cations (Na, Ca and Sr) are more readily leached. In clay-bearing rocks with a carbonate content, the elements Mn, Pb and Sr are chiefly contained in the carbonate component and anomalous values of these elements may provide a signal for the presence of carbonate.

4.5 Platinum metal group element (PGE) plots

The platinum groups elements (PGEs) consist of Ru, Rh, Pd, Os, Ir and Pt (Table 4.10). The noble metal Au and the base metals Cu and Ni are often included on PGE plots. The PGEs can be divided on the basis of their associations into two sub-groups — the Ir-group (IPGEs — Os, Ir and Ru) and the Pd-group (PPGEs — Rh, Pt and Pd). Gold is often associated with the latter group.

The platinum group elements are very strongly fractionated into a sulphide phase and are useful as a measure of sulphur saturation in a melt. They are also potentially useful as an indicator of partial melting in the mantle, although at present the appropriate partition coefficients are not sufficiently well known. PGEs occur at the ppb level (1 part in 10^9) in basic and ultrabasic igneous rocks but may be concentrated in coexisting chromitites and sulphides. The IPGEs are often associated with chromite as alloys or sulphides in dunites whilst the PPGEs and Au are often associated with the sulphides of Fe, Ni and Cu and are found in norites, gabbros and dunites (Barnes *et al.*, 1985).

Table 4.10 The platinum group elements (PGEs)*

Element	Symbol	Atomic no.	Charge	Ionic radius† (Å)	Melting point (°C)
Ruthenium	Ru	44	2+	0.74	2310
			3+	0.68	
			4+	0.62	
Rhodium	Rh	45	2+	0.72	1966
			3+	0.66	
			4+	0.60	
Palladium	Pd	46	2+	0.86	1552
			3+	0.76	
			4+	0.615	
Osmium	Os	76	2+	0.74	3045
			4+	0.63	
Iridium	Ir	77	2+	0.74	2410
			3+	0.68	
Platinum	Pt	78	2+	0.80	1722
			4+	0.625	

* From compilation of Barnes *et al.* (1985).
† After Shannon (1976) (1Å = 1^{-10} m).

PGE concentrations are normally determined by instrumental neutron activation although the sensitivity of the method decreases in the order Ir> Au> Rh>> Pd> Pt> Os> Ru. In rocks such as ocean-floor basalts PGE concentrations are so low that some elements are below the limit of detection. In this case analysis may be limited to the elements Au, Pd and Ir.

4.5.1 Presenting PGE data

The platinum group elements may be presented in the same way as are the REE and incompatible elements and normalized to either chondrite meteorites or to the primitive mantle.

Chondrite normalization

Naldrett *et al.* (1979) showed that if PGE and Au concentrations are chondrite-normalized and plotted in order of decreasing melting point (see Table 4.10) they define smooth curves rather like REE patterns (Figure 4.27). Normalizing values currently in use are given in Table 4.11, columns 1 to 3. The analogy with the REE is not close, however, because the PGEs are not ordered from light to heavy in keeping with their order in the periodic table. Further, the two groups of PGEs, the Ir-group and the Pd-group, behave differently; the Ir-group tend to be compatible during mantle melting whereas the Pd-group are incompatible. In rocks with very low concentrations of PGEs only Au, Pd and Ir may be measurable. This allows the slope of the chondrite-normalized PGE pattern to be determined from the Ir/Pd ratio, although of course the detail of the pattern is unknown. Au is not used in this instance because it is much more mobile than Pd and is not a reliable indicator of the PGE slope.

Using the terminology developed for REE patterns, depletion and enrichment

Table 4.11 Normalizing values for PGEs, noble metals and associated transition metals (in ppb)

		Chondrite values			Primitive mantle		Fertile mantle	Archaean mantle
	(Ref.)	(1)	(2)	(3)	(4)	(5)	(6)	(7)
	Ni				2110000	2110000		
	Cu				28000	28000	28000	
	Os	510	514	700	3.3	(4.0–5.6)		
IPGEs	Ir	510	540	500	3.6	3.5	4	3.4
	Ru		690	1000	4.3			
	Rh		200					
PPGEs	Pt	1060	1020	1500		(7.0)	7	7.5
	Pd	510	545	1200	4.0		4	5
	Au	160	152	170	1.0	0.5	1	0.75–1.5
	Re	35				0.1		

(1) Sun (1982): C1 chondrites.
(2) Compilation of Naldrett and Duke (1980): C1 chondrites.
(3) Cocherie *et al.* (1989).
(4) Compilation of Brugmann *et al.* (1987): primitive mantle.
(5) Jagoutz *et al.* (1979): average of six primitive mantle nodules.
(6) Compilation of Sun *et al.* (1991): fertile mantle.
(7) Sun (1982): Archaean mantle based upon komatiites.

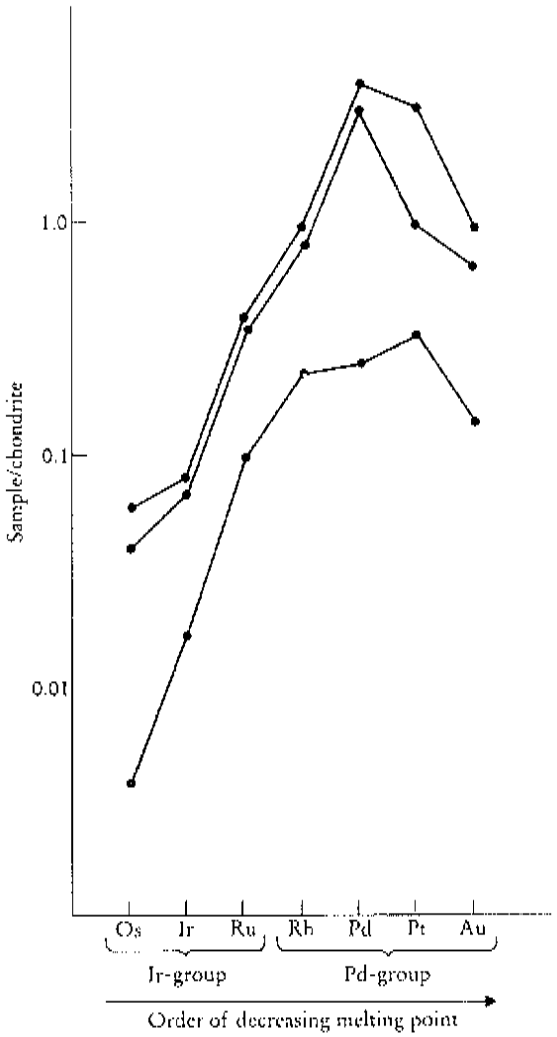

Figure 4.27 Chondrite-normalized platinum group element plot. The data are for komatiite-massive sulphide ores from Alexo Mine, northen Ontario (from Barnes and Naldrett, 1986). The chondrite-normalizing values are given in Table 4.11, column 2 and are taken from Naldrett and Duke (1980).

relative to the chondrite-normalized curve may be described as anomalous, although in this case there is no *a priori* reason why these variations do constitute anomalies. This is illustrated in the ultramafic and basaltic rocks described by Barnes *et al.* (1985) which show positive Pd anomalies and negative Pt and Au anomalies.

Primitive mantle normalization

Brugmann *et al.* (1987) present a primitive mantle-normalized PGE (Pd, Ru, Os, Ir) – Au – Cu – Ni plot (Figure 4.28). The elements are broadly arranged in order of increasing compatibility in the primitive mantle from left to right across the diagram. Primitive mantle values are listed in Table 4.11. Also shown are estimated values for the Archaean mantle (Sun, 1982) and the fertile mantle (Sun, *et al.*, 1991) to illustrate the observation of Brugmann *et al.* (1987) that the estimated

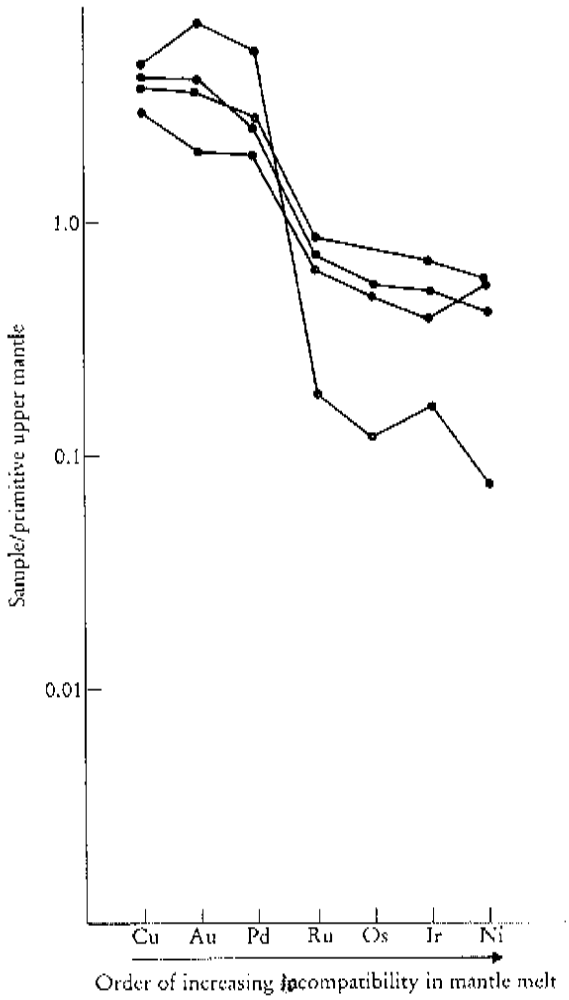

Figure 4.28 Primitive upper mantle-normalized platinum group element (plus Ni, Cu and Au) plot (after Brugmann *et al.*, 1987). The data are for Gorgona Island komatiites from Brugmann *et al.* (1987). The normalizing values are also taken from the compilation of Brugmann *et al.* (1987) and are given in Table 4.11, column 4.

concentrations of PGEs in the upper mantle have not changed since the late Archaean. There is some debate over the significance of the mantle concentrations of PGEs. They range between 0.005 and 0.01 times chondrite, indicating that the mantle may never have had chondritic abundances of PGEs. Garnet and spinel lherzolite xenoliths, on the other hand, show flat chondritic PGE patterns, indicating that the mantle does at least have chondritic PGE *ratios*.

4.5.2 Interpreting PGE patterns

The fractionation of the PGEs is principally governed by their partitioning between solid and melt phases. Unfortunately, partition coefficient data are not available for many minerals for the PGEs. One dominant control is that of a sulphide liquid, for

whilst sulphide melt/silicate melt partition coefficients are not well known experimentally, they are thought to be very large. Campbell *et al.* (1983) suggest that *Kd* values for Pt and Pd between a sulphide melt and a silicate melt may be as high as 160 000 and 120 000 respectively. Barnes *et al.* (1985) state that sulphide/silicate melt *Kd* values for the PGEs are in the order Os> Ir> Ru> Rh> Pt> Pd. Thus PGE fractionation may be used as a measure of the level of sulphur-saturation of melt. The extreme fractionation of sulphur undersaturated basaltic melts may be due to the compatibility of the IPGEs in olivine (Brugmann *et al.*, 1987), indicating that they are retained in mantle melting or during fractional crystallization. Barnes *et al.* (1985) investigated the extent to which PGE patterns may be modified by alteration and concluded that, whilst Pt and Au may be mobilized, this is not the dominant process.

4.6 Transition metal plots

The elements of the first transition series (Sc, Ti, V, Cr, Mn, Fe, Co, Ni, Cu and Zn) vary in valence state and in geochemical behaviour. Quadrivalent Ti is a high field strength, incompatible element whilst divalent Mn, Co, Ni, Cu and Zn and trivalent V and Cr are compatible elements (see Figures 4.1 and 4.2). Transition element plots have been mainly used with basalts as a means of exploring the geochemical behaviour of the first transition series. There is no geochemical reason

Table 4.12 Normalizing values used for transition metals (ppm)

Chondrite concentrations						Primitive mantle concentrations				
(Ref.)	(1)	(2)	(3)	(4)	(5)	(6)	(7)	(8)	(9)	(10)
Sc	5.8				5.21				17	17
Ti	410	720	440	660	610	1300	1300	1230		1300
V	49	94	42	50	49	82	87	59	97	77
Cr	2300	3460	2430	2700	2300	3140	3000	1020		3140
Mn	1720	2590	1700	2500	1720	1010	1100	1000		1010
Fe		219000	171000	250700	265000	61000	65000	67000		60800
Co	475	550	480	800	470	110	110	105		105
Ni	9500	12100	9900	13400	9500	2110	2000	2400		2110
Cu	115	140	110	100		28	30	26		28
Zn	350	460	300	50		50	56	53		50

(1) Langmuir *et al.* (1977).
(2) Kay and Hubbard (1978) from Mason (1971): chondrites, with Cu and Zn from carbonaceous chondrite.
(3) Sun (1982): CI chondrites.
(4) Bougault *et al.* (1980).
(5) Wood *et al.* (1979b).
(6) Sun (1982): primitive mantle (nodules).
(7) Sun (1982): primitive mantle (partial melting model).
(8) Kay and Hubbard (1978): model mantle.
(9) Sun and Nesbitt (1977): Archaean mantle.
(10) Jagoutz *et al.* (1979): average of six primitive ultramafic nodules.

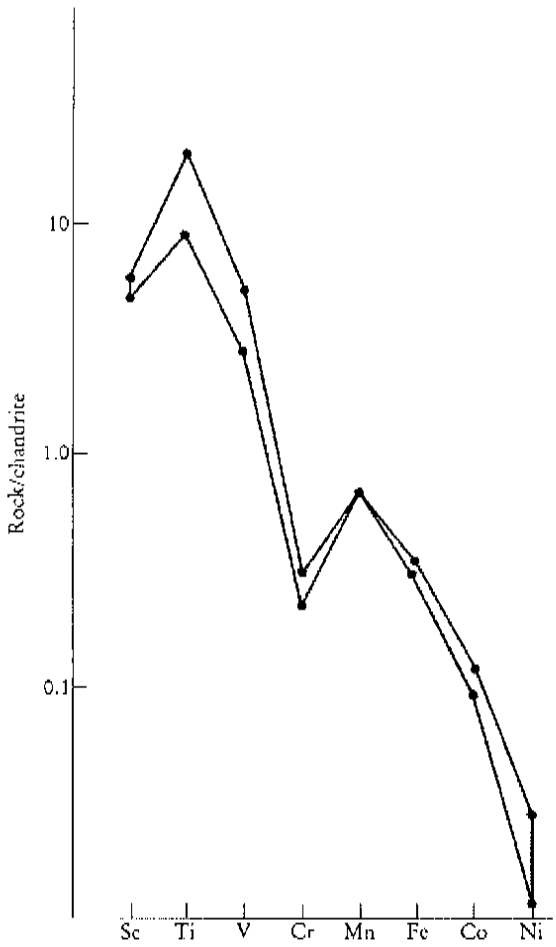

Figure 4.29 Transition metal concentrations in MORB (from Langmuir *et al.*, 1977) normalized to chondritic values. The normalizing values are taken from Langmuir *et al.* (1977) with the exception of Fe, which was taken from Wood *et al.* (1979b) — Table 4.12.

for them behaving as a coherent group nor is there any reason why they should have been present in the primitive earth in chondritic concentrations.

Mid-ocean ridge basalts from the Famous area of the Atlantic show consistent trends on chondrite-normalized plots (Table 4.12, Figure 4.29). They show progressive depletion from Ti to Ni, and have a positive Ti anomaly and a negative Cr anomaly. Cu and Zn are omitted because they are more variable and their concentrations may not reflect the original igneous values (Langmuir *et al.*, 1977). An alternative normalization scheme is to use estimated primitive mantle concentrations, (Figure 4.30). These values are given in Table 4.12, columns 6 to 10.

In summary, the elements Cu and Zn may be quite mobile during metamorphism and alteration and concentrations may diverge from expected smooth patterns. Anomalies in Ni and Cr concentrations may reflect the role of olivine (Ni) and clinopyroxene or spinel (Cr). Ni and Cu can also be concentrated into sulphide melts. Ti anomalies indicate the role of Fe–Ti oxides.

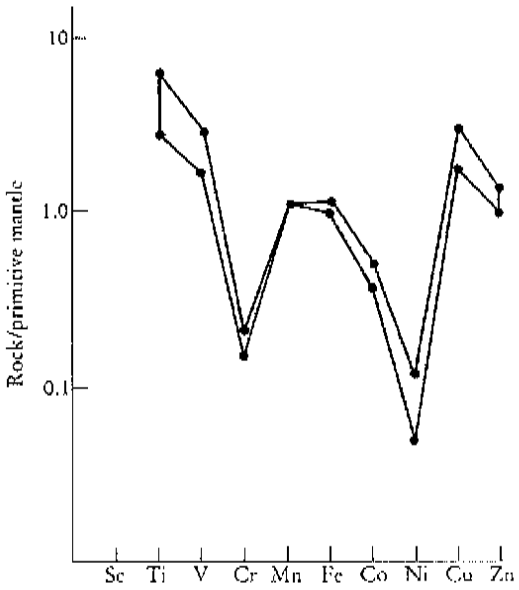

Figure 4.30 Transition metal concentrations in MORB (from Langmuir *et al.*, 1977) normalized to primitive mantle values. The normalizing values are taken from Sun (1982) — Table 4.12, column 6.

4.7 Bivariate trace element plots

So far in this chapter we have concentrated on the display of trace element data on multi-element plots. This approach has the advantage of utilizing a large number of elements and allowing broad conclusions to be drawn on their geochemical behaviour. Multi-element plots have one particular disadvantage, however, for only a few samples can be shown on a single diagram before it becomes becomes cluttered and confused. Thus the simple bivariate plot is superior to a multivariate plot when a large number of samples are plotted and in particular when geochemical trends are sought. Variation diagrams are discussed in detail in Section 3.3 and many of the principles outlined there and applied to major elements are equally valid for trace element plots.

4.7.1 The selection of trace elements in igneous rocks for plotting on bivariate graphs

Many igneous rocks have had a complex history of solid–liquid equilibria in their journey from the source region to their site of emplacement. In addition they may also have interacted with fluids during or after their solidification. The task for the

igneous geochemist, therefore, is to work out which trace elements are indicative of which processes in this complex history. The clues come from a knowledge of mineral/melt (and the lesser known mineral/fluid) partition coefficients and the physical laws which govern the concentrations of trace elements in igneous rocks. Most fruitful are trace elements which show extreme behaviour, such as the highly incompatible and the highly compatible elements. Further clues may come from the inspection of multi-element plots, for this allows the identification of element pairs or ratios which can be used in trace element modelling and in subdividing rocks into similar suites.

Incompatible element plots

Incompatible element concentrations are particularly sensitive to partial melting processes (see for example Figures 4.11a and 4.12a). The more highly incompatible an element is, the more sensitive it is to degrees of partial melting. This is true for both batch melting and fractional melting but is most extreme in fractional melting. Incompatible element concentrations also vary during fractional crystallization, although the effect is most strongly marked in AFC processes.

(a) Identification of igneous source characteristics from incompatible element plots The ratio of a pair of highly incompatible elements whose bulk partition coefficients are very similar will not vary in the course of fractional crystallization and will vary little during batch partial melting. Thus the slope of a correlation line on a bivariate plot of two such highly incompatible elements gives the ratio of the concentration of the elements in the source. In the case of mantle melting, the following groups of elements have almost identical bulk partition coefficients during mantle melting: Cs–Rb–Ba, U–Nb–Ta–K, Ce–Pb, Pr–Sr, P–Nd, Zr–Hf–Sm, Eu–Ti, Ho–Y. Bivariate plots of element pairs taken from within these groups can be expected to show to a first approximation the ratio of the elements in the source (Sun and McDonough, 1989). In addition the elemental pairs Y–Tb, La–Ta, La–Nb, Ta–Th, Ti–Zr and Ti–Y are also often assumed to have very similar bulk partition coefficients and are used in a similar way. Any variation in the ratio reflects heterogeneity in the source (Bougault *et al.*, 1980) resulting from source mixing or contamination.

This approach has been very fruitful in some areas of igneous petrology but is not universally applicable. Firstly, the relationship does not hold for very small degrees of melting for there is divergence between the enrichment paths of highly incompatible and moderately incompatible trace elements — see Figures 4.12(a) and (c). If a small degree of melting is suspected it may be recognized from the approximation $C_L/C_0 = 1/F$ derived from the batch melting equation for the case when D is very small (Section 4.2.2). Secondly, this method is difficult to apply to granitic rocks. This is because few trace elements are highly incompatible in granitic melts, chiefly because of the large number of possible minor phases incorporating many of the trace elements traditionally regarded as incompatible. The source region of granitic rocks is more easily characterized by the study of radiogenic isotopes (see Chapter 6).

(b) Identification of igneous source characteristics from incompatible element ratio–ratio plots Ratio–ratio plots of highly incompatible elements minimize the effects of fractionation and allow us to examine the character of the mantle source. Different mantle sources plot on different correlation lines (Figure 4.31). This approach was

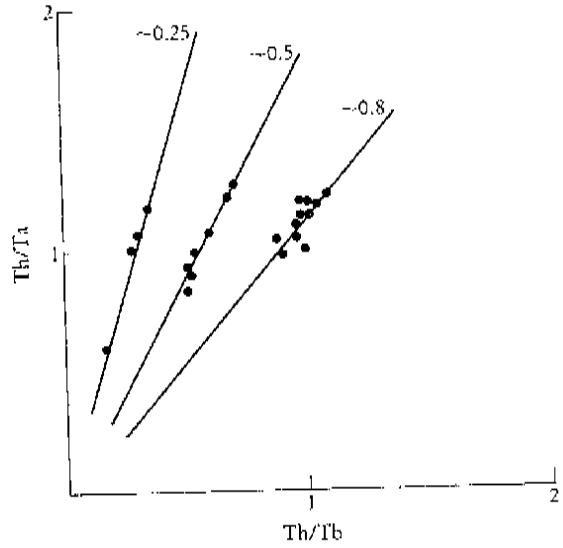

Figure 4.31 Bivariate ratio plot of Th/Ta vs Th/Tb for basalts from the Red Sea Rift (data from Eissen *et al.*, 1989). The three trends showing (Th/Tb)/(Th/Ta) ratios of approximately 0.25, 0.5 and 0.8 are thought to indicate three different mantle sources.

used by Saunders *et al.* (1988) who used the highly incompatible elements Th,U, Pb, K, Ba, Ce and Nb and the element pairs Th–Ce, K–Ce, U–Pb and Ba–Ce each ratioed to Nb, in order to explore the ratios Th/Ce, K/Ce and U/Pb in MORB. Where the three elements have identical bulk partion coefficients the ratio will not change during partial melting or fractional crystallization. Ratio–ratio plots do have some inherent problems and the reader should take note of possible spurious correlations arising from the common denominator effect discussed in Section 2.5.

(c) Calculation of partition coefficients from reciprocal concentration trace element plots Minster and Allegre (1978) showed that, from a rearrangement of the batch melting equation, a bivariate plot of the reciprocals of incompatible elements can be used to obtain information about partition coefficients during melting. Provided the mass fractions of the minerals in the melt remain constant, a linear trend on such a diagram characterizes the batch melting process. Further, the slope and intercept of the trend can provide information about the difference in bulk partition coefficient between the two elements. If the samples are first normalized to the most enriched sample, elements with the same bulk partition coefficient will have a slope of 1 and an intercept of zero. If the bulk partition coefficients for the two elements change at different rates during melting then a curvilinear trend will be produced (Bender *et al.*, 1984).

Compatible element plots

Compatible trace element concentrations change dramatically in an igneous liquid during fractional crystallization (Figure 4.13). Thus bivariate plots of compatible elements, plotted against an index of fractionation (e.g. mg number) can be used to

test for fractional crystallization. The effect is not so marked in *in situ* crystallization except when a large melt fraction is returned to the magma chamber (Figure 4.14d). In AFC processes when the rate of assimilation is high and the trace element concentration in the wallrock is less than in the melt, compatible elements are strongly depleted (Figure 4.16a and b)

During partial melting, however, highly compatible elements are buffered by the solid phase with respect to solid–melt equilibria during partial melting (Figures 4.11b, 4.12d). This means that their concentration in the source, even if it has undergone some partial melting, is largely unchanged.

4.7.2 Bivariate plots in sedimentary rocks

Bivariate trace element plots in sedimentary rocks are mostly used to detect mixing processes in sediments. Norman and De Deckker (1990) suggest that linear correlations amongst a diverse group of elements over a broad range of concentrations may be taken as indicative of mixing of two sedimentary components. Condie and Wronkiewicz (1990) and McLennan and Taylor (1991) have exploited the geochemical differences between elements such as Th and La (indicative of a felsic igneous source) and Sc and Cr (indicative of a mafic source) and have used plots such as Th/Sc vs Sc and Cr/Th vs Sc/Th as indicators of contrasting felsic and mafic provenance. Floyd *et al.* (1989) quantified such mixing processes with the general mixing equation of Langmuir *et al.* (1978) — see Section 4.9.3.

4.8 Enrichment–depletion diagrams

Enrichment–depletion diagrams are a convenient way of showing relative enrichment and depletion in trace (and major) elements. They can be useful, for example, in demonstrating the extent of elemental enrichment and depletion in an igneous suite by comparing the chemistries of early and late members of a series. Hildreth (1981) compares the relative concentrations of the early and late members of the Bishop's tuff (Figure 4.32). The x-axis of the graph shows the elements arranged by atomic number and the y-axis the concentration of an element in the latest erupted ejecta ratioed to that for the earliest erupted ejecta. Alternatively the values on the y-axis may be recorded on a logarithmic scale.

Enrichment–depletion diagrams are also useful as a way of displaying element mobility; this has been used particularly in alteration zones associated with hydrothermal mineralization. For example, Taylor and Fryer (1980) show the relative mobilities of trace and major elements in the zones of potassic and propylitic alteration associated with a porphyry copper deposit. In this case the enrichment/depletion is measured relative to the unaltered country rock.

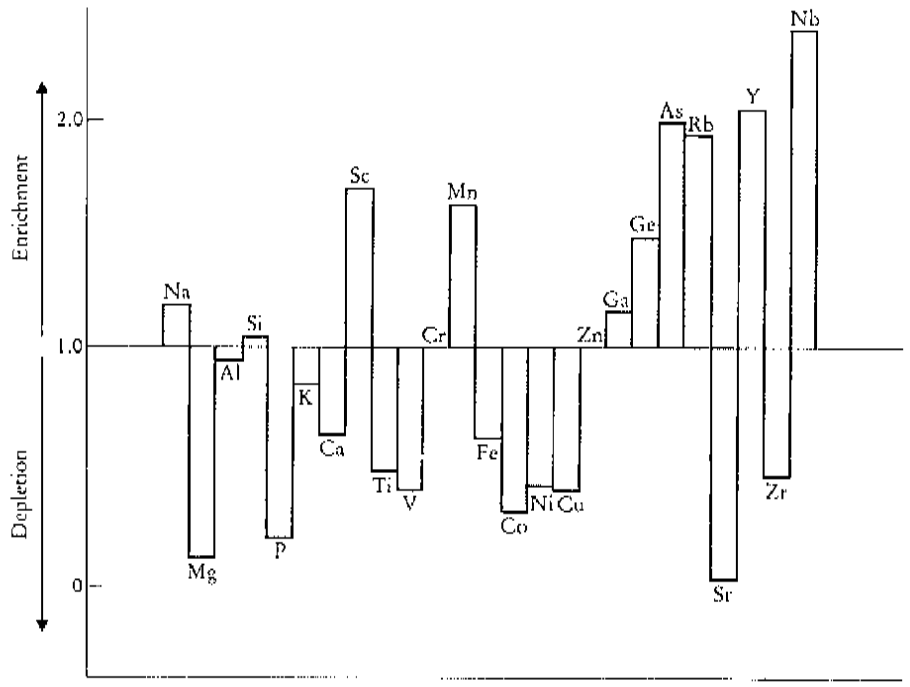

Figure 4.32 Enrichment–depletion diagram showing the enrichment factors for selected major and trace elements from the Bishop's tuff, arranged in order of increasing atomic number. The diagram compares the relative concentrations of the early and late members of the Bishop's tuff and is thought to be a measure of the zonation of the magma chamber. Data from Hildreth (1981).

4.9 Modelling trace element processes in igneous rocks

One of the most important uses of trace elements in modern igneous petrology is in the modelling of geochemical processes. Trace element modelling depends upon the mathematical expressions which describe the equilibrium partitioning of trace elements between minerals and melt during igneous processes (Section 4.2.2) and a precise knowledge of trace element partition coefficients (see Tables 4.1 to 4.3). For successful geochemical modelling, three conditions should be fulfilled. Firstly, trace element concentrations must be determined with great accuracy; otherwise it is impossible to discriminate between competing hypotheses (Arth, 1976). Secondly, partition coefficients must be known accurately for the conditions under which the process is being modelled and, thirdly, the starting composition must be known. This latter condition is not always fulfilled; and sometimes a reasonable assumption of the starting composition must be made which is later refined as the model is developed.

Calculated compositions are plotted on a bivariate graph and compared with an observed trend of rock compositions, or plotted on a multivariate diagram such as an REE diagram and the calculated composition compared with a measured composition. Below we describe these two modes of presentation in some detail.

4.9.1 Vector diagrams

Changes in trace element concentrations may be modelled on a bivariate plot using vectors to show the amount and direction of change which will take place as a consequence of a particular process. **Mineral vectors** show the trend of a fractionating mineral phase or mineral assemblage. These are illustrated in Figure 4.33 for the fractionation of plagioclase, clinopyroxene, orthopyroxene, hornblende, biotite and orthoclase from a granitic melt. **Partial melting** vectors are used to show changing melt and source compositions during the partial melting of a given source composition and mineralogy. The effects of different melting models, source

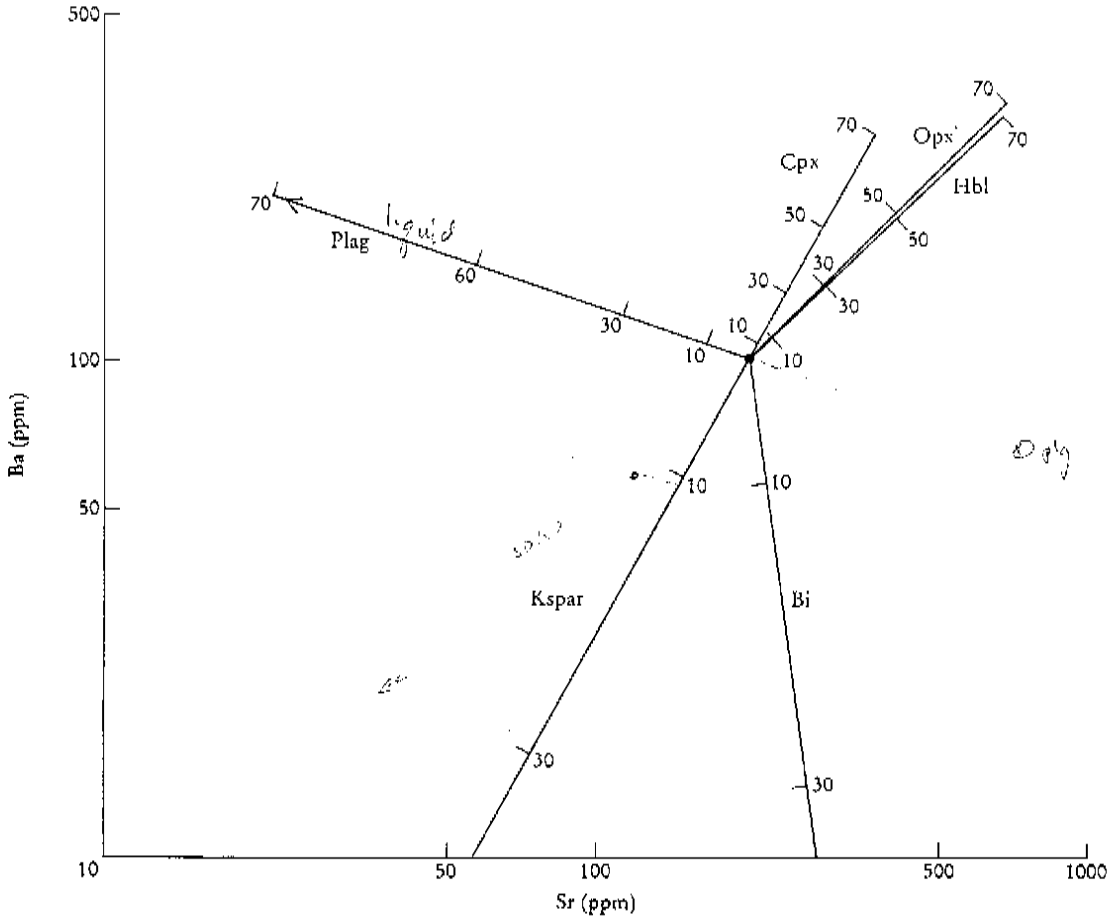

Figure 4.33 Mineral vector diagram showing fractional crystallization trends in a granitic source containing 200 ppm Sr and 100 ppm Ba. Fractionation trends are shown for 10, 30, 50 and 70 % fractional crystallization of the minerals clinopyroxene (Cpx), orthopyroxene (Opx), hornblende (Hbl), biotite (Bi), orthoclase (Kspar) and plagioclase (Plag). The direction of the lines shows the compositional change in the residual liquid when the specified phase is progressively removed during fractional crystallization. The partition coefficients for Ba and Sr are taken from Table 4.3 and the vectors calculated from the Rayleigh fractionation equation (Eqn [4.18]). Details of the calculation are given in Table 4.13. The logarithmic scale is used to produce a straight-line trend.

Table 4.13 Data used in the calculation of mineral vectors shown in Figure 4.33

Partition coefficients for rhyolitic liquids (from Table 4.3)

	Opx	Cpx	Hbl	Bi	Plag	Ksp
Ba	0.003	0.131	0.044	6.360	0.360	6.120
Sr	0.009	0.516	0.022	0.120	2.840	3.870

Initial composition

Ba	100
Sr	200

Calculated compositions (from Eqn [4.18])

	Opx	Cpx	Hbl	Bi	Plag	Ksp
10 % fractional crystallization						
Ba	111.1	109.6	110.6	56.9	107.0	58.3
Sr	222.0	210.5	221.7	219.4	164.8	147.8
30 % fractional crystallization						
Ba	142.7	136.3	140.6	14.8	125.6	16.1
Sr	284.8	237.7	283.5	273.7	103.8	71.9
50 % fractional crystallization						
Ba	199.6	182.6	194.0	2.4	155.8	2.9
Sr	397.5	279.7	393.9	368.1	55.9	27.4
70 % fractional crystallization						
Ba	332.1	284.7	316.1	0.2	216.1	0.2
Sr	659.5	358.2	649.2	577.0	21.8	6.3

compositions and mineralogies may all be explored in this way. Figure 4.34, for example, illustrates the differing melting paths during fractional and batch melting and the different degrees of enrichment caused by the two processes. Whilst vector diagrams select only two out of a vast array of possible elements, they have the advantage of being able to display data from a large number of samples. This means that it is possible to view trends in the data. Hence both mineral and partial melting vectors are compared with observed trends on bivariate plots in order to test the validity of a particular model.

4.9.2 Modelling on multivariate diagrams

Multivariate diagrams such as REE plots and spider diagrams are also used in petrogenetic modelling, although by their nature they are unable to show more than a few samples clearly on a single diagram. In this case the same operation is performed on each element in the plot and the resultant data array is compared with a measured rock composition. The process is illustrated in Figures 4.35 and 4.36 which show respectively the effect of olivine fractionation on a komatiite liquid and the partial melting of a primitive mantle source. Repetitive calculations such as

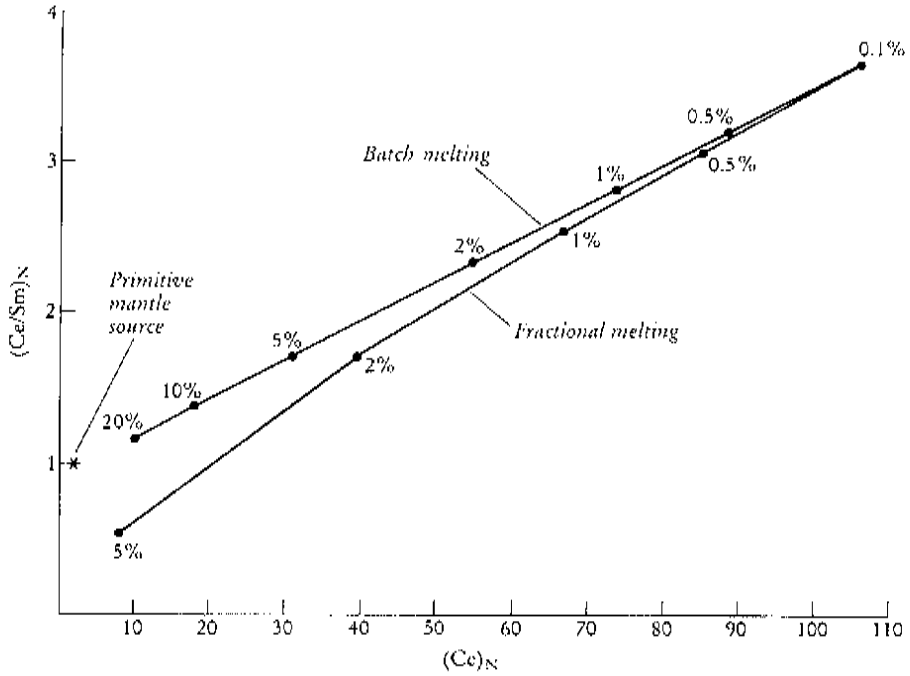

Figure 4.34 Vector diagram showing the change in normalized (Ce/Sm) vs Ce concentrations during the partial melting of a primitive mantle source with the mineralogy: olivine 55 %, orthopyroxene 25 %, clinopyroxene 11 % and garnet 9 %. The initial normalized concentrations of Ce and Sm in the primitive mantle were taken as 2.12 and 2.19 respectively. The vector for modal batch melting between 0.1 % and 20 % melting was calculated from Eqn [4.10]. The vector for single melt increments formed during modal fractional melting between 0.1 and 5 % melting was calculated from Eqn [4.11]. The partition coefficients were taken from Table 4.1. Details of the calculation are given in Table 4.14 and the same data are also illustrated in Figure 4.36.

Table 4.14 Data used in the calculation of partial melting vector diagram (Figure 4.34) and REE diagram (Figure 4.36)

	Primitive mantle composition			Basaltic *Kd* values from Table 4.1				Weighted mean of bulk partition coeff.
	Concn. (ppm)	Nakamura values	Normalized values	Ol	Opx	Cpx	Gt	(Ol 55 %, Opx 25%, Cpx 11 %, Gt 9 %)
La	0.708	0.329	2.15	0.007	0.020	0.056	0.001	0.015
Ce	1.833	0.865	2.12	0.006	0.020	0.092	0.007	0.019
Nd	1.366	0.630	2.17	0.006	0.030	0.230	0.026	0.038
Sm	0.444	0.203	2.19	0.007	0.050	0.445	0.102	0.074
Eu	0.168	0.077	2.18	0.007	0.050	0.474	0.243	0.091
Gd	0.595	0.276	2.16	0.010	0.090	0.556	0.680	0.150
Dy	0.737	0.343	2.15	0.013	0.150	0.582	1.940	0.283
Er	0.479	0.225	2.13	0.026	0.230	0.583	4.700	0.559
Yb	0.481	0.220	2.19	0.049	0.340	0.542	6.167	0.727
Lu	0.074	0.034	2.17	0.045	0.420	0.506	6.950	0.811

(*Continued*)

Table 4.14 (Continued)

	Assumed mantle composition (normalized)		Batch modal partial melting — Eqn [4.10]						
	Source	Calculated bulk partition coeff. for mineral assemblage (Ol 55 %, Opx 25 %, Cpx 11 %, Gt 9 %)	0.1 %	0.5 %	1 %	2 %	5 %	10 %	20 %
La	2.15	0.015	135.17	108.36	86.82	62.13	33.53	18.97	10.15
Ce	2.12	0.019	105.79	88.46	73.43	54.80	31.12	18.09	9.85
Nd	2.17	0.038	55.11	50.20	45.17	37.63	25.08	16.12	9.40
Sm	2.19	0.074	29.01	27.65	26.12	23.52	18.11	13.09	8.43
Eu	2.18	0.091	23.85	22.94	21.89	20.06	16.04	12.02	8.01
Gd	2.16	0.150	14.26	13.94	13.57	12.88	11.18	9.16	6.73
Dy	2.15	0.283	7.57	7.49	7.40	7.22	6.73	6.05	5.04
Er	2.13	0.559	3.81	3.80	3.78	3.75	3.67	3.53	3.29
Yb	2.19	0.727	3.01	3.00	3.00	2.99	2.95	2.90	2.80
Lu	2.17	0.811	2.68	2.68	2.67	2.67	2.65	2.62	2.56
Ce	2.12		105.70	88.46	73.43	54.80	31.12	18.09	9.85
Ce/Sm	0.97		3.65	3.20	2.81	2.33	1.72	1.38	1.17

	Assumed mantle composition (normalized)		Calculated composition assuming fractional modal melting — Eqn [4.11]				
	Source	Calculated bulk partition coeff. for mineral assemblage (Ol 55 %, Opx 25 %, Cpx 11 %, Gt 9 %)	0.1 %	0.5 %	1 %	2 %	5 %
La	2.15	0.015	134.89	103.53	74.26	38.01	4.89
Ce	2.12	0.019	105.65	85.93	66.30	39.31	7.93
Nd	2.17	0.038	55.09	49.82	43.91	34.05	15.63
Sm	2.19	0.074	29.00	27.59	25.92	22.85	15.52
Eu	2.18	0.091	23.85	22.90	21.78	19.67	14.39
Gd	2.16	0.150	14.26	13.94	13.55	12.79	10.73
Dy	2.15	0.283	7.57	7.49	7.39	7.21	6.66
Er	2.13	0.559	3.81	3.80	3.78	3.75	3.66
Yb	2.19	0.727	3.01	3.00	3.00	2.99	2.95
Lu	2.17	0.811	2.68	2.68	2.67	2.67	2.65
Ce	2.12		105.65	85.93	66.30	39.31	7.93
Ce/Sm	0.97		3.64	3.11	2.56	1.72	0.51

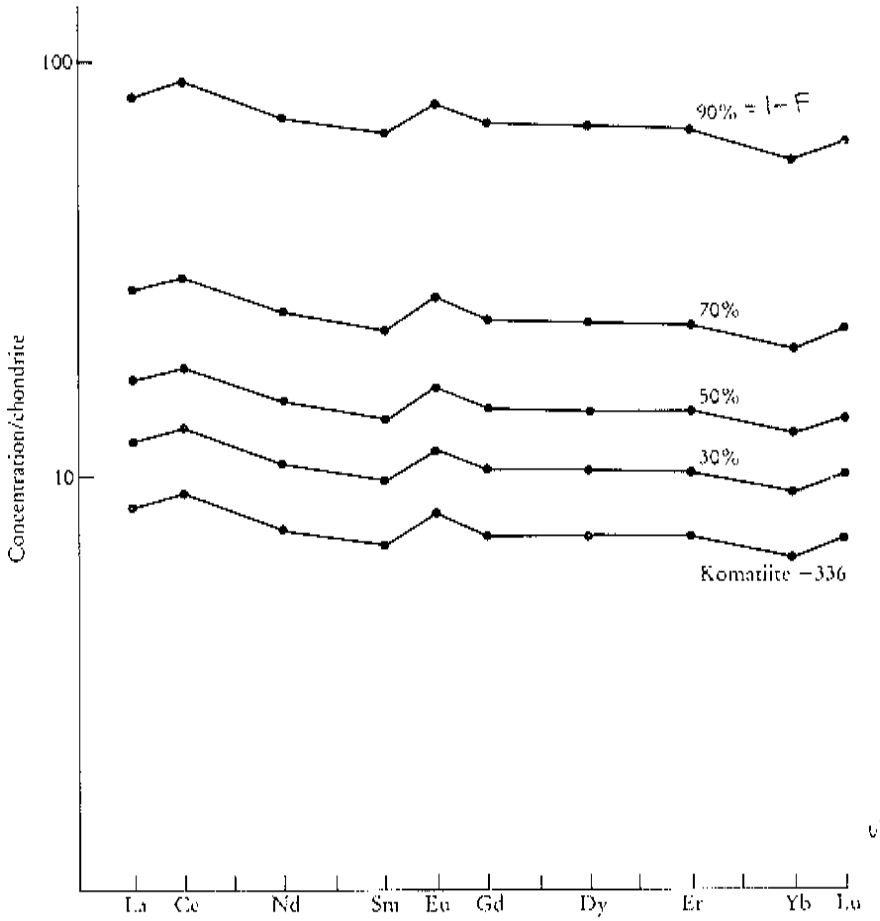

Figure 4.35 Chondrite-normalized REE patterns calculated for olivine fractionation from a komatiite melt (komatiite–336) at 30 %, 50 %, 70 % and 90 % fractional crystallization. The partition coefficients were taken from Table 4.1. The details of the calculations made for each of the ten REE shown using Eqn [4.18] are given in Table 4.15.

Table 4.15 Data used in the calculation of the REE diagrams shown in Figure 4.35

	Starting composition of Sula Mountains komatiite 336				Calculated values (from Eqn [4.18]) at a given % fractional crystallization				
	Concn (ppm)	Nakamura values	Normalized values	*Kd* for olivine (Table 4.1)	10 %	30 %	50 %	70 %	90 %
La	2.79	0.3290	8.48	0.0067	9.4	12.1	16.9	28.0	83.5
Ce	7.93	0.8650	9.17	0.0060	10.2	13.1	18.3	30.3	90.4
Nd	4.73	0.6300	7.51	0.0059	8.3	10.7	15.0	24.8	74.1
Sm	1.40	0.2030	6.90	0.0070	7.7	9.8	13.7	22.8	67.9
Eu	0.63	0.0770	8.18	0.0074	9.1	11.7	16.3	27.0	80.4
Gd	2.01	0.2760	7.28	0.0100	8.1	10.4	14.5	24.0	71.2
Dy	2.46	0.3430	7.17	0.0130	8.0	10.2	14.2	23.5	69.6
Er	1.61	0.2250	7.16	0.0256	7.9	10.1	14.1	23.1	67.5
Yb	1.41	0.2200	6.41	0.0491	7.1	9.0	12.4	20.1	57.2
Lu	0.24	0.0339	7.08	0.0454	7.8	10.0	13.7	22.3	63.8

these are done most easily by computer and the results displayed, ideally, on a graphics screen. Holm (1990) describes such a method using a spreadsheet.

4.9.3 Petrogenetic modelling — examples

In this section we illustrate the way in which trace element modelling has been used to identify differing petrogenetic processes in igneous rocks.

Partial melting

A numerical example showing the effects of between 0.1 % and 20 % partial melting on the REE concentrations of a primitive mantle source is given in Table 4.14. The results are displayed graphically on a vector diagram (Figure 4.34) and on a multivariate plot (Figure 4.36). Both diagrams show the extreme enrichment of the light REE relative to the heavy REE in the partial melts — a property which increases as the percentage of melting decreases. This type of modelling has been used extensively and many examples can be found in the geochemical literature. The results of partial melting calculations may equally well be presented on spider diagrams. For example, Thompson *et al.* (1984) calculated chondrite-normalized spidergrams for the dynamic melting of mantle lherzolite for comparison with measured oceanic basalt compositions.

Crystal fractionation

The modelling of fractional crystallization on vector diagrams and REE plots is described above in Sections 4.9.1 and 4.9.2 respectively and is illustrated in Figures 4.33 and 4.35. Details of the calculations are given in Tables 4.13 and 4.15.

Vector diagrams can be used to identify a fractionating phase on a bivariate plot. If, for example, on a plot of Ba vs Sr, the rock compositions define a liquid trend which could have been produced by crystal fractionation, then the slope of the trend can be compared with a mineral vector diagram such as Figure 4.33 and the phase responsible for the fractional crystallization trend can be identified. In addition, it is possible, from the compositional range in the two elements, to make an estimate of the amount of fractional crystallization that has taken place. When there is more than one fractionating phase present a composite vector must be calculated, although when this is the case it is not always possible to find a unique composition for the fractionating mineral assemblage.

Multivariate diagrams are used to compare calculated and measured rock compositions. Provided the composition of a parental melt is known, the composition of derivative liquids can be calculated and compared with the composition of liquids which are thought to have been derived from the parental melt. This is the approach used by Arth (1981), who modelled the REE chemistry of andesites and dacites in New Britain by fractional crystallization from basaltic and basaltic andesites. Arth estimated the mineralogy of the fractionating assemblage from the proportions of phenocrysts present in the lavas and calculated REE patterns which show excellent agreement with the observed REE patterns in the rocks.

Crystal contamination and AFC processes

Komatiitic magmas are thought to have had exceptionally high liquidus temperatures and to have been frequently contaminated with continental crust. Trace element data in support of this hypothesis are illustrated qualitatively by Arndt and Jenner (1986) on a REE diagram. Similarly, Condie and Crow (1990)

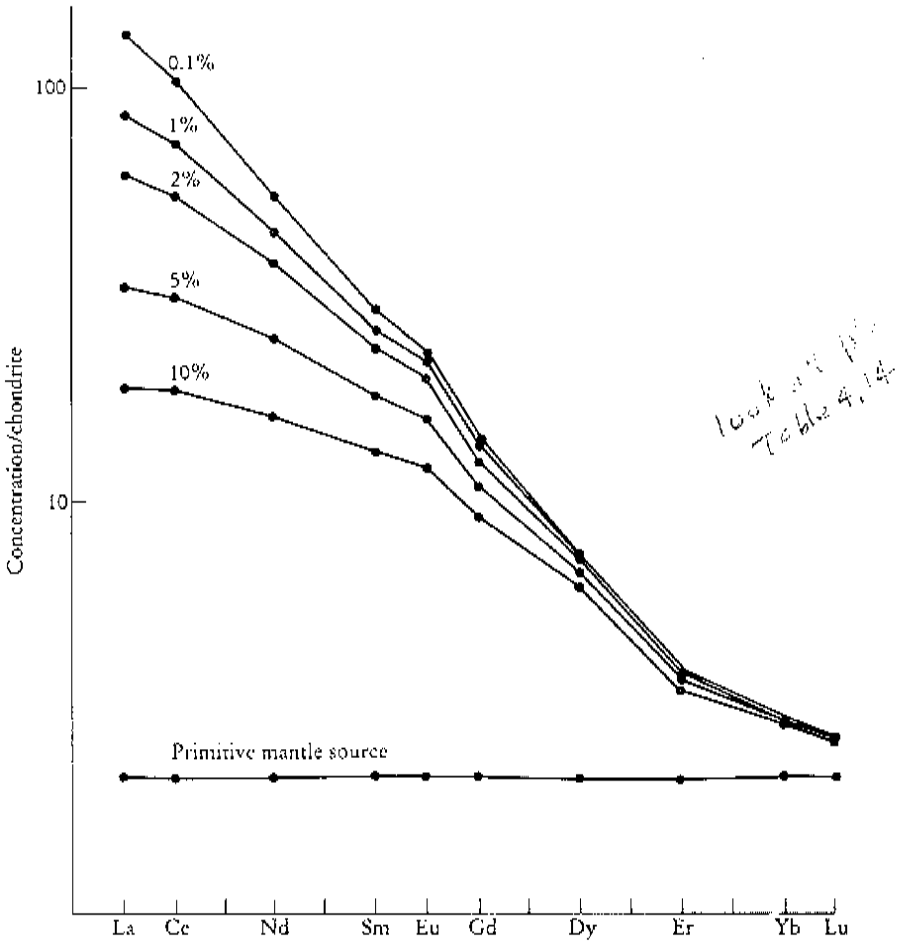

Figure 4.36 Chondrite-normalized REE paterns calculated for modal batch partial melting of a primitive mantle source with *ca* 2.15 chondritic concentration of REE and with the mineralogy — olivine 55 %, orthopyroxene 25 %, clinopyroxene 11 % and garnet 9 %. Curves are shown for 0.1 to 10 % partial melting. The calculations were made for the ten REE shown using Eqn [4.10] — see Table 4.14 for the details.

proposed that Archaean and early Proterozoic basalts erupted on the Kaapvaal craton in southern Africa were komatiitic in origin but contaminated with continental crust. They support this hypothesis by showing that AFC vectors, calculated from the equations of DePaolo (1981b) (see Section 4.2.2), coincide with observed trends on bivariate Zr–Ni and Hf–Th diagrams. They also use MORB-normalized spidergrams to show conformity between measured basaltic compositions and calculated spidergrams for varying degrees of assimilation and fractional crystallization from a komatiitic liquid.

Open system processes

The behaviour of the REE in a periodically replenished, periodically tapped, continuously fractionated (RTF) magma chamber (Section 4.2.2) is described by O'Hara and Matthews (1981). Using chondrite-normalized values of Ce/Yb to represent the slope of the REE diagram, and Sm values as a measure of REE

concentrations, they show on a bivariate plot of normalized Ce/Yb vs Sm the effects of the RTF process on partial melts of a variety of mantle sources coupled with crystal fractionation.

Recognizing RTF processes in a lava sequence requires a very detailed and complete geochemical section. Norman and Leeman (1990), in a study of Oligocene andesites and basalts from southwest Idaho, USA recognized a cyclicity in the trace and major element chemistry up the stratigraphic section. On bivariate Ba–Sc and Th–Sc plots they show that the scatter in the data cannot be accommodated within calculated fractional crystallization and AFC trends alone, and requires the recharge of the magma chamber by the addition of more mafic magmas during evolution of the magma chamber.

Magma and source mixing

A set of general mixing equations is given by Langmuir *et al.* (1978) which may be used to identify magma mixing and mixing in an igneous source region. The equations of Langmuir *et al.* (1978) predict that mixing between two elements produces a straight line whereas mixing between an element and a element ratio or between two ratios produces an asymptotic curve.

The two types of mixing, magma mixing and source mixing, can be differentiated by using differences in behaviour between compatible and incompatible elements. For example, since highly incompatible element ratios do not change during partial melting or fractional crystallization, a mixing curve based upon incompatible element ratios is ambiguous and can indicate either magma mixing or source mixing. Compatible element ratios, on the other hand, are strongly fractionated during partial melting and will not reflect the ratios of the source region. Thus, if mixing is in the source region a compatible element plot will show a scattered trend whereas the mixing of two melts will produce a simple mixing line.

Demonstrating element mobility

Two types of trace element plot lend themselves to the investigation of element mobility. Firstly, the MORB-normalized multi-element diagram of Pearce (1983) (Figure 4.23, Section 4.4.1) was constructed to show the difference in behaviour between elements which are mobile and those which are not. Brewer and Atkin (1989) found that this diagram successfully differentiated between the behaviour of mobile elements such as Sr, K, Rb and Ba and the immobile elements Nb, Ce, P, Zr, Ti and Y during the greenschist facies metamorphism of basalts. A second approach is to use the enrichment–depletion diagram described in Section 4.8 (Figure 4.32), although this type of diagram can only be used when the composition of the unaltered rock is known.

4.9.4 Inversion techniques using trace elements

Trace element inversion methods make use of the variability in elemental concentrations in a suite of cogenetic igneous rocks to determine unknowns such as the composition and mineralogy of the source, the physical process causing the variation — crystal fractionation, partial melting or other process — and the degree of partial melting, crystal fractionation or other process. Thus, the inverse method, with its emphasis on constraining the model from the trace element data, offers a much greater possibility of a unique solution to a geochemical problem. Inverse methods can in principle be applied to all petrological processes, although only

fractional crystallization and partial melting are illustrated here. The methods outlined here are discussed in detail by Allegre and Minster (1978).

The first step in using the inverse approach to the study of trace elements is to identify the likely physical process which accounts for the variation in the data. This may be done by plotting selected trace elements on bivariate plots. For example, elements which are compatible will vary drastically in concentration during fractional crystallizsation, whilst highly incompatible elements will vary most in abundance during partial melting (Minster and Allegre, 1978).

Constraining fractional crystallization using an inversion method

A worked example of the inverse approach to fractional crystallization is given by Minster *et al.* (1977) for a suite of basaltic lavas from the Azores. In this case the unknowns are (1) the initial concentration of the trace elements in the parent magma, (2) the bulk partition coefficients for the elements and (3) the degree of crystallization corresponding to each sample. The initial concentrations of trace elements in the melt were estimated using Ni. The likely Ni concentration in a parental melt was calculated by melting a model mantle. On this basis a parental melt from the lava suite was thus identified. Bulk partition coefficients were calculated using the method of Allegre *et al.* (1977) as follows. It can be shown from the Rayleigh Fractionation Law (Eqn [4.18]) that the slope of a log-log plot of a highly incompatible trace element against any other trace element is proportional to the bulk partition coefficient D (see Figure 4.37). Where $D < 1$ the slope is $(1 - D)$ and where $D > 1$ the slope is $(D - 1)$. Minster *et al.* (1977) calculated bulk partition coefficients by assuming that the highly incompatible element Ta had a bulk partition coefficient of zero. The slopes of log–log plots of the data against Ta were used to estimate bulk partition coefficients for other elements. The degree of

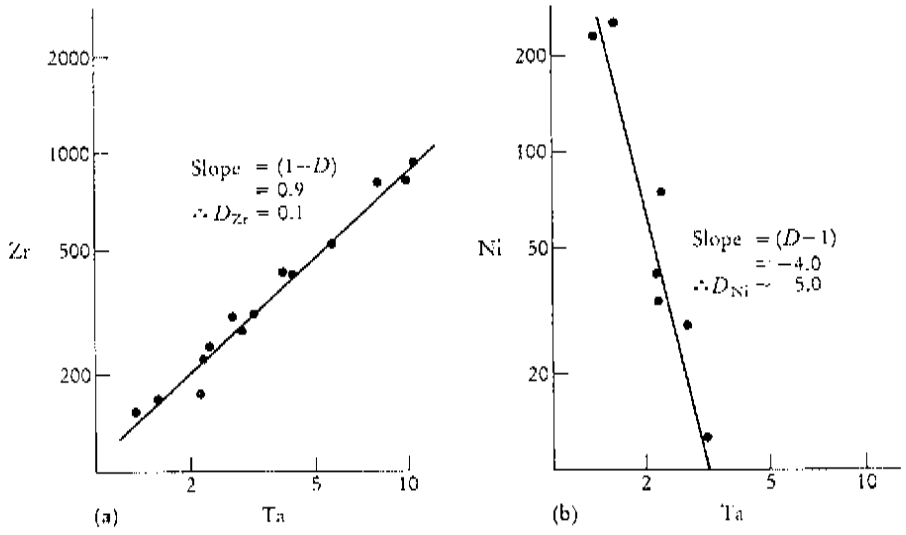

Figure 4.37 Log–log trace element plots showing the calculation of the bulk partition coefficient D during crystal fractionation, after the method of Allegre *et al.* (1977). (a) Plot of moderately incompatible element Zr against highly incompatible element Ta. The slope of the logarithmic plot is 0.9; hence the bulk partition coefficient $D = 0.1$. (b) Plot of compatible element Ni against highly incompatible element Ta. The slope of the logarithmic plot is *ca* −4.0, hence the bulk partition coefficient D is *ca* 5.

crystallization for each sample was calculated from a knowledge of the composition of the primary melt and the bulk partition coefficient.

Constraining partial melting using an inversion method

In the case of partial melting the unknowns are (1) the chemistry of the source, (2) the bulk partition coefficient for each element considered and (3) the degree of partial melting for each sample. There are too many unknowns for a direct solution and so a number of initial assumptions have to be made.

Bender *et al.* (1984), in a study of ocean-floor basalts, used the modal batch melting equation (Eqn [4.10]) and made two initial assumptions. Firstly, they selected a reference element (in this case the most incompatible element) and assigned it a bulk distribution coefficient (D). Secondly, an initial value was assumed for the degree of partial melting. This value is subsequently checked and refined by the geological plausibility of the end result. From these two assumptions the concentration in the source (C_0) may be calculated for the reference element: this is usually done for the most enriched sample. From the values obtained for D and C_0 for the reference element, values for the percentage melting (F) can be calculated for all the other samples. The batch melting equation now has two known parameters for each element — the concentration in the melt (C_L) and the percentage melting (F) — and two unknowns, C_0 and D. These unknowns may be found by solving simultaneous equations for pairs of parental magmas and by assuming that in each case a pair of magmas has values of C_0 and D which are constant.

The results of a preliminary calculation are inspected and refined as necessary. A comparison of calculated D values for each pair of parental magmas gives a test of the assumed batch melting model for these rocks. The calculated inverted partition coefficients may be compared with experimentally determined values to see if they are geologically plausible. The relative values of the inverted distribution coefficients are a robust feature of this inversion method over a range D and F values. Values for the composition of the source are more sensitive to values of D and F but solutions are restricted to a small range of geologically plausible possibilities.

4.9.5 A final comment on geochemical modelling

The development of trace element modelling in petrology represents a major advance in geochemistry. However, this approach must be used with some caution for two reasons.

(1) Most of the models developed in Section 4.2.2 of this chapter are idealized and do not always conform to the actual physical conditions of the process being modelled.
(2) Rarely can petrological modelling produce a unique solution. Often problems of this type contain too many unknowns.

For this reason, trace element modelling must be regarded as a means of hypothesis testing and should be used to verify an already constrained model. Wherever possible, trace element studies should be part of a broader approach to a geochemical problem which includes the constraints of the major element and isotopic chemistry.